Politecnico di Torino

Department of Structural, Geotechnical and Building Engineering
Master's degree in Civil and Structural Engineering

Ductility Analysis of Hybrid Reinforcement Concrete: Evaluating Minimum Longitudinal Reinforcement in Beams Across Building Codes

Supervisor:
Prof. Alessandro P. Fantilli

Candidate:
Mohammadhossein Nikoo

2025-2026

Abstract

This research presents a comprehensive analytical evaluation of the structural safety and predictive accuracy of five major international design frameworks, Eurocode 2004, Eurocode 2023, fib Model Code 2010, fib Model Code 2020, and ACI 318, in determining the minimum reinforcement required to prevent brittle fracture in concrete structures. The study systematically maps physical experimental ductility against theoretical code-prescribed reinforcement limits for both conventional lightly reinforced concrete and hybrid fiber-reinforced concrete elements to identify critical disparities between regulatory mathematical models and physical realities.

The analytical methodology leverages an extensive experimental database to assess the transition boundary between brittle fracture and ductile yielding. A critical phase of this investigation involves calculating the theoretical ductility of the codes using the non-dimensional parameter published by Fantilli. By utilizing the relationship between this non-dimensional parameter and the code-prescribed minimum steel areas and fiber volumes, the ultimate predictive capability of each framework is tested against the experimental baseline. Furthermore, the study isolates the influence of specific geometrical and mechanical variables, proving that parameters such as fiber aspect ratio, fiber volume fraction, concrete compressive strength, and longitudinal reinforcement area strictly dictate post-cracking residual strength and directly alter the minimum reinforcement demands calculated by the codes.

The findings demonstrate that for conventional concrete elements lacking fibers, ACI 318 provides the most reliable and mathematically stable framework, whereas the European standards exhibit systemic calculation discrepancies and a pronounced rightward shift that increases the risk of regulatory false positives. The introduction of microscopic steel fibers to create hybrid matrices exposes severe mathematical instabilities within several of the international codes. Specifically, the minimum reinforcement equations in Model Code 2010 and Model Code 2020 frequently calculate physically impossible negative requirements, leading to a complete mathematical breakdown when modeling the non-dimensional structural parameter. Eurocode 2023 avoids negative values but severely overcompensates by mandating excessively high minimum steel areas, failing to optimize the structural benefits of the fibers and forcing material congestion. In contrast, ACI 318 and Eurocode 2004 demonstrate exceptional mathematical stability for hybrid matrices, generating tight, linear interaction domains that seamlessly track the physical brittle-ductile transition and perfectly mimic the shape of the experimental baseline.

Ultimately, the investigation validates the immense structural efficiency gained by transitioning to hybrid fiber-reinforced concrete, proving that precisely calibrated fiber volumes can safely replace significant amounts of macroscopic longitudinal steel while maintaining fully ductile behavior. The study concludes that while ACI 318 and Eurocode 2004 offer accurate predictive models for structural ductility, the theoretical equations governing

minimum reinforcement in the fib Model Codes require urgent recalibration to prevent mathematical anomalies and safely optimize modern engineering applications.

Table of Contents

1 Introduction

Concrete is a widely used construction material that inherently suffers from low tensile strength and brittleness, which traditionally necessitates the use of continuous steel rebars to carry tensile stresses, creating what is known as Reinforced Concrete (RC) [1]. Alternatively, short discontinuous fibers can be randomly dispersed within the cementitious matrix to form Fiber-Reinforced Concrete (FRC), a material designed to improve toughness and provide post-cracking tensile resistance [2]. In the modern design of structural concrete, there is a strong interest in utilizing Hybrid Reinforced Concrete (HRC) [2]. HRC is defined as a composite material where the secondary reinforcing phase consists of both continuous longitudinal steel rebars and short discontinuous fibers randomly dispersed within the matrix [1], [2]. While traditional RC relies solely on continuous steel bars and FRC relies solely on fibers, HRC seeks to leverage the combined benefits of both materials to improve structural performance, enhance serviceability, and reduce the reliance on conventional rebar, particularly in massive concrete members [1], [2], [3]. By leveraging the synergistic interplay between various fiber types, hybrid fiber-reinforced concrete offers a comprehensive enhancement of material properties[4]. This potential has sparked significant global interest, leading to a robust body of literature. A notable contribution by Xu et al. [5] examined the shear resistance of inclined sections in steel fiber-reinforced beams, providing critical perspectives through a comparative analysis of diverse theoretical shear capacity models.

1.1 The Problem of Minimum Reinforcement

The fundamental problem of minimum reinforcement arises from the brittle nature of concrete in tension [2]. In concrete beams subjected to bending, the flexural response up to failure depends heavily on the amount of reinforcement, specifically the steel-bar reinforcement ratio (ρ) and the fiber volume fraction (V_f) [2]. In structural elements containing low amounts of reinforcement, or those with massive cross-sectional areas, the load that produces the first crack (the effective cracking load, P_{cr}^*) can be greater than the ultimate load capacity (P_u) of the reinforcing system [1].

When a lightly reinforced beam cracks under load, the tensile stresses previously carried by the uncracked concrete matrix are abruptly transferred to the reinforcing system [2]. In the post-cracking stage, if the reinforcement is insufficient to bear this transferred load, the system experiences a sudden, catastrophic brittle failure characterized by deflection-softening [1]. Conversely, a ductile failure (deflection-hardening) is guaranteed only when the ultimate load capacity of the cracked beam is greater than or equal to the cracking load ($P_{cr}^* \geq P_u$) [1].

Therefore, a minimum reinforcement area ($A_{s,min}$) must be introduced [1]. The fundamental necessity of this minimum reinforcement is to guarantee a stable post-cracking response, ensuring that the ultimate bending moment is at least equal to the first cracking moment of the reinforced member [1]. In FRC members, a minimum fiber volume fraction ($V_{f,min}$) serves the exact same mechanical purpose, marking the transition from a brittle to a ductile flexural response [1].

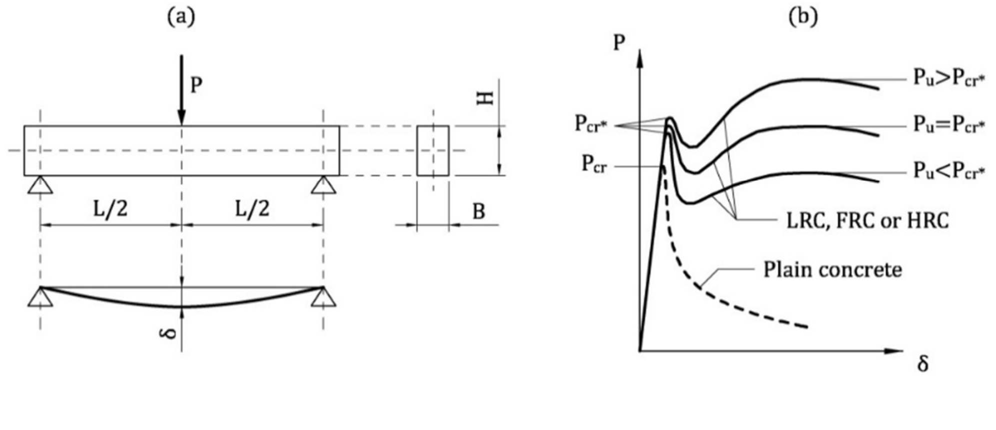

Figure 1.1 Flexural behavior of concrete beam reinforced with rebar and/or fibers: (a) Three-point bending test; (b) applied load (P) vs. midspan deflection (δ) curves in the cases of $(P_{cr}^* \leq P_u)$ brittle response, $(P_{cr}^* = P_u)$ brittle/ductile transition, and $(P_{cr}^* \geq P_u)$ ductile response[6].

1.2 The Need for Minimum Reinforcement

To prevent the sudden and catastrophic collapse immediately following the formation of the first crack, a strictly defined minimum reinforcement area ($A_{s,min}$) must be introduced into the concrete member [1]. The fundamental necessity of this minimum reinforcement is to guarantee a stable post-cracking response, ensuring that the ultimate bending moment capacity is at least equal to the first cracking moment of the reinforced section [2]. In FRC members, a minimum fiber volume fraction ($V_{f,min}$) serves the exact same mechanical purpose, marking the critical transition boundary from a brittle flexural response to a ductile one [1]. Furthermore, providing a minimum amount of reinforcement is essential to ensure adequate crack control under normal serviceability conditions, as it prevents tensile strain from localizing at a single, severely widened crack [3]. Ultimately, by fulfilling both ultimate limit states (preventing sudden brittle failure) and serviceability limit states (controlling crack widths and ensuring immediate post-crack stiffness), the minimum reinforcement acts as a crucial safety threshold in the structural design of concrete beams [1], [3].

1.3 Computation of Minimum Reinforcement

Traditionally, building codes evaluate minimum reinforcement requirements based strictly on the yielding of ordinary steel rebars to fulfill both ultimate and serviceability limit states [1]. However, if the minimum reinforcement of an HRC beam is computed using these conventional LRC building code rules, the structural contribution of the fibers is entirely ignored [1]. This oversight leads to the specification of an uneconomically large amount of steel rebar, effectively rendering the inclusion of fiber-reinforcement useless [1].

To accurately compute the minimum reinforcement in HRC beams, recent methodologies aim to combine the distinct toughening actions of both reinforcing phases.

1.3.1 Scaled Approach[1]

This empirical, multi-scale modeling approach evaluates the brittle/ductile transition by tracking the difference between the ultimate load (P_u) and the cracking load (P_{cr*}) [1]. The condition for minimum reinforcement occurs when the Ductility Index equals zero (DI = 0) [1]. At this threshold, the minimum hybrid reinforcement is computed as a linear combination of the minimum area of rebar ($A_{s,min}$) and the minimum fiber volume fraction ($V_{f,min}$) evaluated from their respective LRC and FRC counterparts [1].

$$DI = \frac{M_u - M_{cr*}}{M_{cr*}} = \frac{P_u - P_{cr*}}{P_{cr*}} \quad (1.1)[1], [6]$$

Building upon this concept, since the ultimate and cracking moments (or loads) depend on the reinforcement amount in Hybrid Reinforced Concrete (HRC) beams, DI is essentially a function of both $A_{s,min}$ and V_f [1]. To quantify this, a non-dimensional reinforcement ratio r, is introduced as the parameter governing the brittle/ductile transition [1], [6]:

$$r = \frac{A_s}{A_{s,min}} + \frac{V_f}{V_{f,min}} \qquad (1.2)[1]$$

Defining r in this manner aligns with the findings of Falkner and Henke (as cited in[1]), who demonstrated that the effects of rebar and fibers in HRC members can be superposed at the ultimate limit state. Consequently, a linear relationship between DI and r is attained. The intersection between this linear function and the horizontal axis (DI = 0) occurs at $r \cong 1$ corresponding to the minimum hybrid reinforcement threshold. This behavior can be described by the following symbolic equation:

$$DI = \zeta \,.\, (r - 1) \qquad (1.3)[1],[6]$$

Where the slope ζ, represents the reinforcement type. The slope is equal to 1 for beams reinforced solely with rebar[7], and ζ= 0.7 for FRC beams, it is used to be equal to 0.8 for HRC beams [8].

Considering LRC and FRC beams as the two limit cases, the values of ζ = 1 and ζ= 0.7 define an envelope that bounds the $DI - r$ relationship for HRC beams, as illustrated in **Fig 1.2** [7], [8].

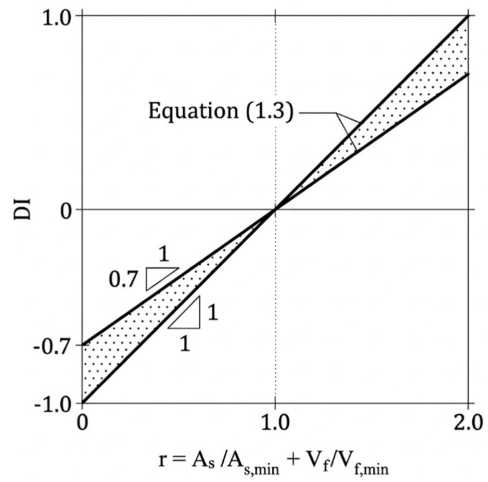

Figure 1.2 Proposed $DI - r$ envelope for HRC beams Eq. (1.3) [1]

From a practical point of view, it is highly useful to analyze all possible reinforcement configurations for Hybrid Reinforced Concrete (HRC) beams to satisfy the threshold requirement of $P_u = P_{cr*}$ (or equivalently, DI = 0). To achieve this condition, it is sufficient to simply impose r = 1 into **Eq 1.2**.[1]

$$\frac{A_s}{A_{s,min}} + \frac{V_f}{V_{f,min}} = 1 \quad (1.4)[1]$$

Consequently, the minimum reinforcement threshold in HRC elements can be achieved through a linear combination of $A_{s,min}$ and $V_{f,min}$ [1].

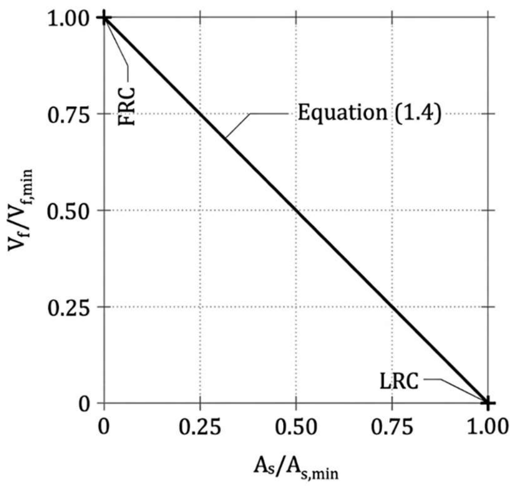

Figure 1.3: The condition of minimum ductility (DI = 0) given by **Eq 1.4**, when rebar and fibers are used to reinforce concrete beams.[1]

The minimum reinforcement thresholds for both LRC and FRC beams are derived using the same design-by-testing framework, expressed through the following relationships[1]:

$$A_{s,min} = \frac{\zeta . A_s}{DI + \zeta} \quad (1.5)[1]$$

$$V_{f,min} = \frac{\zeta . V_f}{DI + \zeta} \quad (1.6)[1]$$

1.3.2 Fracture Mechanics Approach (Updated Bridged Crack Model)[2]:

This approach assumes the cementitious matrix is linear-elastic and perfectly brittle, while applying nonlinear constitutive laws to describe the yielding of steel rebars and the pull-out of short fibers [2]. The required minimum reinforcement is computed using scale-dependent dimensionless numbers: the bar-reinforcement brittleness number (N_p) and the fiber-reinforcement brittleness number ($N_{p,f}$) [2]. The combination of the critical values of these two numbers defines the exact percentages of rebar (ρ_{min}) and fibers ($V_{f,min}$) required to guarantee a stable post-cracking response, explicitly accounting for the scale dependence of the beam [2].

$$N_p = \rho \frac{\sigma_y}{K_{IC}} h^{\frac{1}{2}} \quad (1.7)[2]$$

$$N_{p,f} = V_f \frac{\alpha \sigma_s}{K_{IC}} h^{\frac{1}{2}} = V_f \frac{\overline{\sigma_s}}{K_{IC}} h^{\frac{1}{2}} \quad (1.8)[2]$$

Within the comprehensive framework provided by the Universal Beam Cracking Model (UBCM), the flexural response of HRC beams is governed by two primary dimensionless parameters, known as brittleness numbers[2]:

Bar-reinforcement brittleness number (N_p): As defined in **Eq. (1.7)**, this parameter depends on the steel-bar reinforcement ratio (ρ), the steel yield strength (σ_y), the matrix fracture toughness (K_{IC}), and the beam depth (h)[2].

Fiber-reinforcement brittleness number ($N_{p,f}$): An analogous expression **Eq. (1.8)** is obtained for the fiber phase by substituting the bar-reinforcement parameters (ρ and σ_y) with the fiber volume fraction (V_f) and the equivalent slippage strength of the fibers (σ_s), respectively. It should be noted that σ_s intrinsically accounts for the fiber orientation factor (α)[2].

The minimum reinforcement conditions predicted by the UBCM can be effectively synthesized in a nomograph (Figure1.4). In this diagram, each data point represents a specific combination of the two reinforcement brittleness numbers, N_p and $N_{p,f}$, required to ensure a stable post-peak response in the composite beam.[2]

Analysis of the numerical dataset reveals that, under critical conditions, the relationship between N_p and $N_{p,f}$ can be accurately interpolated using a linear regression. This linear function essentially defines the minimum reinforcement threshold for HRC beams.[2] It acts as a strict boundary line that divides the nomograph into two distinct domains: one representing combinations of N_p and $N_{p,f}$ that yield a stable response, and the other representing an unstable response[2].

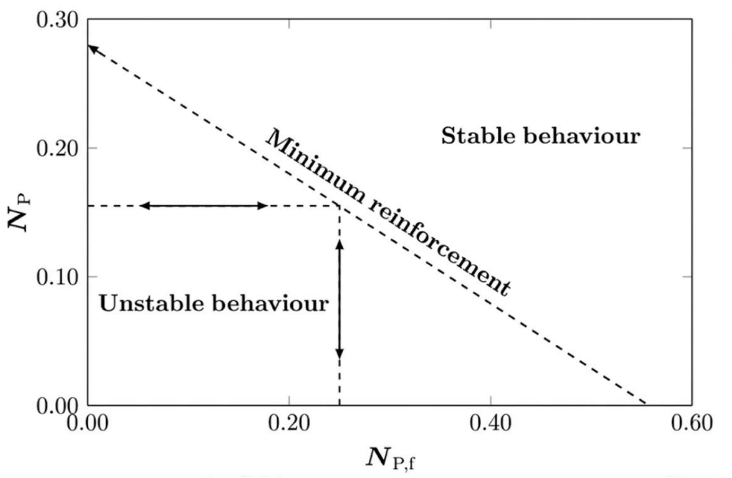

Figure 1.4: Minimum reinforcement design diagram for hybrid-reinforced concrete beams. [2]

From a practical standpoint, for a given value of N_p (which corresponds to a specific steel-bar reinforcement ratio, ρ), this diagram allows for the direct determination of the corresponding $N_{p,f}$ value (representing the required fiber volume fraction, V_f) needed to satisfy the minimum reinforcement condition, and vice versa. Consequently, the nomograph presented in **Fig 1.4** serves as a highly practical quantitative tool for evaluating the exact amount of reinforcing fibers required to partially or entirely replace traditional steel bars in HRC flexural members[2].

1.4 The Effect of Fiber

Cementitious matrices, most notably concrete, are characterized by inherently low tensile strength and a propensity for brittle failure. The integration of short, discontinuous fibers into these matrices significantly augments their mechanical performance, specifically improving fracture toughness, ductility, and energy absorption capacity under dynamic loading. While the past forty years have yielded extensive research into fiber-reinforced concrete (FRC) with a primary focus on steel fiber reinforcement there remains a notable paucity of research concerning the geometric and material design of the fibers themselves. Consequently, many commercially available steel fibers are based on designs established over three decades ago, highlighting a lack of recent innovation in fiber optimization[9]. Investigating the mechanical influence of steel fibers, Yang et al. [10] and Cui et al.[11] established that increased volume fractions and reinforcement ratios not only restrict crack widths but also bolster the horizontal load-bearing capacity of concrete piles. The micro-structural benefits were further highlighted by Sakthipriya et al. [12], who noted that dense, uniform fiber distribution is critical for enhancing both static and dynamic properties. Beyond steel, the effects of synthetic and natural fibers have been widely documented: Wang et al. [13] modeled the shrinkage behavior of polyester fibers, noting a performance threshold for fiber length, while Fu [14] and Zhang [15] demonstrated how basalt, cellulose, and carbon fibers mitigate brittleness and thermal sensitivity in various concrete grades. Furthermore.

1.5 Fiber Mechanics

The characteristic stress-elongation behavior of fiber-reinforced cementitious composites (FRC) reveals two critical mechanical parameters: the first-cracking strength, σ_{cc} and the ultimate post-cracking tensile strength, σ_{pc} **(Fig 1.5)**[9]. The theoretical significance and the constitutive relationship between these properties have been extensively documented in prior literature (Naaman and Reinhardt, 1996; Naaman, 2002)[9]. Whereas σ_{cc} is fundamentally governed by the tensile capacity of the cementitious matrix, the post-cracking performance is dictated exclusively by fiber reinforcement parameters and the interfacial bond mechanisms between the fiber and the matrix[9]. Consequently, the optimization of σ_{pc} is a primary determinant in the structural efficacy and performance enhancement of the composite system.[9]

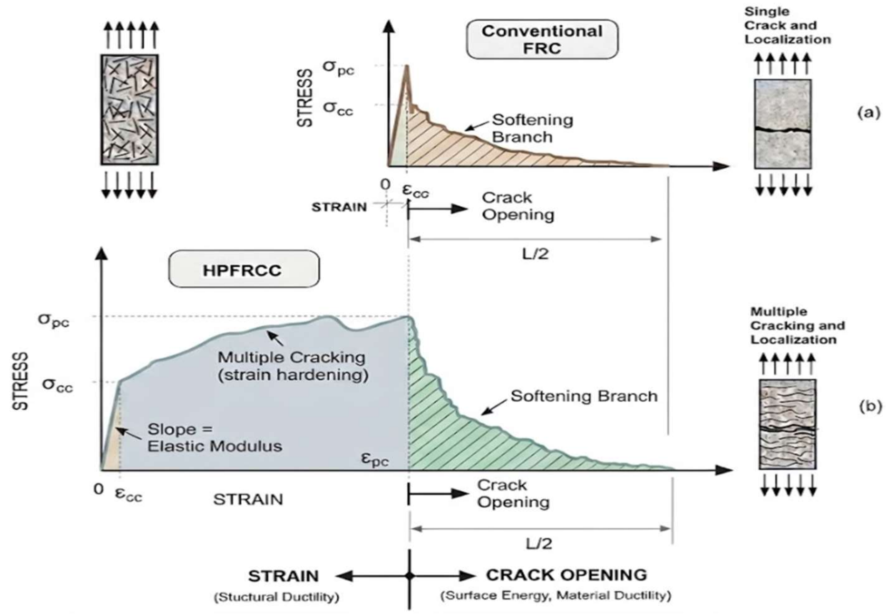

Figure 1.5: tensile stress-strain (σ-ε) response of a fiber-reinforced cementitious composite. (HPFRCC: High Performance Fiber Reinforced Cement Composites)[9]

1.6 Fiber Residual Tensile Strength

The ultimate post-cracking tensile strength of the composite, σ_{pc}, can be obtained from the classical approach, assuming a predominant fiber pull-out failure mechanism, may be analytically estimated using the fundamental governing equation[9]:

$$\sigma_{pc} = \beta \, . V_f \, . \tau_f \, . \frac{l_f}{\Phi_f} \qquad (1.9)\ [9]$$

$$\tau_f = 0.1 \, . \sqrt{f_c} \qquad (1.10)\ [6]$$

in which τ_f the residual bond strength at the fiber-matrix interface[6], V_f is the volume fraction of fibers, l_f is the fiber length, Φ_f is the fiber diameter, $\frac{l_f}{\Phi_f}$ is the aspect ratio, and β is the orientation factor and equal to 0.5 in 3D random fiber orientation.[16]

2 Formulation of Minimum Reinforcement in Building Codes

The evolution of minimum reinforcement philosophy emphasizes a shift from purely preventing brittle collapse to managing post-cracking energy dissipation, a goal shared by Eurocode 2 (EN 1992-1-1:2004), the updated Eurocode 2 (EN 1992-1-1:2023), the fib Model Code 2010, the state-of-the-art fib Model Code 2020, and ACI 318-19. While traditional standards like EC2:2004 and ACI 318-19 primarily focus on conventional steel to ensure the ultimate resisting moment exceeds the cracking moment, the newer EC2:2023 and the fib series have expanded this logic to include the synergistic effects of Hybrid Reinforced Concrete (HRC), which combines macro-synthetic or steel fibers with traditional rebars. The fib Model Code 2010 was a pioneer in standardizing the contribution of fibers to the residual tensile strength of a section, a concept that the fib Model Code 2020 has further matured into a unified design approach where fibers and rebars work in tandem to meet minimum reinforcement requirements. In an HRC system, the fibers act as a bridge across micro-cracks, delaying the localization of macro-cracks and allowing for a reduction in conventional steel area while still maintaining the ductile failure mechanism mandated by these global codes. By integrating these materials, the latest versions of the Eurocode and the fib Model Codes recognize that the "minimum reinforcement" is no longer just a bar count but a performance-based metric where the combined toughness of the fiber-matrix and the yield capacity of the longitudinal steel ensure that any cracking is distributed and controlled. This transition towards HRC in modern standards reflects a more sophisticated understanding of material science, ensuring that even if the concrete matrix fails, the combined internal resistance of fibers and bars prevents the catastrophic, "snap-through" failure that these codes were originally written to avoid.

2.1 Eurocode 2 (EN1992-1-1:2004)

The traditional Eurocode 2 framework addresses minimum longitudinal tension reinforcement primarily to mitigate the risk of brittle failure and control crack widths. For standard RC beams, Section 9.2.1.1 [17]dictates that the area of longitudinal tension reinforcement, $A_{s,min}$, must not fall below a prescribed threshold relative to the mean width of the tension zone (b_t) and the effective depth (d)[17].

The recommended formulation is given as:

$$A_{s,min} = 0.26\left(\frac{f_{ctm}}{f_{yk}}\right)b_t d \geq 0.0013 b_t d \qquad (2.1)\ [17]$$

Where f_{ctm} represents the mean tensile strength of the concrete class (table 3.1in EN 1992-1-1:2004 [17]), and f_{yk} is the characteristic yield strength of the reinforcement. The values are provided in **Table 2.2**.

$$f_{ctm} = \begin{cases} 0.30 \, . \, f_{ck}^{\frac{2}{3}} & for\ concrete\ classes\ \leq C50/60 \\ 2.12 \, . \ln\left(1 + \frac{f_{cm}}{10}\right) & for\ concrete\ classes > C50/60 \end{cases} \qquad (2.2)\ [17]$$

$$f_{cm} = f_{ck} + 8 \qquad (2.3)\ [17]$$

2.2 Eurocode 2 (EN 1992-1-1:2023)

For conventionally reinforced concrete beams without the inclusion of steel fibers, the minimum longitudinal reinforcement provisions fundamentally follow the legacy framework established in Eurocode 2 (EN 1992-1-1:2004), incorporating the updated mean compressive strength formulation as defined in **Eq. (2.6)**.

The updated Eurocode 2 (EN 1992-1-1:2023) adopts a more generalized, performance-based approach to minimum reinforcement. According to Section 12.2 of Eurocode 2 EN 1992-1-1:2023 [18] the primary objectives of providing $A_{s,min}$ are to ensure distributed cracking, provide sufficient deformation capacity for structural robustness, and avoid sudden, brittle failures resulting from unpredicted cracking.

While the generalized fundamental requirement dictates that a section's nominal moment resistance must at least equal the cracking moment, the code provides specific simplified formulations based on the state of stress. For members evaluated under pure tension models, the required minimum reinforcement is directly proportional to the gross concrete area and the material strengths, calculated as:

$$A_{s,min} = A_c \, . \, \frac{f_{ctm}}{f_{yk}} \qquad (2.4)[18]$$

where:

A_c is the total area of the concrete cross-section.

f_{ctm} is the mean tensile strength of the concrete, which defines the stress at which the concrete will initially crack.

f_{yk} is the characteristic yield strength of the reinforcing steel, representing the capacity of the reinforcement to bridge the crack and maintain structural integrity.

By satisfying this condition, the design ensures that upon the formation of the first crack, the reinforcement possesses adequate capacity to absorb the tensile forces previously carried by the uncracked concrete without immediately yielding.

Based on the provisions of Eurocode 2 (EN 1992-1-1:2023. Table 5.1 [18]), both the 28-day mean compressive strength, f_{cm} , and the mean tensile strength of concrete, f_{ctm} , can be derived from its characteristic compressive strength, f_{ck} (expressed in MPa), utilizing the empirical relationships below:

$$f_{ctm} = \begin{cases} 0.30 \,.\, f_{ck}^{\frac{2}{3}} & for\ concrete\ classes\ \leq 50\ MPa \\ 1.1 \,.\, f_{ck}^{\frac{1}{3}} & for\ concrete\ classes > 50\ MPa \end{cases} \quad (2.5)[18]$$

$$f_{cm} = f_{ck} + 8\ MPa \quad (2.6)[6], [18], [19]$$

Table 2.1 presents the mean tensile strength (f_{ctm}) values for standard compressive strength classes, extracted directly from Eurocode 2 (EN 1992-1-1:2023, Table 5.1 [18]) to streamline structural evaluation and design procedures.

Furthermore, the Eurocode 2 (EN 1992-1-1:2023) states that the lower, $f_{ctk,0.05}$, and upper bound, $f_{ctk,0.95}$, values for the characteristic tensile strength are estimated at 0.7 and 1.3 of the mean tensile strength, f_{ctm}, respectively, and 5% and 95% fractile [16], [17], [18].

Table 2.1: Mean tensile strength (f_{ctm}) for standard concrete compressive strength classes (f_c), as provided by Eurocode 2 (EN 1992-1-1:2023).

f_{ck} (Mpa)	f_{cm} (Mpa)	$f_{ctk,0.05}$ (Mpa)	$f_{ctk,0.95}$ (Mpa)	f_{ctm} (Mpa)
12	20	1.1	2.0	1.6
16	24	1.3	2.5	1.9
20	28	1.5	2.9	2.2
25	33	1.8	3.3	2.6
30	38	2.0	3.8	2.9
35	43	2.2	4.2	3.2
40	48	2.5	4.6	3.5
45	53	2.7	4.9	3.8
50	58	2.9	5.3	4.1
55	63	3.0	5.4	4.2
60	68	3.1	5.6	4.3
70	78	3.2	5.9	4.5
80	88	3.3	6.2	4.7
90	98	3.5	6.4	4.9

2.2.1 Application to HRC Beams (Annex L[18])

The new Eurocode explicitly incorporates fiber-reinforced concrete into this framework. Section L.12. (EN 1992-1-1:2023) [18] applies the same foundational inequality but modifies the calculation of the resisting moment. In this context, $M_{R,min}$ is defined as the bending strength of the section containing $A_{s,min}$, calculated by explicitly including the tensile contribution of the fibers. Section L.12.2.1(EN 1992-1-1:2023)[18] also applies a restrictive rule which the minimum longitudinal reinforcement in beams should not be replaced by steel fibers[18].

2.3 Fib Model Code 2010

The 2010 fib Model Code addresses the minimum reinforcement required specifically for crack control in flexural elements. To control cracking elements under bending, a minimum area of reinforcement ($A_{s,min}$) must be provided to balance the tensile stresses just before cracking, while explicitly accounting for the residual tensile strength provided by fiber reinforcement. (According to Section 7.7.4.3 [19]),

The required minimum reinforcement is calculated as:

$$A_{s,min} = k_c \, . \, k \, . \, (f_{ctm} - f_{Ftsm}) \frac{A_{ct}}{\sigma_s} \tag{2.7)[19}$$

Where:

f_{ctm}: is the average value of the tensile strength of the concrete matrix.

f_{Ftsm}: is the average value of the residual tensile strength of the fibers.

A_{ct}: is the tensile part of the concrete cross-section, evaluated by considering a stress field at the elastic limit.

σ_s: is the maximum allowable tensile stress in the reinforcement at the cracking stage, which can be taken as equal to the yield stress of the steel.

k_c: is a coefficient that accounts for the stress distribution in the cross-section just before cracking and the change in the inner lever arm (taken as k_c = 1 for rectangular cross-sections).

k: is a coefficient accounting for non-uniform self-equilibrating stresses, which lead to a reduction of the cracking force.

According to Eurocode 2 (EN 1992-1-1:2004 [17]) and Model Code 2010 (section 7.2.3[19]), mean value of compressive strength f_c at an age of 28 days, f_{cm}, and the mean tensile strength of concrete, f_{ctm}, can be estimated from the characteristic compressive strength, f_{ck} (expressed in MPa), using the **Eq. 2.2** and **Eq. 2.3** [6], [17], [19].

To facilitate practical design and evaluation, the corresponding values for the mean tensile strength, evaluated at various standard compressive strength classes by Eurocode 2 (EN 1992-1-1:2004 in the table 3.1[17]) and fib Model Code 2010, (in the table 7.2.1[19]) are summarized in **Table 2.2**:

Table 2.2: Mean tensile strength (f_{ctm}) for standard concrete compressive strength classes (f_c), as provided by the fib Model Code 2010.

f_{ck} (Mpa)	f_{cm} (Mpa)	$f_{ctk,0.05}$ (Mpa)	$f_{ctk,0.95}$ (Mpa)	f_{ctm} (Mpa)
12	20	1.1	2.0	1.6
16	24	1.3	2.5	1.9
20	28	1.5	2.9	2.2
25	33	1.8	3.3	2.6
30	38	2.0	3.8	2.9
35	43	2.2	4.2	3.2
40	48	2.5	4.6	3.5
45	53	2.7	4.9	3.8
50	58	2.9	5.3	4.1
55	63	3.0	5.5	4.2
60	68	3.1	5.7	4.4
70	78	3.2	6.0	4.6
80	88	3.4	6.3	4.8
90	98	3.5	6.6	5.0

Crucially, the code states that if the calculated $A_{s,min}$ is negative, it indicates that the minimum reinforcement requirements can be satisfied entirely by the fiber reinforcement without the need for conventional steel bars.[19]

2.4 Fib Model Code 2020

The fib Model Code 2020 aligns closely with the updated Eurocode 2 philosophy regarding the fundamental requirement that $M_{R,min} \geq M_{cr}$ [16], [18]. Section 30.13.6.2[16] outlines the ductility behavior of cross-sections in HRC structures, emphasizing that minimum reinforcement must ensure the applicability of limit design models and constructability.

To control the crack width in the HRC beams subjected to bending, the Model Code prescribes minimum reinforcement area formulation equal to the fib Model 2010, **Eq. (2.7),** also it has been mentioned directly in fib Model 2020 that the coefficient of non-uniform self-equilibration stresses (k) which leads to reduce in crack force is based on the web and flange dimensions.

where:

$$k = \begin{cases} 1 & for\ webs\ with\ h \leq 300mm\ or\ flanges\ with\ width \leq 300mm \\ 0.65 & for\ webs\ with\ h \geq 800mm\ or\ flanges\ with\ width \geq 800mm \end{cases} \quad (2.8)\ [16]$$

By interpolation for intermediate values, k can be obtained.

For elements acting as components within reinforced concrete systems, a baseline amount of reinforcement, $A_{s,min}$ is mandatory to achieve several structural objectives:

Promote an even distribution of cracks and accommodate internal forces arising from restricted movements that were not directly accounted for during the structural analysis.

Guarantee adequate ductility, which enhances the overall resilience of the structure by enabling the redistribution of loads through secondary load paths.

Preventing sudden or brittle collapse triggered by unexpected crack formation.

Validate the underlying assumptions required for applying limit state design methodologies.

Facilitate practical execution and constructability on site.

According to model code 2020 (section 14.6.1.2 [16]), the mean tensile strength of concrete, can be estimated from the characteristic compressive strength, using the following empirical relationships:[16]

$$f_{ctm} = 1.8\ .\ln(f_{ck}) - 3.1 \quad (2.9)[16]$$

Furthermore, the fib Model Code 2020 states that the lower, $f_{ctk,min}$, and upper bound, $f_{ctk,max}$, values for the characteristic tensile strength are estimated at 70% and 130% of the mean tensile strength, f_{ctm}, corresponding to the 5% and 95% fractiles, respectively [16],[17].

To assist with practical design and evaluation, **Table 2.3** summarizes the mean tensile strength values for standard compressive strength classes, as originally detailed in Table 14.6.3 of the fib Model Code 2020 [16]:

Table 2.3: Mean tensile strength (f_{ctm}) for standard concrete compressive strength classes (f_c), as provided by the fib Model Code 2020.

f_{ck} (Mpa)	$f_{ctk,min}$ (Mpa)	$f_{ctk,max}$ (Mpa)	f_{ctm} (Mpa)
12	1.0	1.8	1.4
16	1.3	2.5	1.9
20	1.6	2.9	2.3
25	1.9	3.0	2.7
30	2.1	3.5	3.0
35	2.3	3.9	3.3
40	2.5	4.3	3.5
45	2.6	4.9	3.8
50	2.8	5.1	3.9
55	2.9	5.3	4.1
60	3.0	5.6	4.3
70	3.2	5.9	4.5
80	3.4	6.2	4.8
90	3.5	6.5	5.0

2.5 ACI 318-19

The American Concrete Institute standard approach focuses exclusively on traditional RC non-prestressed beams. Section 9.6.1[20] mandates that a minimum area of flexural reinforcement must be provided at every section where tension reinforcement is required by analysis.

The required area is determined as the larger of two empirical formulations, limited by a maximum yield strength (f_y) of 80,000 psi[20]:

$$A_{s,min} = max\left[\left(\frac{3\sqrt{f'_c}}{f_y}b_w d\,,\left(\frac{200}{f_y}\right)b_w d\right)\right] \qquad (2.10)\ [20]$$

Where f'_c is the specified compressive strength of concrete (Pounds per Square Inch), and b_w is the web width (Inch). ACI 318 includes a notable exception (Section 9.6.1.3 [20]): the minimum reinforcement requirements need not be satisfied if the area of steel provided at every section is at least one-third greater than the amount required by standard structural analysis.[20]

3 Application of Code Rules and Standards

The transition from the theoretical regulatory frameworks established in the previous chapter to the quantitative assessment of structural safety requires a strictly defined analytical methodology. While international building codes provide generalized boundary conditions intended to prevent brittle failure, applying these rigid mathematical formulas to complex, real-world structural elements necessitate a systematic and standardized approach.

The primary objective of this chapter is to bridge the gap between pure code philosophy and practical engineering analysis. This involves translating the abstract minimum reinforcement provisions into measurable, comparative performance metrics. By establishing a uniform set of analytical assumptions, such as the governing limit states, idealized stress blocks, and fracture mechanics models, the inherent safety margins embedded within the divergent global standards can be evaluated on an equal footing.

To achieve this, the subsequent sections outline the sequential execution of this analytical procedure. The methodology begins with the curation of an appropriate experimental testbed to serve as the baseline for calculation. It then proceeds to define the boundary conditions and extract the governing mechanical parameters, ultimately detailing the precise mathematical execution of the code rules required to quantify the true structural ductility of the elements**.**

3.1 Selection of Experimental Beams

To practically apply and evaluate the minimum reinforcement building code formulations detailed in Part 2, a comprehensive dataset of experimental beams has been selected from the existing literature.

To ensure a rigorous, balanced, and statistically significant evaluation across all material configurations relevant to this study, the selected beams are evenly categorized into two distinct reinforcement strategies: 86 of Lightly Reinforced Concrete (LRC) specimens, and 108 of Hybrid Reinforced Concrete (HRC) specimens. This parametric diversity captures structural behaviors at, below, and above the critical minimum reinforcement thresholds across varying concrete strengths and geometrical scales. The design of reinforced concrete (RC) flexural members is mainly based on the consideration of strength and ductility[21]. By organizing the experimental database into these two distinct LRC and HRC categories, this study is perfectly positioned to track how different international building codes manage that delicate balance across the critical minimum reinforcement threshold.

3.2 Geometric and Material Properties of the Selected Beams

To systematically apply the analytical minimum reinforcement formulations prescribed by the Eurocode, fib Model Code, and ACI 318, the specific geometric dimensions and material characteristics of each selected specimen must be defined. Based on the available experimental data, all structural parameters and inverted calculations utilized for these specific specimens are thoroughly documented in **Appendix A and B**. To systematically apply the analytical minimum reinforcement formulations prescribed by the Eurocode, fib Model Code, and ACI 318, the complete structural parameters of each selected specimen must be distinctly defined. The variables required for these theoretical verifications include the cross-sectional width (B), overall depth (H), concrete compressive strength (f_c), mean concrete tensile strength (f_{ctm}), yield strength of conventional steel (f_y), provided area of longitudinal tension steel (A_s), and the steel fiber volume fraction (V_f) or dosage. The effective depth, (d) can be reasonably assumed to be 0.8.H for the beams [6].

3.3 Analytical Scenarios and Evaluation Procedures

To systematically assess the structural safety and required reinforcement across the selected database, the analytical procedure was divided into specific evaluation scenarios. These scenarios isolate the mechanical variables for the Lightly Reinforced Concrete (LRC) and Hybrid Reinforced Concrete (HRC) specimens, allowing for a direct comparison between the empirical building codes and the unified theoretical framework proposed by Fantilli et al.[1]

3.3.1 Evaluation of Lightly Reinforced Concrete (LRC)

For the LRC specimens, the baseline experimental Ductility Index (DI) and its corresponding non-dimensional reinforcement ratio (r) were established using the reference data from Fantilli et al[1]. To evaluate the regulatory frameworks, the absolute minimum reinforcement area ($A_{s,min}$) was calculated for each beam using the equations provided by the five international building codes.

Using these newly calculated $A_{s,min}$ values, the reinforcement ratio (r) was recalculated utilizing **Eq. (1.2)**. The primary objective of this scenario is to conduct a direct comparison between the code-prescribed $A_{s,min}$ requirements, the theoretical $A_{s,min}$ proposed by Fantilli et al[1], and the divergence in their resulting non-dimensional (r) values.

3.3.2 Scenarios for Hybrid Reinforced Concrete (HRC)

To systematically assess the structural performance and material optimization of the Hybrid Reinforced Concrete (HRC) dataset, the analytical procedure was divided into three distinct scenarios. These pathways evaluate the intersection of code-mandated reinforcement limits, experimental ductility, and theoretical fiber volume requirements.

Scenario 1: Evaluation of Code-Mandated Minimum Steel and Resulting Ductility

The primary objective of this scenario is to quantify how the absolute minimum reinforcement areas dictated by international building codes influence the overall post-cracking ductility of the HRC elements. The procedure begins by calculating the updated non-dimensional reinforcement ratio (r) utilizing **Eq. (1.2)**. Subsequently, this updated ratio is substituted into **Eq. (1.3)** to compute the corresponding theoretical Ductility Index (DI). To evaluate the safety margins and efficiency of the empirical code provisions, two direct comparative analyses are conducted: the code-prescribed minimum steel area ($A_{s,min}$) is evaluated against the experimental minimum steel area, and the resulting theoretical Ductility Index is compared directly with the documented experimental Ductility Index.

Scenario 2: Back-Calculation of Minimum Fiber Volume for Target Ductility

In the second scenario, the analytical framework is inverted to determine the specific fiber volume fraction necessary to achieve an experimentally validated ductility threshold. The methodology initiates by establishing the required non-dimensional reinforcement ratio (r) utilizing **Eq. (1.3)**, strictly adopting the baseline experimental Ductility Index (DI) established in Fantilli's unified approach introduced in **Eq. (1.1)**. Once this target ratio is defined, it is integrated into **Eq. (1.2)** to back-calculate the newly required minimum fiber volume fraction ($V_{f,min}$). The scenario concludes with a critical comparison between the baseline minimum fiber volume proposed by Fantilli and the newly derived composite fiber requirement.

Scenario 3: Ultimate Limit State Evaluation for Fiber Volume Optimization

The final scenario establishes a theoretical boundary condition by evaluating the requisite fiber volume under strict ultimate limit state assumptions, specifically at the exact transition point between ductile and brittle failure. In this phase, a revised minimum fiber volume fraction is determined utilizing **Eq. (1.4)** under the governing conditions that the Ductility Index equals zero and the non-dimensional reinforcement ratio equals one. Following this calculation, a comparative assessment is performed to observe how the theoretical minimum fiber volume fluctuates when derived through the target-ductility methodology of Scenario 2 versus the strict limit-state boundaries imposed in Scenario 3.

4 Analysis of Results and Discussion

This chapter presents the quantitative evaluation of the minimum reinforcement provisions across the selected experimental database. Applying the analytical scenarios. The structural performance of the 194 selected beams was evaluated against the rigid boundary conditions of five international building codes: Eurocode 2004, Eurocode 2023, fib Model Code 2010, fib Model Code 2020, and ACI 318.

The primary objective of this phase is to move beyond the theoretical equations and explicitly measure the actual post-cracking safety margins provided by these global standards. By normalizing the code-prescribed reinforcement areas ($A_{s,min}$) into the non-dimensional reinforcement ratio (r) and calculating the corresponding Ductility Index (DI), the potential vulnerability of each code is exposed.

To provide a clear comparative analysis, the findings are separated into two primary categories. Section 4.1 details the baseline mechanical behavior of the Lightly Reinforced Concrete (LRC) elements under purely conventional steel reinforcement. Section 4.2 subsequently explores the Hybrid Reinforced Concrete (HRC) elements, evaluating how the introduction of steel fibers alters the requisite reinforcement thresholds and structural ductility.

4.1.1 Evaluation of Minimum Reinforcement Areas ($A_{s,min}$) for LRC

An analytical comparison between the theoretically prescribed minimum longitudinal reinforcement areas and the experimentally validated baselines indicates a substantial, non-linear divergence among international regulatory frameworks. To facilitate a comprehensive evaluation of this Lightly Reinforced Concrete (LRC) scenario, ten representative specimens were systematically selected from the extensive experimental database. The theoretical minimum reinforcement provisions dictated by five prominent design standards, Eurocode 2004, Eurocode 2023, the *fib* Model Code 2010, the *fib* Model Code 2020, and ACI 318, are visually juxtaposed against the physical experimental baselines in the subsequent graphical representations. It must be noted that all underlying numerical calculations and corresponding structural parameters utilized to generate these comparative models are comprehensively detailed in **Table 3** in **Appendix A**.

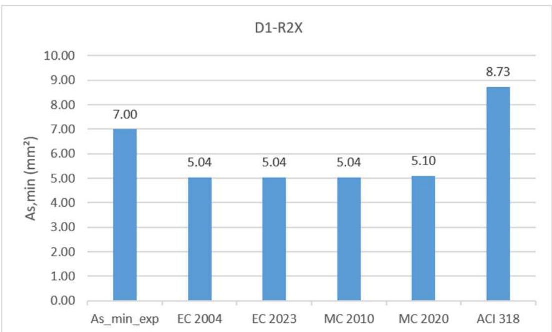

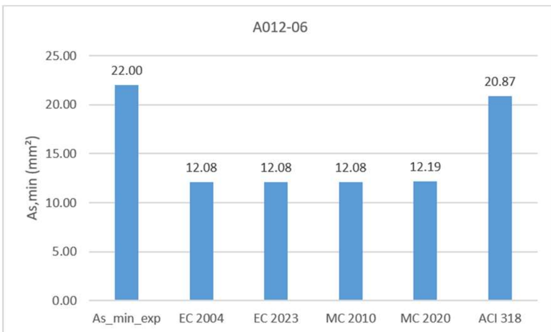

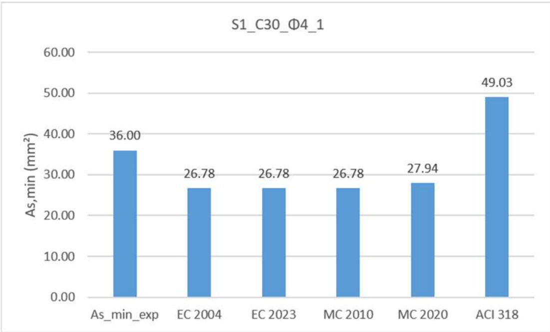

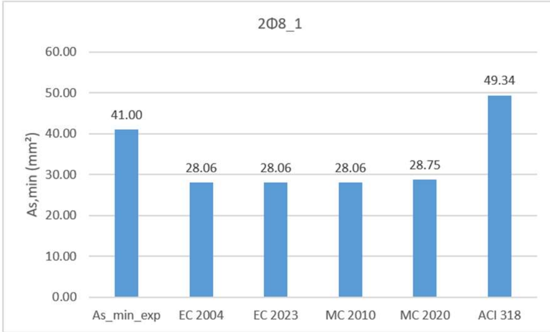

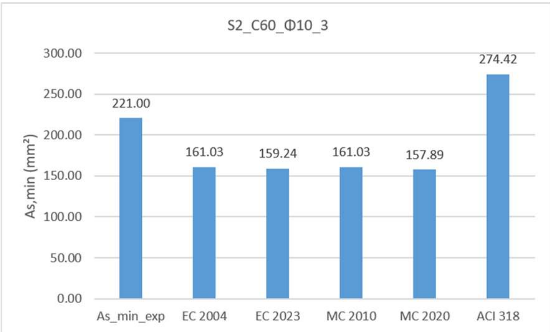

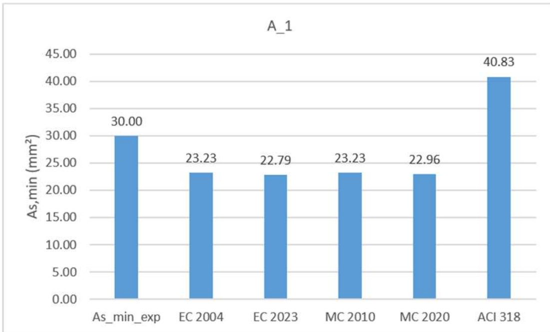

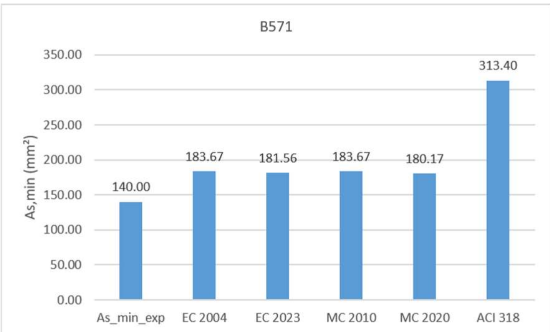

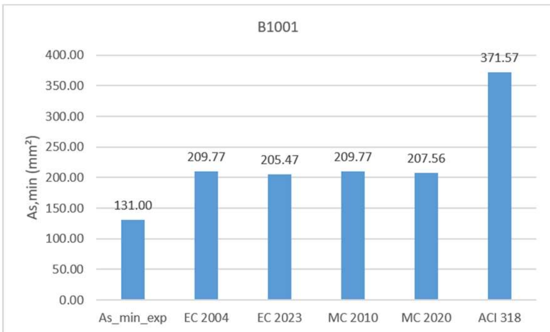

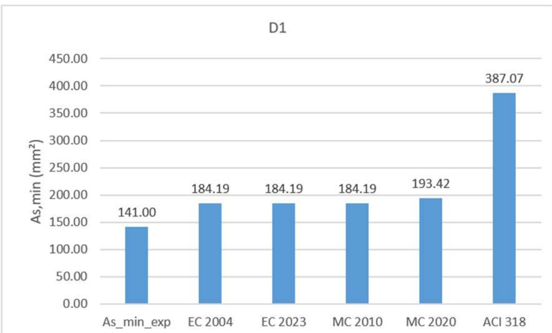

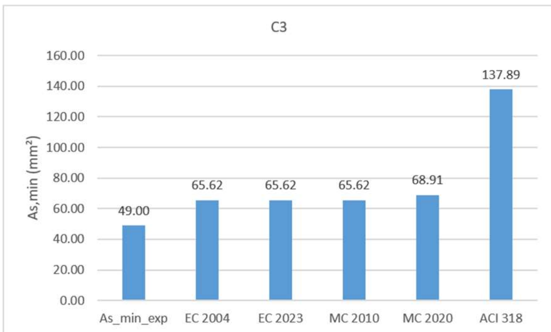

The graphical evidence presented in the preceding diagrams demonstrates that the discrepancies among these design codes do not scale uniformly; rather, they are distinctly influenced by the geometrical limits of the cross-section and the concrete compressive strength. When the physical geometry of an element is highly restricted, the mathematical divergence between opposing code philosophies is naturally suppressed. In micro-elements, the gross

cross-sectional area is small enough that differing theoretical multiplier effects yield negligible physical discrepancies. For example, in Sample D1-R2X, the experimental baseline dictates a safe minimum reinforcement area of 7.00mm². Consequently, the European code provisions remain tightly clustered around 5.04mm² to 5.10mm², while ACI318 dictates a marginal increase to 8.73mm². A similarly scaled specimen, Sample A012-06, requires 22.00mm² experimentally, with the European frameworks uniformly predicting approximately 12.00mm² and ACI 318 prescribing 20.87mm². In such minimal applications, a clear consensus emerges where the disagreement between code provisions exerts almost zero physical or economic impact on constructability.
However, as structural scale increases into standard control geometries, the European frameworks, including both the legacy Eurocode 2004 and the updated Eurocode 2023, begin to systematically under-predict the required yield force. This exposes specific elements to a dangerous under-reinforcement trap. For a standard baseline element like Sample S1_C30_Φ4_1, the experimental physical requirement is 36.00mm², yet the European frameworks strictly mandate between 26.78mm² and 27.94mm². This under prediction becomes physically hazardous in elements like Sample 2Φ8_1, where physical experimentation dictates an area of 41.00mm² to bridge the primary flexural crack safely, but the European consensus demands merely 28.06mm² to 28.75mm². A beam detailed strictly to these European standards is theoretically assumed safe but physically lacks the tensile capacity to prevent brittle failure. Conversely, ACI 318 dictates 49.34mm² for the same specimen, effectively securing the structural limit state through a more conservative empirical approach.

This dangerous discrepancy within the European codes scales aggressively in the presence of High Strength Concrete (HSC). As observed in Sample S2_C60_Φ10_3, against an experimental necessity of 221.00mm², Eurocode 2004, Eurocode 2023, and the *fib* Model Codes limit the longitudinal steel to a severely deficient range of 157.89mm² to 161.03mm². This proves that the fundamental tension-zone models utilized across these European standards critically destabilize in higher-strength matrices. In these high-strength applications, ACI 318 consistently operates as a highly conservative upper bound. For Sample A_1, against an experimental baseline of 30.00mm², the European codes prescribe approximately 23.00mm², whereas ACI318 enforces an empirical demand of 40.83mm², ensuring ductility at the cost of material efficiency.

Ultimately, as the uncracked gross area of the concrete expands macroscopically, ACI318 begins to mathematically over-penalize the cross-section, leading to severe reinforcement congestion. This extreme geometrical penalty is best illustrated by Sample B1001, an Ultra High Strength Concrete specimen requiring 131.00mm² experimentally. While the European codes cluster closely around 205.00mm² to 209.00mm², ACI 318 demands an economically unviable 371.57mm². This penalty is strictly geometrical, as proven by the normal-strength, deep-beam Sample D1; against a baseline of 141.00 mm², the European codes reasonably predict between 184.19mm² and 193.42mm², whereas the sheer height of the element causes the ACI 318 formula to spike to 387.07mm². This step-by-step graphical divergence confirms that conventional design codes fail to uniformly balance post-cracking ductility and material efficiency, fluctuating between dangerous inadequacy in the European frameworks and severe material congestion in ACI 318.

4.1.2 Ductility and Safety Margin Divergence (DI) for LRC

Following the comparative evaluation of the absolute minimum reinforcement areas, it is critical to quantify how these code-prescribed theoretical limits influence the structural safety margins and post-cracking ductility of the Lightly Reinforced Concrete (LRC) elements. By integrating the mandated reinforcement provisions into the non-dimensional framework, the theoretical Ductility Index (DI) can be calculated and juxtaposed against the experimentally validated baselines. The following graphical representations illustrate the fundamental divergence in ductility expectations dictated by Eurocode 2004, Eurocode 2023, the *fib* Model Codes, and ACI 318. All corresponding structural parameters and index calculations are comprehensively detailed in **Table 5** in **Appendix A.**

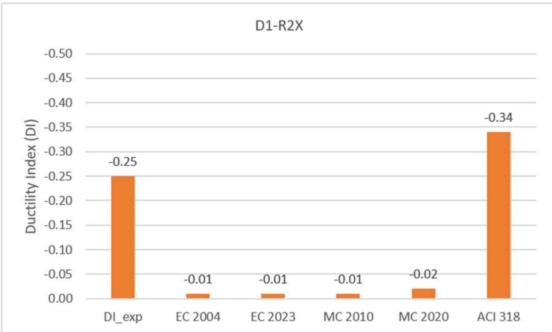

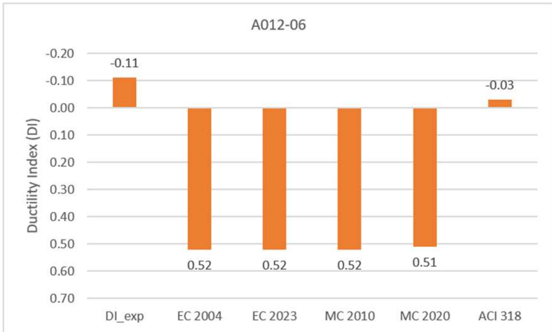

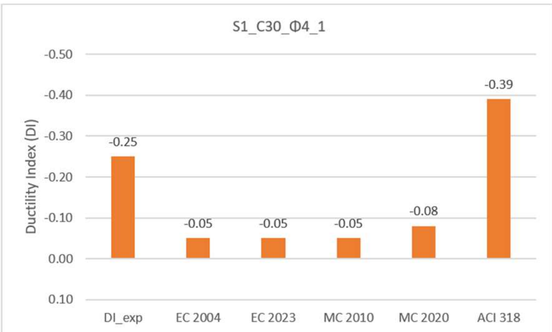

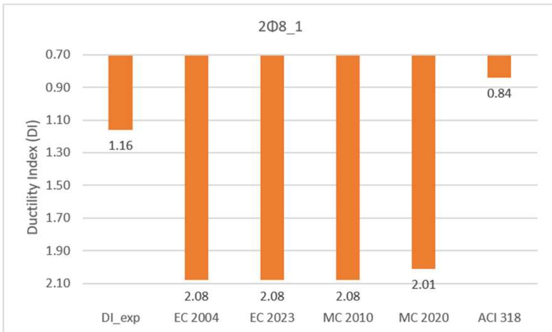

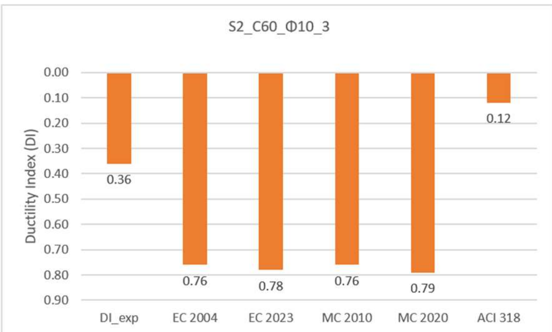

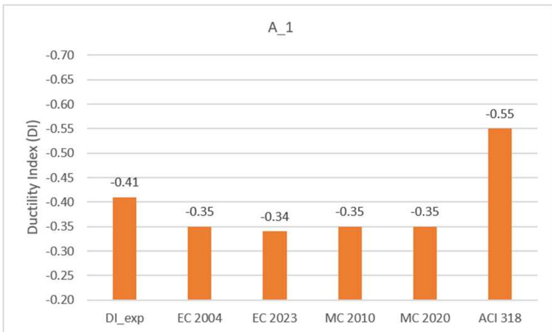

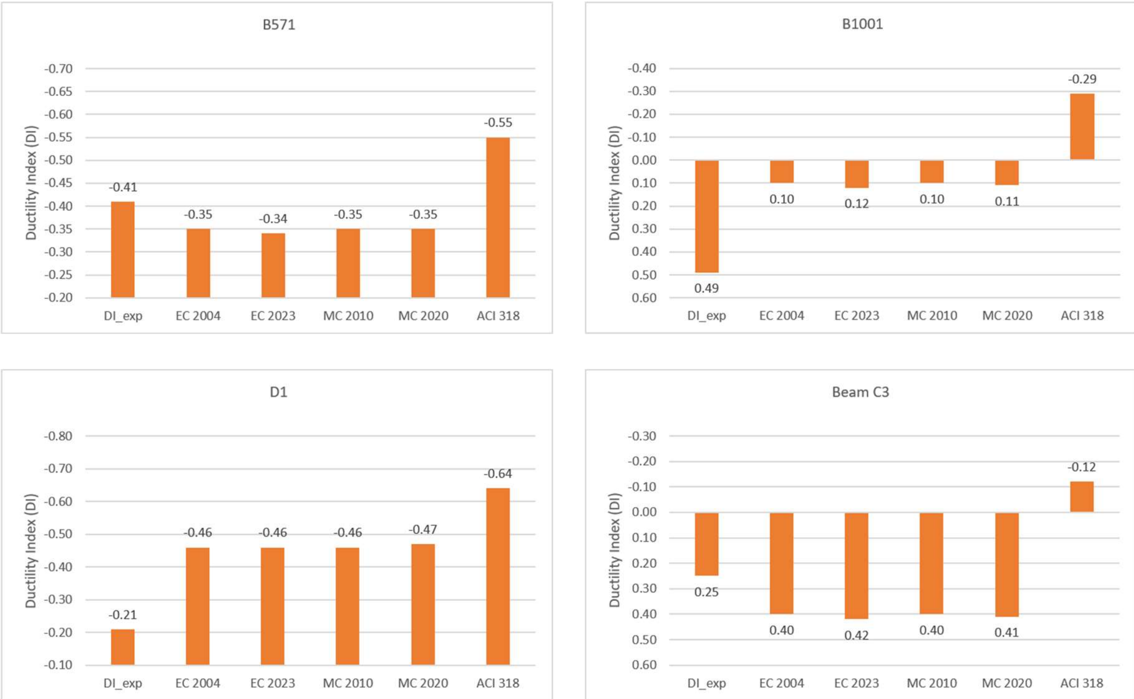

The analytical evaluation of the Ductility Index (DI) reveals that the discrepancies in minimum reinforcement areas propagate aggressively into the theoretical safety margins of the elements. In micro-elements where the geometrical variations are restricted, the resulting ductility indices exhibit minor but distinct analytical shifts. For example, in Sample D1-R2X, the experimental baseline establishes a DI of -0.25. While the European provisions converge near a theoretical DI of -0.01, ACI 318 forces a ductility shift to -0.34, demonstrating that even in consensus geometries, the mathematical safety margins do not perfectly align. This behavior is similarly reflected in Sample A012-06, where the baseline DI of -0.11 contrasts sharply with the European consensus of 0.52 and the ACI 318 prediction of -0.03.
The divergence becomes structurally critical in standard control geometries and high-strength matrices, directly mirroring the under-reinforcement trap identified in the previous section. In Sample 2Φ8_1, the experimental ductility dictates a DI of 1.16 to safely bridge primary flexural cracking. However, because the legacy European frameworks severely under-predict the required longitudinal steel, the corresponding theoretical DI spikes artificially to a highly divergent 2.08. ACI 318, utilizing its conservative empirical approach, maintains a DI of 0.84, remaining much closer to the physical reality. This severe ductility distortion within the European codes is further exacerbated in the high-strength Sample S2_C60_Φ10_3. Against an experimental baseline DI of 0.36, the European codes yield a structurally deficient range between 0.76 and 0.79, while ACI 318 provides a conservative index of 0.12.

Conversely, the extreme geometrical and material penalties imposed by ACI 318 in macroscopic and Ultra-High-Strength Concrete (UHSC) elements result in the complete suppression of ideal ductility. This is most prominently demonstrated by the UHSC Sample B1001. The experimental baseline establishes a functioning DI of 0.49. While the European codes estimate a closely clustered DI range of 0.10 to 0.12, the massive reinforcement congestion mandated by ACI 318 forces the Ductility Index into a negative state of -0.29. This trend is corroborated by the macroscopic Sample C3, where the baseline DI is 0.25, the European consensus averages around 0.41, and ACI 318 drops entirely to -0.12. Ultimately, this graphical data confirms that the standard international codes fail to provide a unified, scale-independent safety margin, forcing structural elements to fluctuate between theoretical brittleness in the European frameworks and severe over-reinforcement congestion under ACI 318.

4.2.1 Evaluation of Minimum Reinforcement Areas ($A_{s,min}$) for HRC

To systematically assess the structural performance and material optimization of the Hybrid Fiber-Reinforced Concrete (HRC) dataset, the analytical procedure is divided into distinct methodological phases. The primary objective of this initial phase is to quantify how the absolute minimum longitudinal reinforcement areas ($A_{s,min}$) prescribed by standard international building codes influence the overall post-cracking ductility of the HRC elements.

By calculating the updated non-dimensional reinforcement ratio (r) and integrating it into the established theoretical framework, the corresponding theoretical Ductility Index (DI) is computed for each design standard, Eurocode 2004, Eurocode 2023, the *fib* Model Code 2010, the *fib* Model Code 2020, and ACI 318. To rigorously evaluate the safety margins and the efficiency of the empirical code provisions when fibers are introduced, these theoretical indices are compared directly against the documented experimental Ductility Index of each specimen. All foundational numerical calculations and structural parameters utilized for these HRC elements are comprehensively detailed in **Table 8** in **Appendix B.**

The subsequent graphical representations illustrate this comparative evaluation across the selected representative HRC specimens:

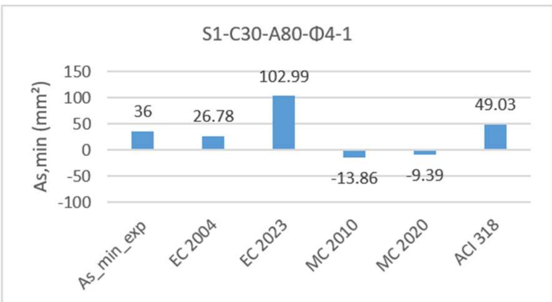

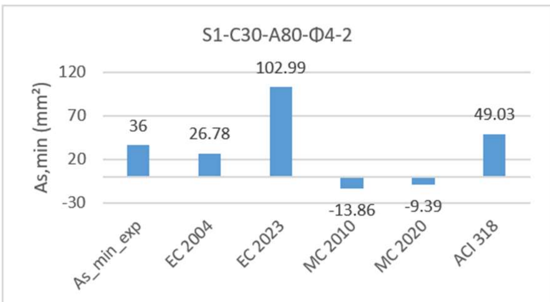

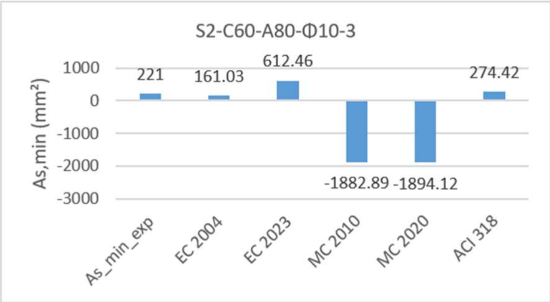

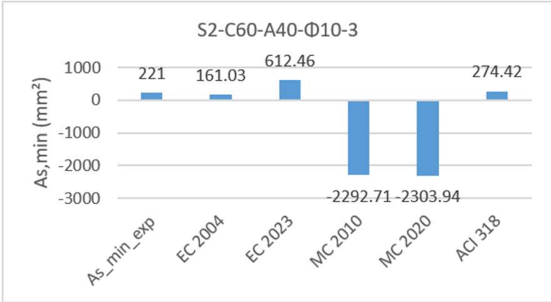

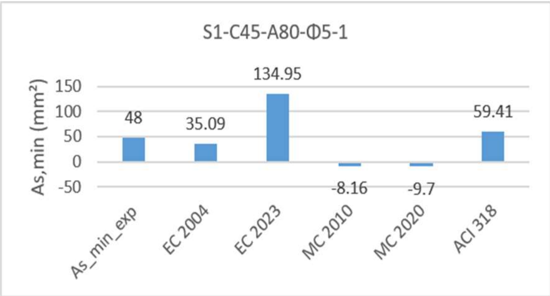

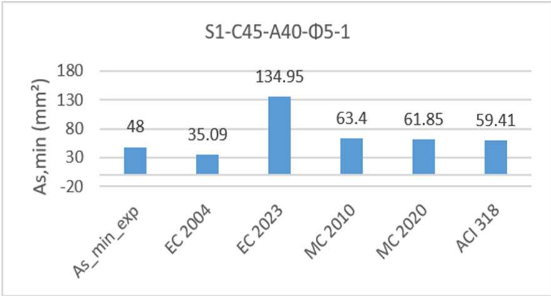

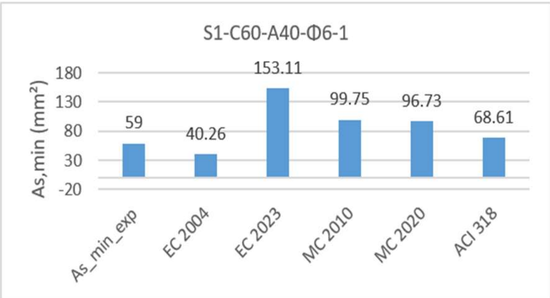

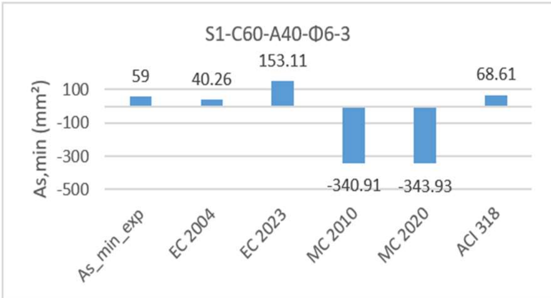

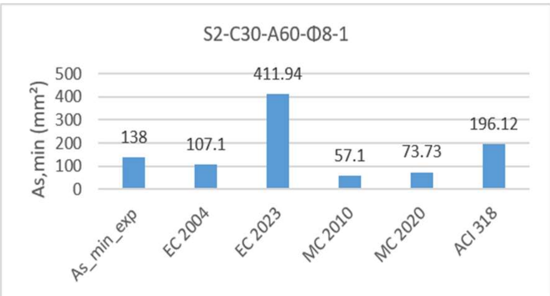

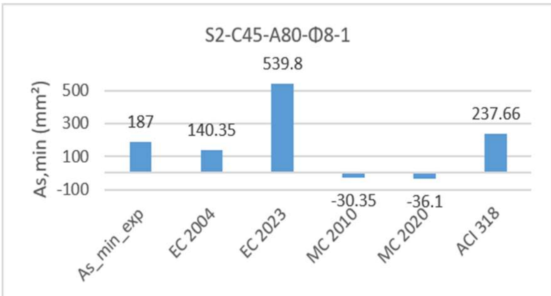

The most notable regulatory behavior emerges within the *fib* Model Codes (MC 2010 and MC 2020). For the vast majority of the evaluated HRC specimens, integrating the fiber volume into the standard code equations results in negative minimum reinforcement areas. According to the specific normative provisions within these frameworks (Section 7.7-13 of MC 2010 and Section 30.7-6 of MC2020), a negative theoretical area explicitly signifies that the minimum reinforcement requirement can be satisfied entirely by the residual tensile strength of the fiber reinforcement alone[16], [19], theoretically eliminating the need for macroscopic longitudinal steel. However, when juxtaposed against the physical experimental baselines, this regulatory assumption reveals a potential non-conservative gap. For instance, in the high-strength specimen S2-C60-A40-Φ10-3, the physical experiment dictates a safe minimum steel area of 221.00 mm² to properly bridge primary flexural cracking, whereas the Model Codes calculate a deep negative state (e.g., -2292.71 mm²), theoretically stripping the element of longitudinal rebars. This indicates that the Model Codes may overestimate the standalone structural capacity of randomly distributed fibers in highly stressed elements.

Conversely, the updated Eurocode 2 (EC 2023) demonstrates severe mathematical overcompensation, imposing massive material congestion. According to the dataset, EC 2023 consistently generates the highest $A_{s,min}$ demands, aggressively penalizing the structural geometry despite the active tensile contribution of the fibers. In specimen S2-C45-A80-Φ8-1, the physical experiment safely bridges primary cracking with only 187.00 mm², yet EC 2023 mandates an excessive 539.80 mm². This mathematical inflation completely negates the economic and structural material optimization intended by utilizing hybrid fiber matrices.

The legacy Eurocode 2004 (EC 2004) and ACI 318 frameworks operate between these two extremes, though with entirely distinct structural behaviors. EC 2004 consistently under-predicts the required steel across the high-strength and highly scaled specimens, maintaining the dangerous under-reinforcement trap identified in the non-fibrous concrete evaluation. For example, in specimen S2-C30-A60-Φ8-1, EC 2004 predicts a deficient 107.10 mm² against an experimental baseline need of 138.00 mm². ACI 318, utilizing its empirical approach, functions as a more reliable conservative boundary. While it occasionally overestimates the required steel prescribing 196.12 mm² for the same S2-C30-A60-Φ8-1 specimen, it avoids both the complete elimination of longitudinal steel seen in the Model Codes and the severe over-congestion trap of EC 2023.

Ultimately, this analytical phase proves that current international frameworks lack a unified, structurally safe methodology for proportionally balancing macroscopic longitudinal steel with randomly distributed fiber reinforcement.

4.2.2 Ductility and Safety Margin Divergence (DI) for HRC

The pronounced mathematical discrepancies observed in the code-prescribed minimum reinforcement areas ($A_{s,min}$) directly distort the theoretical post-cracking ductility of Hybrid Fiber-Reinforced Concrete (HRC) beams. By evaluating the theoretical Ductility Index (DI) against the experimentally validated baselines, the structural consequences of these regulatory divergences become highly visible. The following graphical representations illustrate the fundamental shifts in ductility expectations across the selected HRC specimens. All corresponding structural parameters and index calculations are comprehensively detailed in **Table 10** in **Appendix A.**

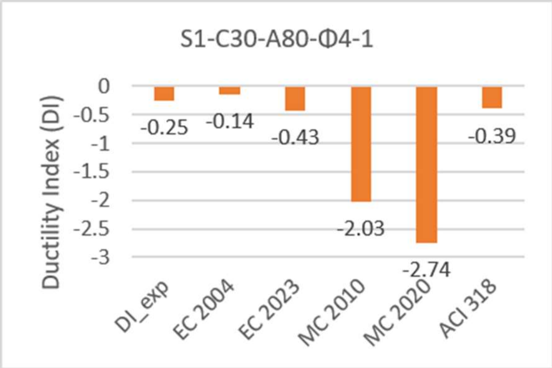
S1-C30-A80-Φ4-1
Ductility Index (DI)
0
-0.5
-1
-1.5
-2
-2.5
-3
-0.25
-0.14
-0.43
-2.03
-2.74
-0.39
DI_exp
EC 2004
EC 2023
MC 2010
MC 2020
ACI 318

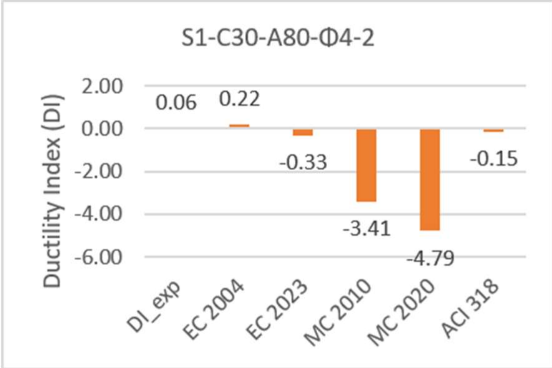
S1-C30-A80-Φ4-2
Ductility Index (DI)
2.00
0.00
-2.00
-4.00
-6.00
0.06
0.22
-0.33
-3.41
-4.79
-0.15
DI_exp
EC 2004
EC 2023
MC 2010
MC 2020
ACI 318

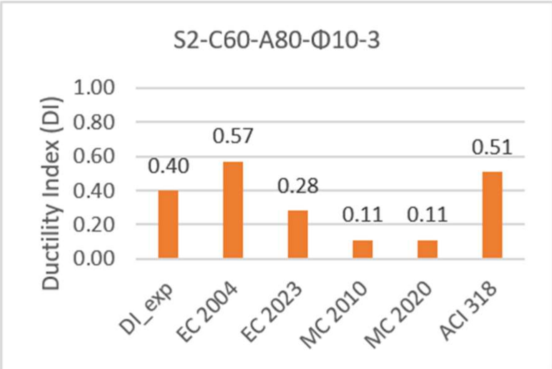
S2-C60-A80-Φ10-3
Ductility Index (DI)
1.00
0.80
0.60
0.40
0.20
0.00
0.40
0.57
0.28
0.11
0.11
0.51
DI_exp
EC 2004
EC 2023
MC 2010
MC 2020
ACI 318

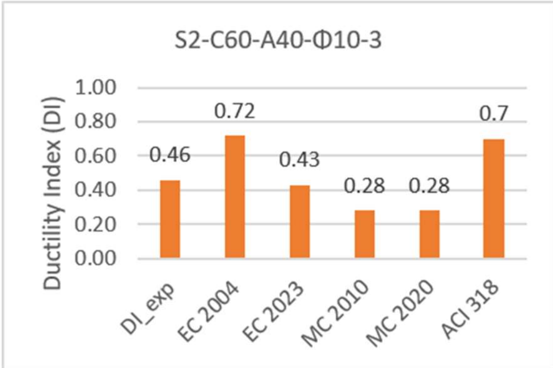
S2-C60-A40-Φ10-3
Ductility Index (DI)
1.00
0.80
0.60
0.40
0.20
0.00
0.46
0.72
0.43
0.28
0.28
0.7
DI_exp
EC 2004
EC 2023
MC 2010
MC 2020
ACI 318

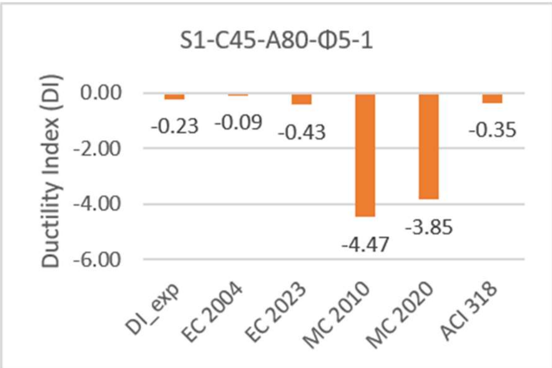
S1-C45-A80-Φ5-1
Ductility Index (DI)
0.00
-2.00
-4.00
-6.00
-0.23
-0.09
-0.43
-4.47
-3.85
-0.35
DI_exp
EC 2004
EC 2023
MC 2010
MC 2020
ACI 318

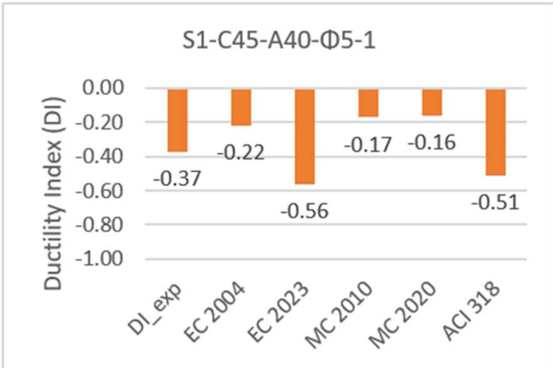
S1-C45-A40-Φ5-1
Ductility Index (DI)
0.00
-0.20
-0.40
-0.60
-0.80
-1.00
-0.37
-0.22
-0.56
-0.17
-0.16
-0.51
DI_exp
EC 2004
EC 2023
MC 2010
MC 2020
ACI 318

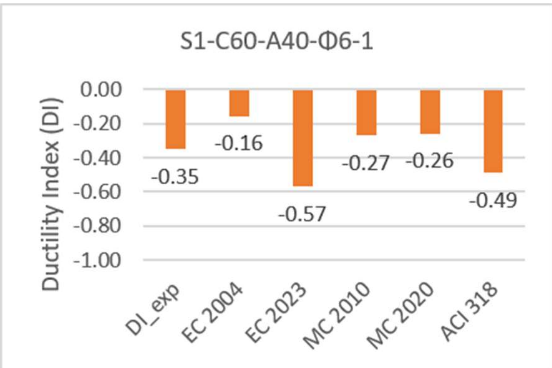
S1-C60-A40-Φ6-1
Ductility Index (DI)
0.00
-0.20
-0.40
-0.60
-0.80
-1.00
-0.35
-0.16
-0.57
-0.27
-0.26
-0.49
DI_exp
EC 2004
EC 2023
MC 2010
MC 2020
ACI 318

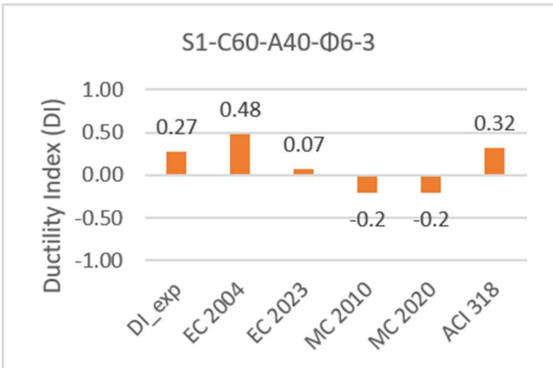
S1-C60-A40-Φ6-3
Ductility Index (DI)
1.00
0.50
0.00
-0.50
-1.00
0.27
0.48
0.07
-0.2
-0.2
0.32
DI_exp
EC 2004
EC 2023
MC 2010
MC 2020
ACI 318

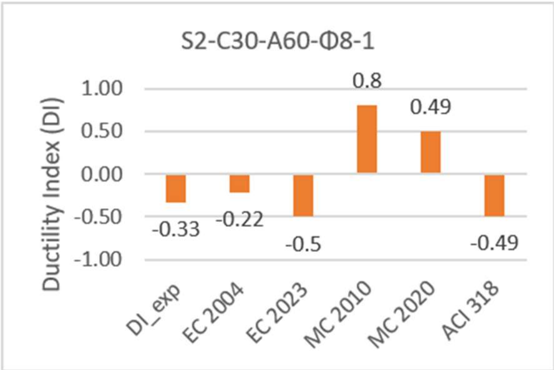

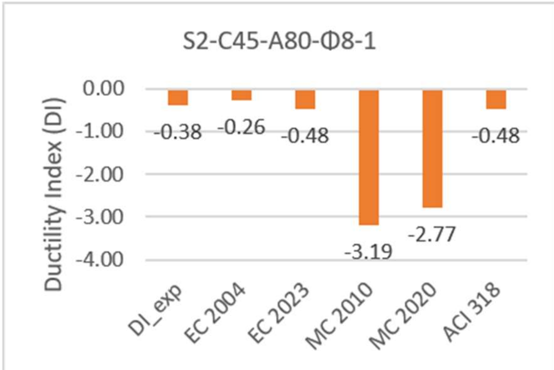

The most severe structural anomaly manifests within the *fib* Model Codes (MC 2010 and MC 2020). As established in the prior evaluation, these frameworks frequently yield negative reinforcement areas, theoretically assuming the fibers alone can sustain the post-cracking tensile stresses. This assumption drives the corresponding Ductility Index into mathematically extreme and physically unrealistic negative states. For instance, in specimen S1-C30-A80-Φ4-2, the physical element achieves a stable, slightly positive experimental ductility baseline of 0.06. However, the Model Codes collapse entirely, predicting profound negative indices of -3.41 (MC 2010) and -4.79 (MC 2020). This pattern repeats aggressively in specimen S1-C45-A80-Φ5-1, where the experimental DI is -0.23, yet the Model Codes plummet to -4.47 and -3.85. This massive divergence demonstrates that relying entirely on the residual strength of randomly distributed fibers, as permitted by the negative area provisions in the Model Codes, theoretically strips the section of macroscopic ductility.

Conversely, Eurocode 2023 (EC 2023) mathematically suppresses ductility through massive material congestion. Because EC 2023 demands the highest volume of longitudinal steel regardless of fiber presence, it consistently yields a more negative DI than the physical baseline, simulating an artificially brittle, over-reinforced state. In specimen S2-C45-A80-Φ8-1, the baseline ductility is -0.38, but the heavy steel penalty of EC 2023 forces the theoretical DI down to -0.48. The code entirely fails to capture the ductility enhancements provided by the hybrid matrix.

Eurocode 2004 (EC 2004) exhibits the opposite, and arguably more dangerous, behavior. By consistently under-predicting the required steel, it artificially inflates the theoretical ductility. In specimen S2-C60-A40-Φ10-3, the experimental baseline requires a DI of 0.46 to safely yield. EC 2004 predicts a highly flexible DI of 0.72, creating a false sense of security where the physical element would likely experience localized brittle fracture before reaching that state. ACI 318 generally mirrors the baseline more closely than the European codes, though it still exhibits scaling issues, predicting a DI of 0.70 for the same specimen.

This comprehensive phase confirms that when macroscopic longitudinal steel and microscopic steel fibers are combined, current international codes fail to accurately predict the true safety margins and physical ductility of the structural elements.

4.2.3 Back-Calculation of Minimum Fiber Volume ($V_{f,min}$) for HRC

In this second methodological phase, the analytical framework is inverted to determine the specific fiber volume fraction necessary to achieve an experimentally validated ductility threshold. Rather than calculating the resulting ductility from a prescribed area of steel, this procedure establishes the required non-dimensional reinforcement ratio (r) by strictly adopting the baseline experimental Ductility Index (DI) established through Fantilli's unified approach.

Once this target ratio is defined, it is integrated back into the governing theoretical equations to back-calculate the newly required minimum fiber volume fraction ($V_{f,min}$) dictated by the varying foundational assumptions of each international design code. To evaluate material efficiency and regulatory consistency, these code-derived fiber requirements are critically compared against the baseline minimum fiber volume proposed by Fantilli's unified theoretical framework. All structural parameters and inverted calculations utilized for these specific specimens are thoroughly documented in **Table 11 in Appendix B**.

The subsequent graphical representations illustrate this comparative evaluation of required fiber volumes across the selected HRC specimens:

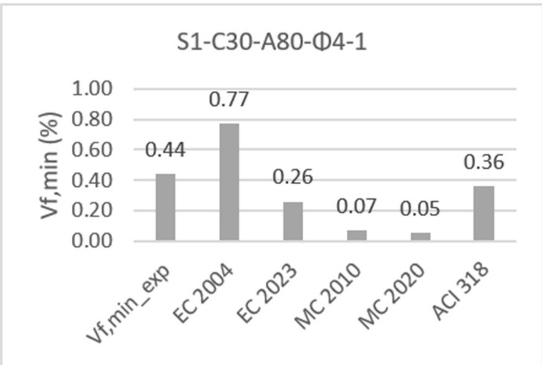

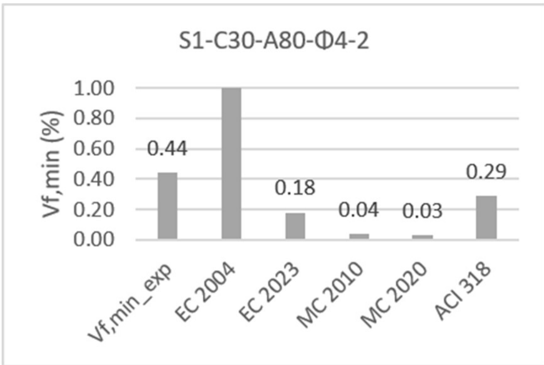

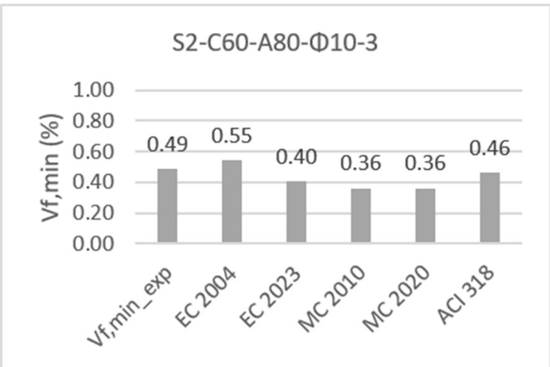

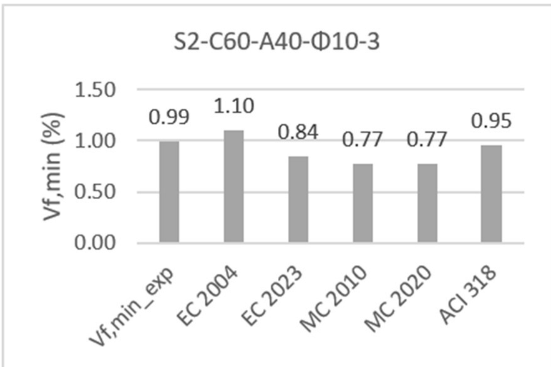

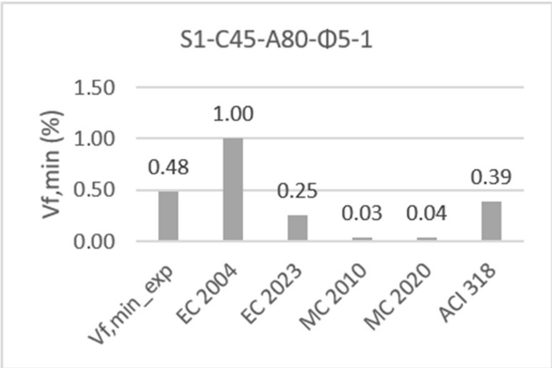

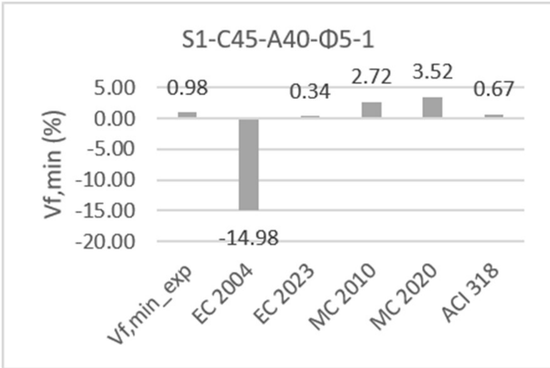

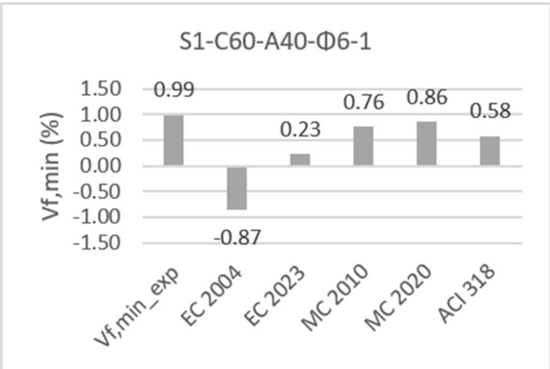

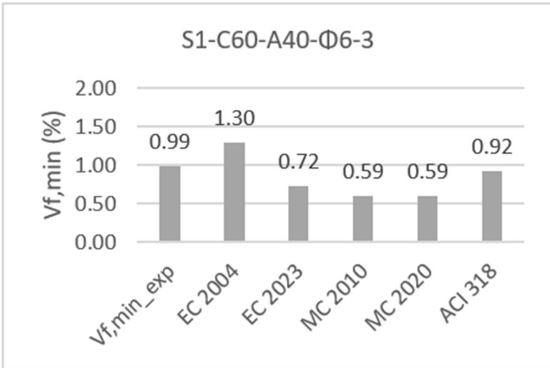

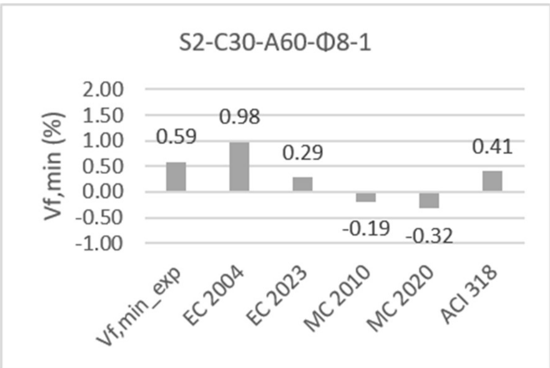

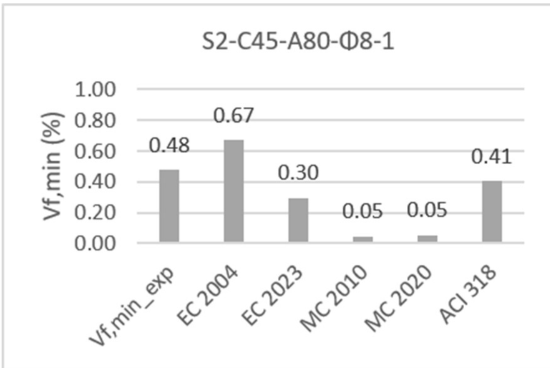

The most profound regulatory distortions occur within the legacy Eurocode 2004 (EC 2004) framework. Because EC 2004 consistently under-predicts the required area of macroscopic longitudinal steel, the inverted calculation forces a massive artificial overcompensation in the required fiber volume to reach the target ductility. This results in severe, often unbuildable, material penalties. For example, in specimen S1-C30-A80-Φ4-2, the baseline empirical requirement is a viable $V_{f,min}$ of 0.44%. However, EC 2004 demands an extreme 1.56%, effectively mandating a fiber density that would compromise the workability of the concrete matrix. Even more critically, in specimen S1-C45-A40-Φ5-1, the mathematical inversion of EC 2004's deficient steel parameters yields an impossible $V_{f,min}$ of -14.98%, highlighting a complete breakdown of the code's theoretical equations when applied outside of standard Lightly Reinforced Concrete (LRC) boundaries.

Conversely, the *fib* Model Codes (MC 2010 and MC 2020) consistently underestimate the fiber volume necessary to achieve the target ductility. In specimen S1-C45-A80-Φ5-1, where the experimental baseline requires a 0.48% fiber volume, the Model Codes suggest structurally deficient values of 0.03% and 0.04%, respectively. This aligns directly with the earlier finding that these frameworks theoretically assume the fibers possess disproportionately high residual tensile strength, leading to potentially dangerous under-reinforcement scenarios.

Eurocode 2023 (EC 2023) and ACI 318 offer more mathematically stable, albeit conservative, estimates across the dataset. EC 2023 generally demands slightly less fiber volume than the baseline (e.g., 0.26% vs 0.44% in S1-C30-A80-Φ4-1) because its formulas mandate such massive volumes of longitudinal steel that the structural reliance on the fibers is artificially reduced. ACI 318, utilizing its robust empirical foundations, tends to closely mirror or slightly undercut the baseline experimental requirements, avoiding the extreme mathematical failures observed in the European provisions. Ultimately, this analysis confirms that no single modern code currently provides a universally accurate equation for optimizing fiber volumes while guaranteeing target ductility across diverse structural geometries.

4.2.4 Evaluation of Minimum Fiber Volume when ($r = 1$) for HRC

In this third analytical phase, the methodological focus shifts to the absolute boundary of structural safety: the strict brittle-ductile transition point. Mathematically, this threshold is defined as the point where the non-dimensional reinforcement ratio (r) equals exactly 1.0, which consequently forces the Ductility Index (DI) to equal zero. This represents the precise moment a structural element shifts from a sudden brittle fracture mechanism to safe, ductile yielding.

By anchoring the theoretical framework to $r = 1$, the exact minimum fiber volume fraction ($V_{f,min}$) required to prevent brittle failure is backcalculated using Fantilli's unified equation. This calculation is performed by substituting the code-prescribed minimum steel areas ($A_{s,min}$) for each international framework (Eurocode 2004, Eurocode 2023, MC 2010, MC 2020, and ACI 318) into the equation. These regulatory requirements are then directly compared against the experimental baseline, utilizing the actual longitudinal steel area (A_s) and corresponding fiber volume (V_f) documented in the physical samples. This phase critically evaluates how efficiently and safely each code balances macroscopic steel and microscopic fibers at the absolute limit of structural viability. All structural parameters and inverted calculations utilized for these specific specimens are thoroughly documented in **Table 12 in Appendix B**.

The subsequent graphical representations illustrate this comparative evaluation of the required $V_{f,min}$ at $r = 1$ across the selected HRC specimens:

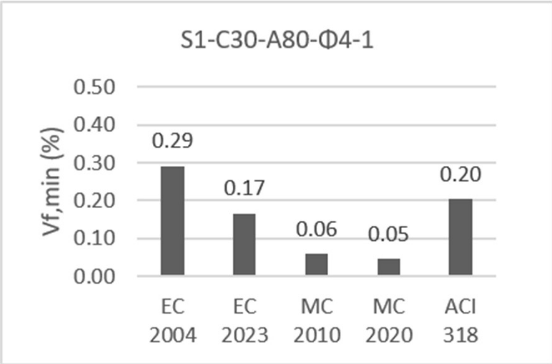
S1-C30-A80-Φ4-1
Vf,min (%)
0.29
0.17
0.06
0.05
0.20
EC 2004
EC 2023
MC 2010
MC 2020
ACI 318

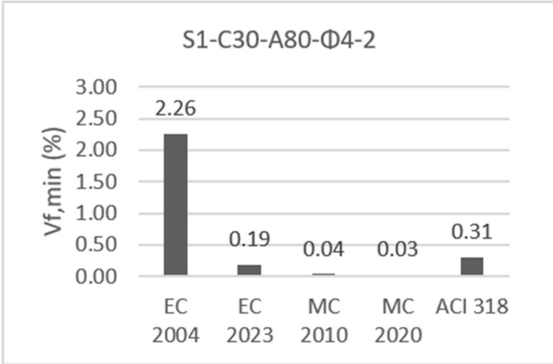
S1-C30-A80-Φ4-2
Vf,min (%)
2.26
0.19
0.04
0.03
0.31
EC 2004
EC 2023
MC 2010
MC 2020
ACI 318

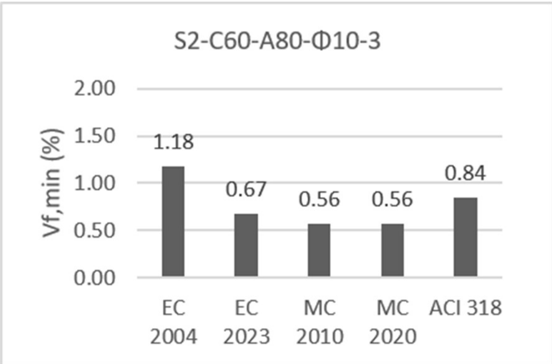
S2-C60-A80-Φ10-3
Vf,min (%)
1.18
0.67
0.56
0.56
0.84
EC 2004
EC 2023
MC 2010
MC 2020
ACI 318

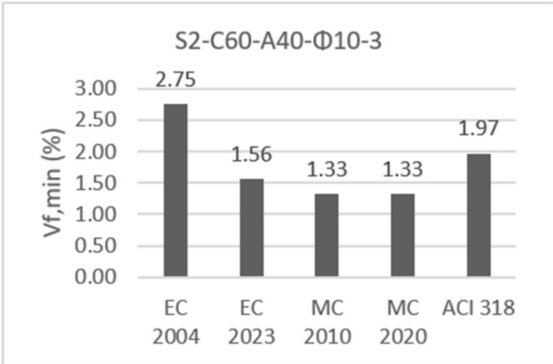
S2-C60-A40-Φ10-3
Vf,min (%)
2.75
1.56
1.33
1.33
1.97
EC 2004
EC 2023
MC 2010
MC 2020
ACI 318

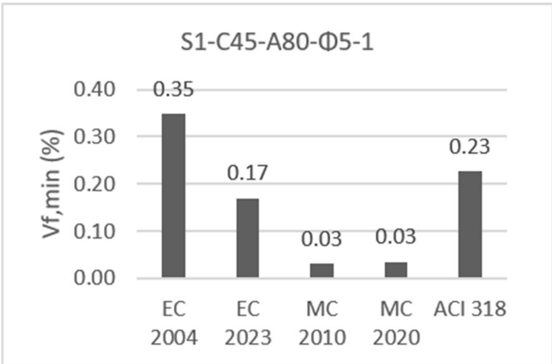
S1-C45-A80-Φ5-1
Vf,min (%)
0.35
0.17
0.03
0.03
0.23
EC 2004
EC 2023
MC 2010
MC 2020
ACI 318

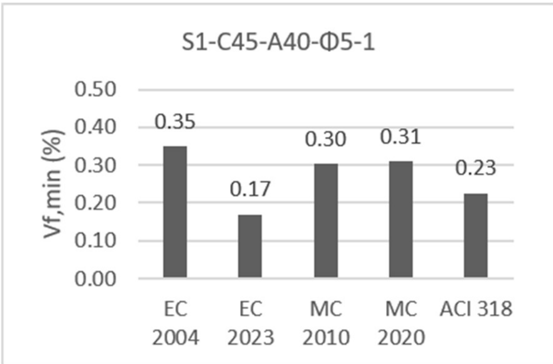
S1-C45-A40-Φ5-1
Vf,min (%)
0.35
0.17
0.30
0.31
0.23
EC 2004
EC 2023
MC 2010
MC 2020
ACI 318

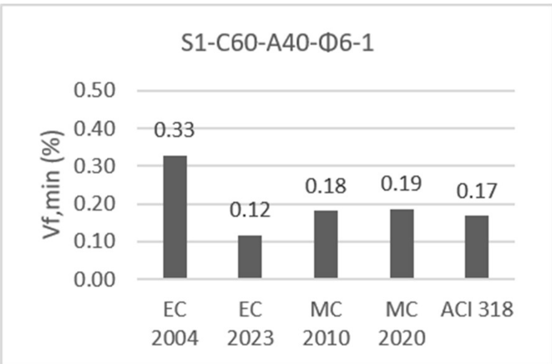
S1-C60-A40-Φ6-1
Vf,min (%)
0.33
0.12
0.18
0.19
0.17
EC 2004
EC 2023
MC 2010
MC 2020
ACI 318

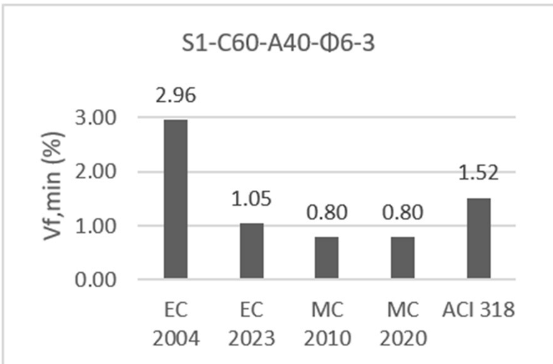
S1-C60-A40-Φ6-3
Vf,min (%)
2.96
1.05
0.80
0.80
1.52
EC 2004
EC 2023
MC 2010
MC 2020
ACI 318

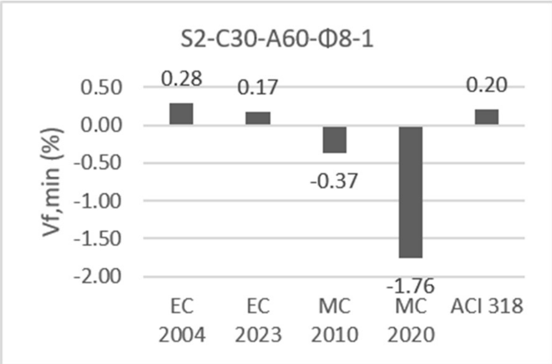

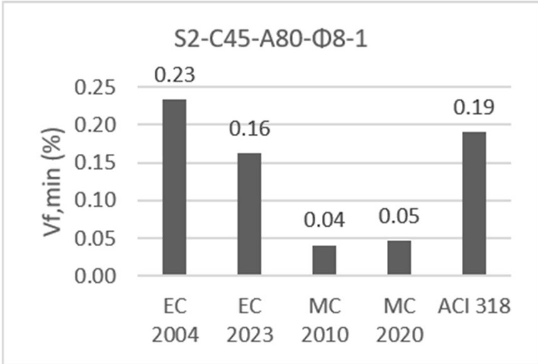

The legacy Eurocode 2004 (EC 2004) framework continues to exhibit extreme material demands at this transitional boundary. Because the code significantly under-prescribes the macroscopic longitudinal steel, the governing equation is forced to mathematically compensate by demanding exceptionally high fiber volumes to theoretically bridge the primary cracking phase. For example, in specimen S2-C60-A40-Φ10-3, EC 2004 requires a massive 2.75% fiber volume, while in specimen S1-C60-A40-Φ6-3, the demand peaks at an extreme 2.96%. These high densities severely risk compromising matrix workability and highlight a critical calibration flaw when legacy LRC codes are applied to hybrid systems.

In stark contrast, the *fib* Model Codes (MC 2010 and MC 2020) yield the lowest required fiber volumes, frequently dropping near zero or entering impossible negative values. For specimen S2-C30-A60-Φ8-1, the calculation yields negative structural requirements of -0.37% (MC 2010) and -1.76% (MC 2020). This mathematical anomaly implies that the code-prescribed longitudinal steel alone is theoretically over-sufficient to prevent brittle fracture at $r = 1$, creating a direct contradiction with the physical behavior and structural necessity of fiber reinforcement in highly stressed concretes.

Eurocode 2023 (EC 2023) and ACI 318 navigate between these two extremes but demonstrate differing structural safety philosophies. EC 2023 consistently requires lower fiber volumes than ACI 318 across the dataset, such as 0.67% compared to 0.84% in specimen S2-C60-A80-Φ10-3. This disparity occurs because EC 2023 inherently mandates a severe congestion of macroscopic longitudinal steel, artificially reducing the structural reliance on the micro-fibers to achieve the $r = 1$ threshold. Conversely, ACI 318 maintains a more balanced and conservative profile, demanding moderate fiber volumes (e.g., 1.52% for S1-C60-A40-Φ6-3) to ensure a safe transition.

Ultimately, this analytical phase demonstrates that relying on disjointed code prescribed steel limits to establish the $r = 1$ threshold creates massive regulatory scatter, proving that standard international frameworks lack the unified mathematical cohesion required to guarantee a safe brittle-ductile transition in HRC elements.

4.3 Analytical Correlation Between Experimental Ductility and Code-Prescribed Reinforcement Limits for LRC Beams

Following the individual parametric evaluations, this section transitions into a multidimensional assessment specifically designed for Lightly Reinforced Concrete (LRC) beams. The primary objective is to visually and mathematically map the actual, physical performance of the test specimens, represented by the baseline experimental ductility index (DI) directly against the theoretical safety thresholds mandated by international design frameworks.

By utilizing normalized ratios on the horizontal axis and plotting the physical ductility on the vertical axis, structural scale effects are completely eliminated. The horizontal zero line (DI= 0) serves as the definitive physical boundary between brittle fracture and ductile yielding. This comprehensive approach isolates regulatory scatter and explicitly reveals whether a specific code accurately predicts safe yielding, mathematically forces an element into a brittle state, or mandates unnecessary material congestion in conventional reinforced concrete.

4.3.1 Evaluation of Experimental Ductility Against Normalized Minimum Longitudinal Steel

This initial correlation evaluates the structural efficiency and safety of the macroscopic longitudinal steel provisions in LRC elements. The vertical axis represents the true physical yielding behavior of the element (DI), while the horizontal axis plots the normalized steel ratio: the actual steel area provided in the physical specimen (A_s) divided by the strict minimum steel area required by the specific regulatory code ($A_{s,min}$).

A horizontal coordinate of 1.0 represents the exact theoretical boundary where the provided steel mathematically matches the code's minimum requirement. Plotting the physical samples onto this domain instantly visualizes regulatory paradoxes. If a sample exhibits a positive, ductile DI (falling in the upper quadrants) but possesses a normalized steel ratio significantly below 1.0, the respective code classifies that safely yielding physical element as dangerously under-reinforced. Conversely, sample points falling into the bottom-right quadrant (where $A_s/A_{s,min}$> 1.0 but DI < 0) highlight a severe regulatory failure known as a false positive, where the code theoretically classifies a physically brittle beam as safely reinforced.

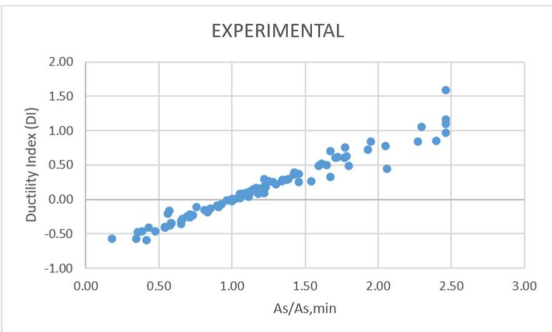

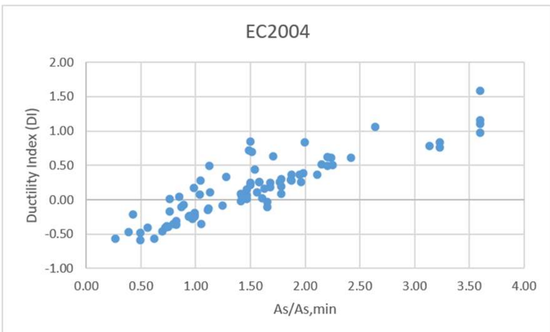

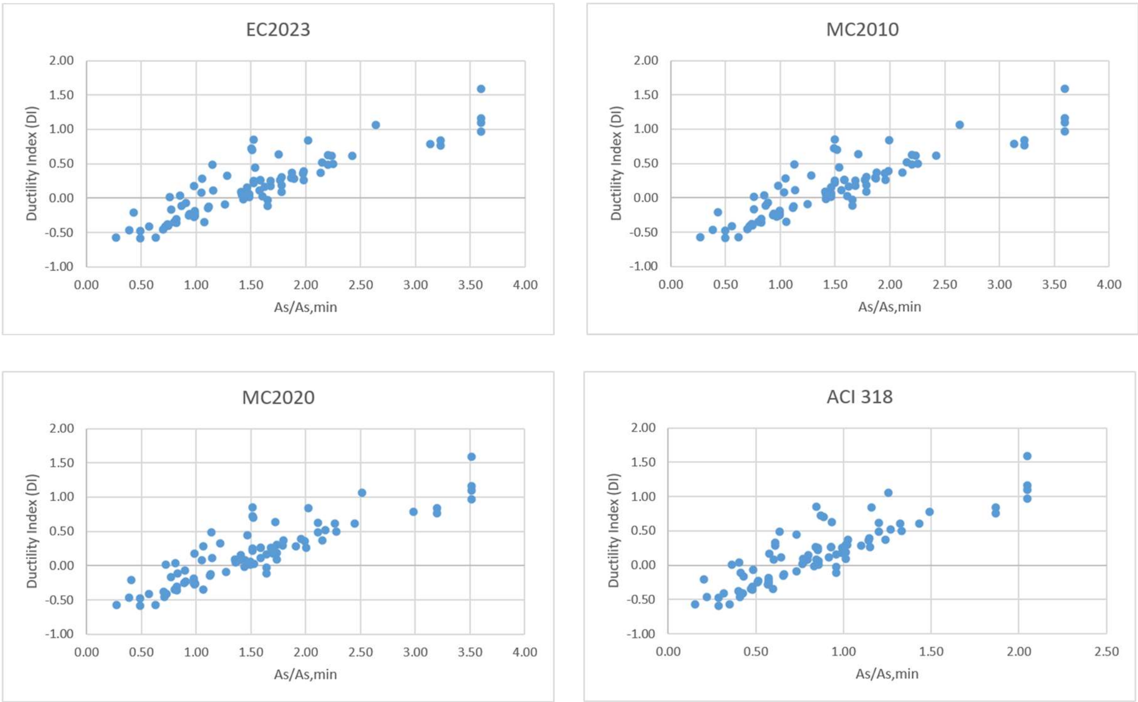

In the baseline experimental diagram, the data aligns in a distinct, tight linear progression. The data crosses the zero-ductility boundary exactly at the 1.0 mark, with the maximum observed ratio reaching approximately 2.50. This confirms the fundamental structural premise that when the provided steel exactly matches the true physical minimum requirement, the element sits perfectly at the brittle-ductile transition point.

The international code projections demonstrate significant deviations from this physical reality.

Regarding Eurocode 2004 and Eurocode 2023, both frameworks exhibit a severe rightward shift in their data clusters, with normalized ratios stretching out to approximately 3.60. This visual shift proves that these codes systematically underestimate the required minimum longitudinal steel, which mathematically inflates the normalized ratio. Most critically, both domains show numerous sample points located in the bottom-right quadrant where the ratio is greater than 1.0 but the experimental ductility is negative. This represents a dangerous regulatory false positive, as the codes theoretically classify these beams as adequately reinforced and safe, yet the physical tests prove they will experience brittle fracture.

The interaction domains for the Model Codes 2010 and 2020 closely mirror the unsafe scatter observed in the Eurocodes. The data spreads widely up to 3.60 on the horizontal axis, and the zero-ductility crossing point fluctuates unpredictably between normalized ratios of roughly 0.70 and 1.50. Like the Eurocodes, the Model Codes suffer from significant false positives, placing physically brittle elements into the mathematically safe zone, thereby failing to guarantee structural ductility.

The ACI 318 interaction domain presents the closest correlation to the experimental baseline. The data cluster is significantly tighter, maximizing around a ratio of 2.10 rather than 3.60. More importantly, the critical transition zone aligns much more closely with the 1.0 boundary. While it exhibits a slight scatter, ACI 318 successfully minimizes the dangerous false positives seen in the European frameworks. The vast majority of physically brittle specimens are correctly identified by the code as under-reinforced.

4.3.2 Evaluation of Experimental Ductility Against Code-Predicted Ductility

Since Lightly Reinforced Concrete elements do not contain fibers, the analytical progression bypasses the fiber interaction domain and moves directly to evaluating the theoretical ductility predictions. In this phase, the physical experimental ductility is plotted on the vertical axis against the theoretical ductility calculated on the horizontal axis. This theoretical ductility is derived using the governing ductility formula, substituting the specific minimum steel areas prescribed by each international standard.

This correlation isolates the mathematical accuracy of the ductility predictions derived from each code. The zero line on both axes represents the absolute brittle-ductile transition boundary. By mapping these values, it becomes evident whether the code-prescribed minimum reinforcement theoretically guarantees the ductile yielding that is physically documented in the experimental baseline, or if the theoretical equations fail to align with the physical behavior.

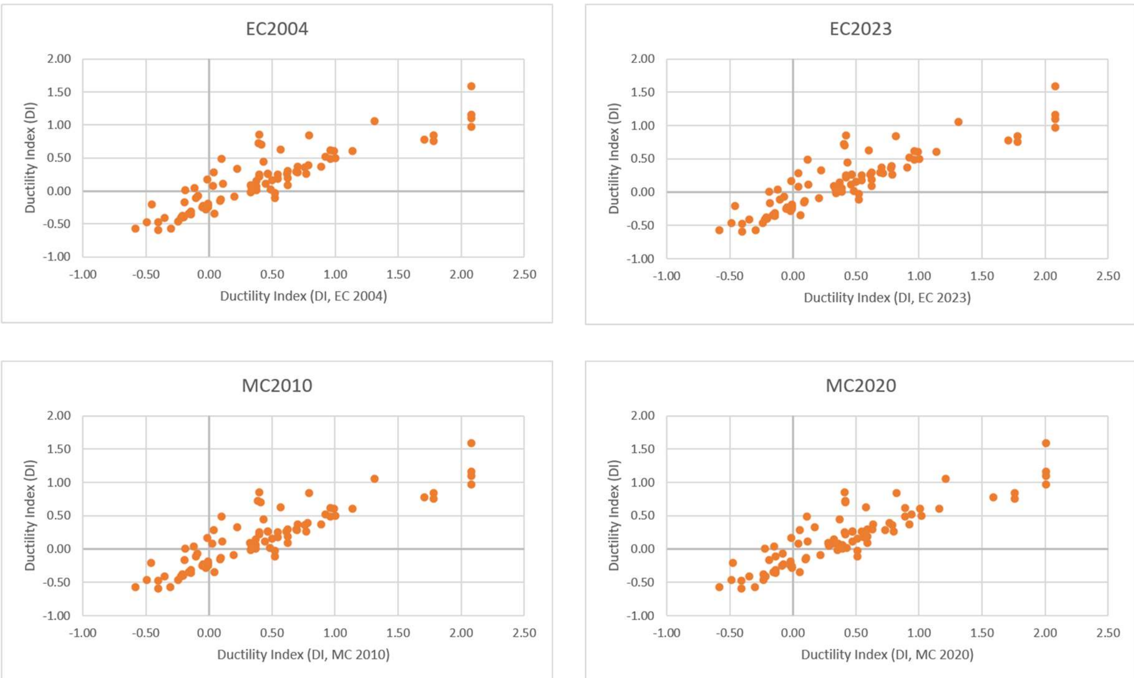

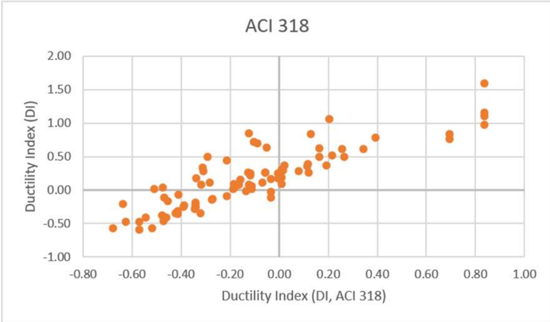

An assessment of Eurocode 2004, Eurocode 2023, and both Model Codes reveal a systemic theoretical overestimation of structural ductility. The data clusters for these four European frameworks are notably shifted to the right, with theoretical ductility values extending up to 2.0 on the horizontal axis. Consequently, a substantial number of physical specimens occupy the bottom-right quadrant of these interaction domains. In this region, the experimental ductility is definitively negative, indicating real-world brittle fracture, yet the code-derived mathematical equations yield a positive ductility prediction. This discrepancy exposes a critical regulatory vulnerability, as the minimum reinforcement formulas mathematically predict a ductile yielding that the physical concrete element cannot actually achieve.

The theoretical interaction domain for ACI 318 demonstrates a significantly higher degree of regulatory safety and mathematical precision. The data distribution is considerably more constrained on the horizontal axis, with maximum theoretical ductility values clustering near 0.8. Most importantly, the ACI 318 framework nearly eliminates the occurrence of unsafe false positives. When the physical specimens exhibit negative experimental ductility, the corresponding theoretical calculations strictly remain in the negative domain, correctly confining the vast majority of the data to the bottom-left quadrant. This alignment proves that the macroscopic longitudinal steel provisions in ACI 318 successfully and safely predict the brittle-ductile transition for standard lightly reinforced elements.

4.3.3 Evaluation of Experimental Ductility Against Non-Dimensional Parameter

This subsequent analytical phase evaluates the interaction between the physical yielding behavior of the conventional Lightly Reinforced Concrete elements and the non-dimensional parameter introduced by Fantilli. Because these conventional elements do not contain steel fibers, the theoretical calculation for this non-dimensional parameter relies exclusively on the macroscopic longitudinal steel provisions.

The vertical axis maps the actual experimental ductility index observed during physical testing. The horizontal axis represents the theoretical non-dimensional parameter, calculated specifically using the minimum longitudinal steel area mandated by each respective international design code. By plotting the experimental ductility against this calculated parameter, the analysis tests the fundamental mathematical validity of the code provisions within the context of established structural mechanics. A reliable regulatory framework should produce a clear, predictable trajectory where the calculated non-dimensional parameter aligns accurately with the physical transition from brittle fracture to ductile yielding.

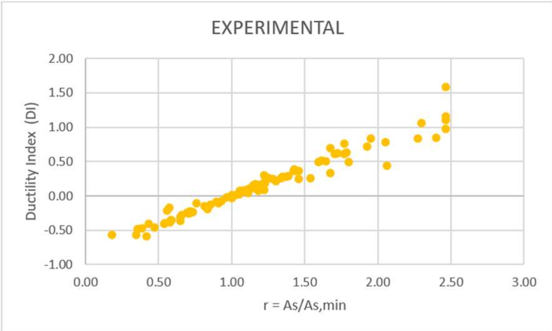

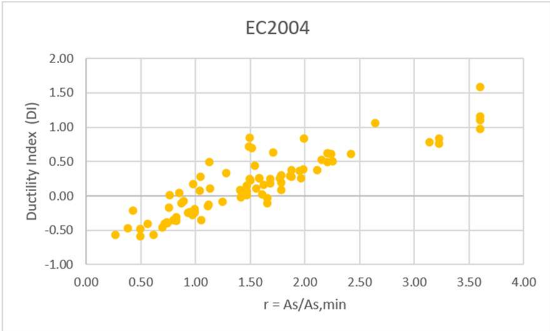

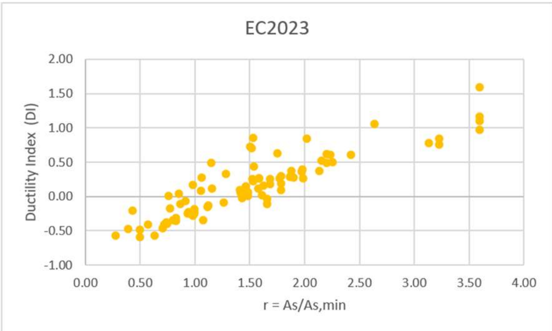

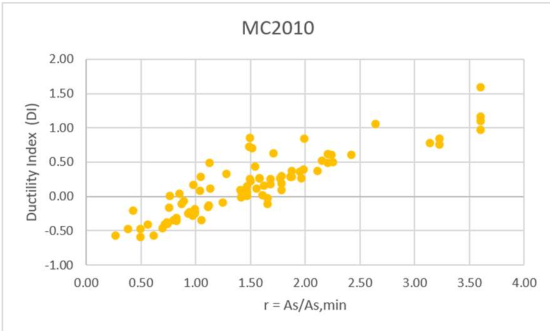

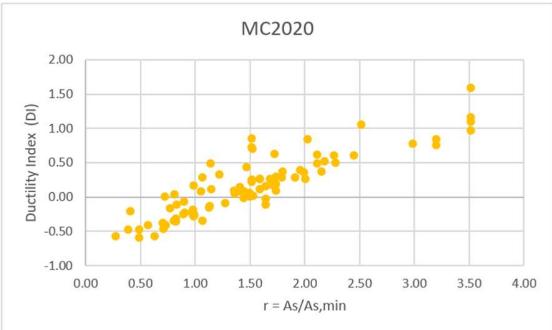

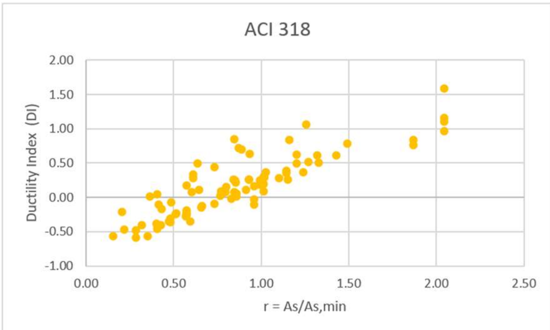

In the experimental baseline diagram, the data forms a highly distinct, tight linear progression that smoothly advances from the negative brittle zone into the positive ductile zone, establishing the true physical behavior of the conventional concrete elements. The maximum non-dimensional parameter in the experimental baseline reaches approximately 2.50, establishing the natural boundary for this specific dataset.

When evaluating the international frameworks, the ACI 318 framework exhibits a shape that is remarkably close to the experimental baseline. The data points for ACI 318 form a tightly clustered linear trajectory that safely tracks across the brittle-ductile transition zone without extreme deviation. Furthermore, its horizontal distribution maximizes near 2.10, remaining structurally proportional to the physical testing limits. This proves that when utilizing the minimum reinforcement areas prescribed by ACI 318, the non-dimensional parameter accurately and reliably represents the true structural mechanics of the Lightly Reinforced Concrete elements.

The European frameworks, encompassing Eurocode 2004, Eurocode 2023, Model Code 2010, and Model Code 2020, all exhibit a generally correct upward trajectory but contain considerably more internal scatters. The data distributions for these four codes are visibly wider and more dispersed horizontally than the experimental baseline. Most notably, their data clusters are severely shifted to the right, extending up to a non-dimensional parameter of approximately 3.60 to 4.00. This pronounced rightward shift and increased structural scatter indicate a noticeable loss of mathematical precision when the specific minimum reinforcement limits of the European codes are applied to calculate the non-dimensional parameter for conventional concrete elements.

4.4 Analytical Correlation Between Experimental Ductility and Code-Prescribed Reinforcement Limits for HRC Beams

Expanding upon the methodology applied to the conventional specimens, this section elevates the evaluation to assess the Hybrid Fiber-Reinforced Concrete dataset. The introduction of steel fibers significantly alters the post-cracking behavior and minimum reinforcement requirements of the concrete matrix, demanding a specialized interaction domain analysis.

As with the lightly reinforced beams, the experimental ductility index is mapped against normalized code parameters to test the regulatory accuracy of Eurocode 2004, Eurocode 2023, the *fib* Model Codes, and ACI 318. This multidimensional phase is critical for determining how effectively current standards balance macroscopic steel and microscopic fibers, and whether they successfully predict the strict brittle-ductile transition when a hybrid matrix is utilized.

4.4.1 Evaluation of Experimental Ductility Against Normalized Minimum Longitudinal Steel

This correlation assesses the longitudinal steel provisions specifically within the complex context of Hybrid Fiber-Reinforced Concrete elements. The vertical axis tracks the physical yielding behavior via the experimental ductility index, while the horizontal axis maps the normalized steel ratio, defined as the actual steel area provided divided by the strict minimum steel area required by the specific code.

Because the theoretical minimum steel calculations for hybrid beams are deeply influenced by the assumed tensile contribution of the fibers, often resulting in extreme mathematical congestion or impossible negative requirements, this specific interaction domain visually exposes severe structural misalignments. A horizontal coordinate of 1.0 represents the exact theoretical boundary where the provided steel matches the code requirement. By mapping these hybrid elements, it becomes explicitly clear whether the international codes safely optimize and reduce the required longitudinal steel in the presence of fibers, or if their theoretical equations inadvertently push the physical elements into a brittle failure mode.

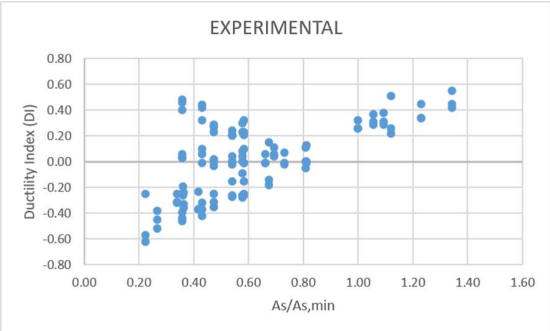

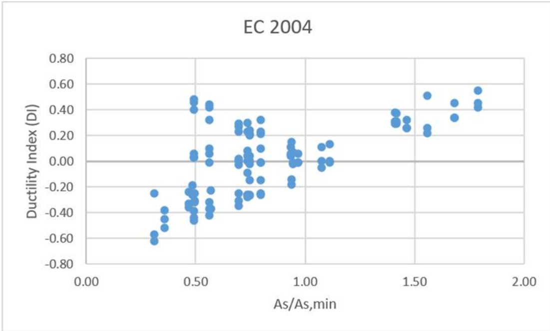

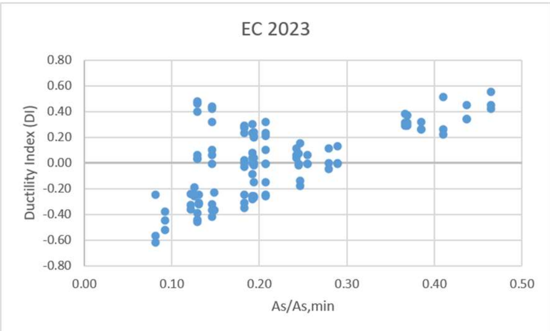

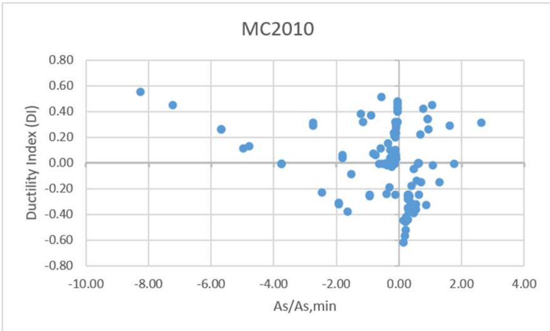

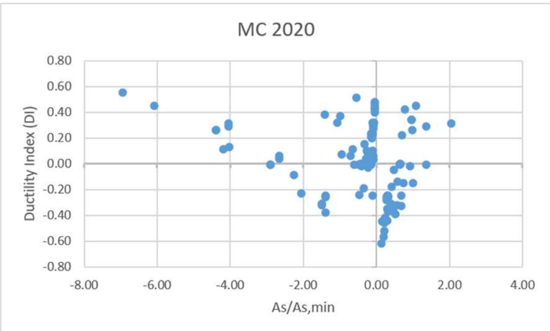

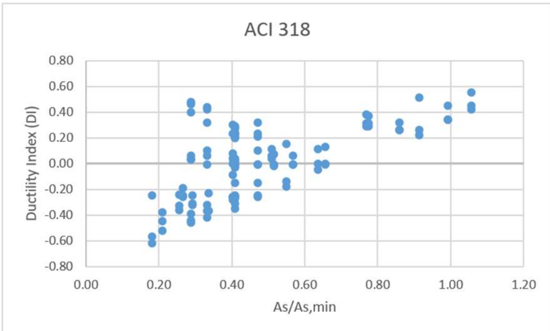

In the experimental baseline diagram, the data distributes naturally across the zero-ductility boundary, with the normalized steel ratio maximizing near 1.40.

The Eurocode 2004 framework exhibits a shift in data distribution, with normalized ratios extending up to approximately 1.80. This interaction domain shows several data points located in the bottom-right quadrant, representing elements with a normalized ratio greater than 1.0

but a negative experimental ductility. These false positives indicate that Eurocode 2004 theoretically classifies these physically brittle hybrid beams as safely reinforced.

Eurocode 2023 presents a drastically different structural approach. The entire data cluster is severely compressed to the left, with the maximum normalized ratio barely reaching 0.50. This extreme compression proves that Eurocode 2023 mandates excessively high minimum longitudinal steel areas for hybrid elements, mathematically shrinking the normalized ratio. While this eliminates false positives by correctly classifying all physically brittle specimens as under-reinforced, it forces severe material congestion and fails to optimize the structural benefits of the steel fibers.

The interaction domains for both Model Code 2010 and Model Code 2020 reveal a critical mathematical breakdown. The data for these codes scatters wildly into the negative domain on the horizontal axis, reaching values as low as -8.00. This visualization proves that the Model Code equations frequently calculate a negative minimum longitudinal steel requirement because the theoretical tensile contribution of the fibers is assumed to mathematically exceed the cracking strength of the concrete matrix. This mathematical anomaly renders these specific provisions highly unstable for evaluating Hybrid Fiber-Reinforced Concrete elements.

The ACI 318 framework provides the most balanced and mathematically stable interaction domain for the hybrid specimens. The data cluster maximizes near a normalized ratio of 1.10, remaining strictly within the logical positive domain. ACI 318 successfully minimizes unsafe false positives while simultaneously avoiding the extreme material over-prescription seen in Eurocode 2023 and the mathematical anomalies present in the Model Codes.

4.4.2 Evaluation of Experimental Ductility Against Normalized Minimum Fiber Volume

This secondary correlation isolates the regulatory effectiveness of the microscopic fiber provisions. The vertical axis continues to map the true physical yielding behavior of the hybrid elements, while the horizontal axis now represents the normalized fiber ratio. This ratio is calculated by dividing the physical experimental fiber volume used in the mixture by the theoretical minimum fiber volume required by each respective design code to guarantee ductility.

Plotting this domain allows for a direct visual assessment of fiber efficiency. A horizontal coordinate of 1.0 marks the boundary where the physical fibers provided exactly match the code's theoretical requirement. By observing where the actual physical failures and successes fall relative to this theoretical boundary, it becomes evident which standards properly calibrate their fiber requirements to prevent brittle fracture, and which mathematically overestimate or underestimate the necessary fiber volumes.

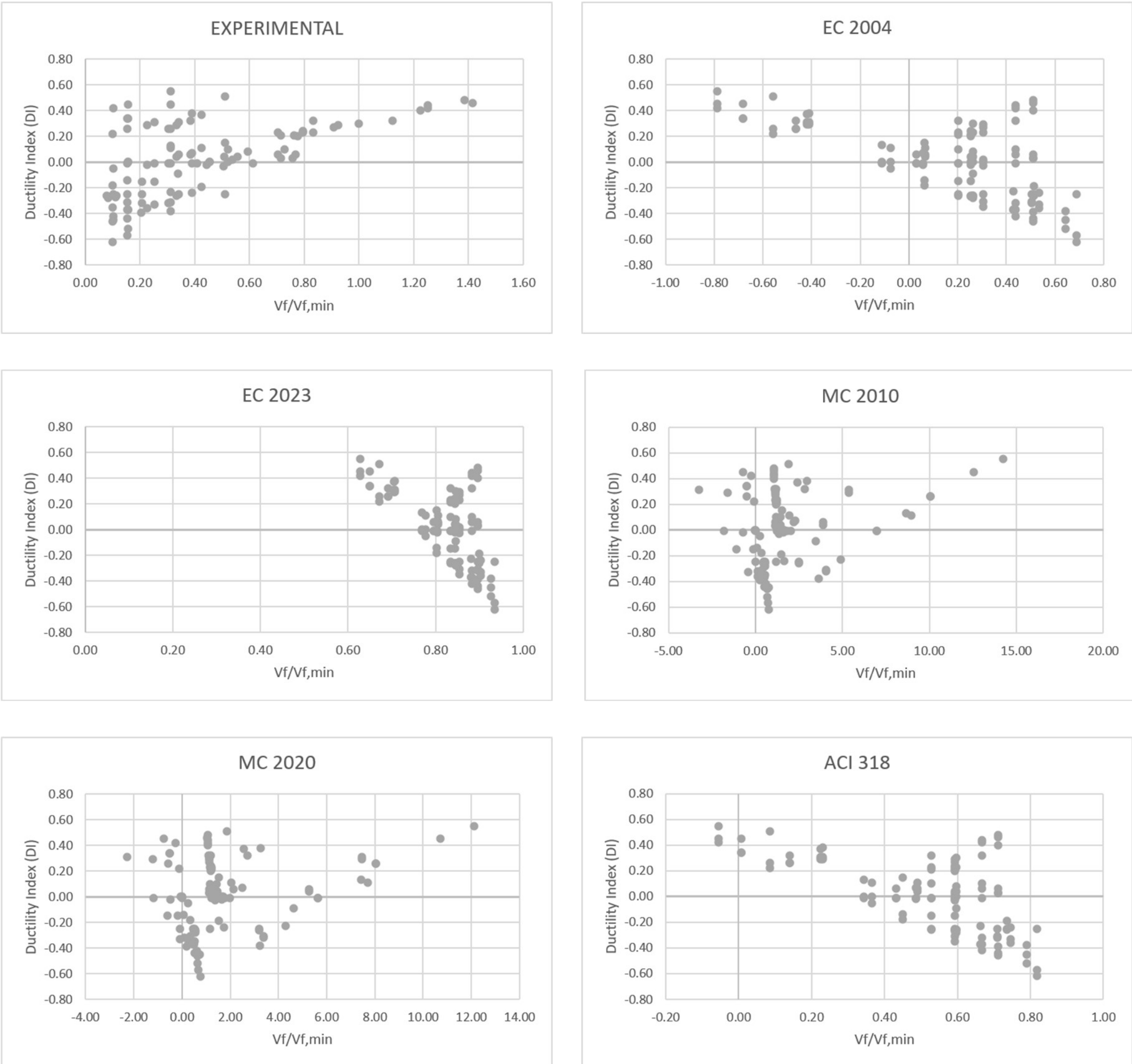

In the experimental baseline diagram, the data distributes across the positive horizontal axis, reaching a maximum ratio of approximately 1.40.

The Eurocode 2004 interaction domain reveals a critical mathematical anomaly. A significant portion of the data points fall into the negative domain on the horizontal axis, reaching values as low as roughly negative 0.80. Because the physical fiber volume provided in the mixture is always a positive real quantity, a negative ratio proves that the Eurocode 2004 equations mathematically calculate a negative minimum required fiber volume for these specific hybrid beams. This renders the code provision physically meaningless for these applications.

Eurocode 2023 avoids the negative ratio anomaly, with all data points falling between 0.60 and 1.00 on the horizontal axis. However, the data cluster exhibits a distinct downward trend, where an increase in the normalized fiber ratio corresponds to a decrease in physical experimental ductility. This inversely proportional relationship contradicts fundamental structural logic, indicating a severe misalignment in the theoretical fiber contribution equations.

The Model Code 2010 and Model Code 2020 frameworks display the most extreme mathematical instability. The data scatters widely across the horizontal axis, extending up to approximately 15.00 in the positive direction and dropping down to roughly negative 4.00 in the negative direction. This wild fluctuation confirms that the Model Code formulas for minimum fiber volume are highly sensitive and produce erratic, unreliable requirements when evaluating complex hybrid matrices.

The ACI 318 interaction domain also suffers from mathematical inconsistencies. Similar to Eurocode 2004, it produces negative normalized ratios extending down to slightly below zero. Furthermore, the data displays a downward trajectory similar to Eurocode 2023, where higher mathematically normalized ratios align with lower experimental ductility.

Ultimately, this visual correlation proves that none of the evaluated international codes currently possess a stable, reliable mathematical model for prescribing minimum fiber volumes in Hybrid Fiber-Reinforced Concrete elements.

4.4.3 Evaluation of Experimental Ductility Against Code-Predicted Ductility

This final analytical phase mirrors the theoretical ductility evaluation performed on the conventional specimens but applies it directly to the Hybrid Fiber-Reinforced Concrete dataset. The physical experimental ductility is plotted on the vertical axis against the theoretical ductility index calculated on the horizontal axis.

This correlation tests the ultimate predictive capability of the codes when both macroscopic steel and microscopic fibers are present. The zero lines mark the absolute transition between a brittle and ductile state. By observing these domains, we can definitively state whether the current international equations can safely predict the actual physical yielding behavior of a hybrid element based on its prescribed minimum reinforcement.

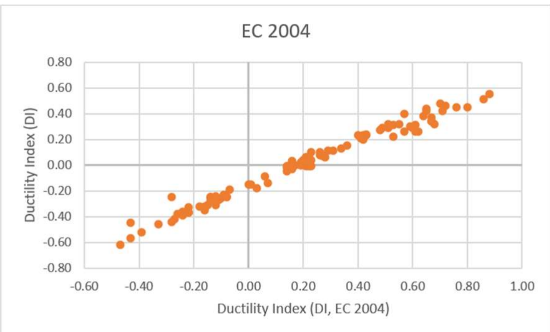

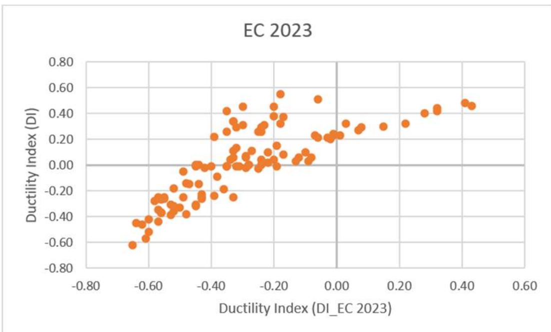

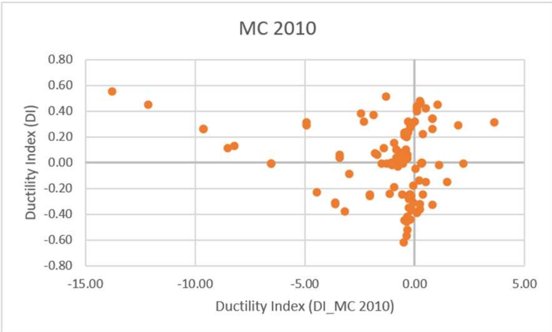

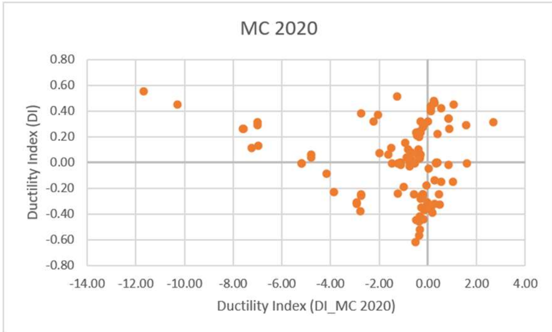

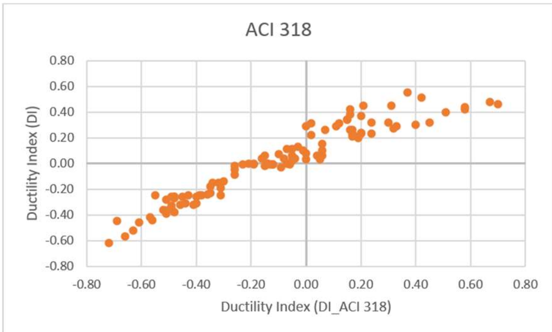

The theoretical interaction domains for Model Code 2010 and Model Code 2020 reveal severe mathematical instability when applied to hybrid elements. The data scatters erratically across the horizontal axis, with theoretical ductility values ranging from positive 5.00 down to extreme negative values of negative 15.00. This immense scatter proves that the underlying theoretical formulas for minimum reinforcement in the Model Codes are fundamentally unstable when steel fibers are introduced, rendering them incapable of safely predicting the brittle-ductile transition.

Eurocode 2023 exhibits a more constrained data distribution compared to the Model Codes but still demonstrates noticeable scatter and regulatory vulnerabilities. Several data points fall into the bottom-right quadrant, representing physical specimens that experienced brittle fracture but were theoretically predicted by the code to yield in a ductile manner. These false positives indicate that Eurocode 2023 overestimates the theoretical ductility of certain hybrid beams, which compromises structural safety.

In stark contrast, Eurocode 2004, and ACI 318 present highly stable and accurate interaction domains for the Hybrid Fiber-Reinforced Concrete elements. Both frameworks produce tight linear distributions that align well with the zero-axis origin. The vast majority of the data is correctly confined to the bottom-left and top-right quadrants, practically eliminating the risk of dangerous false positives. This strong alignment confirms that the theoretical ductility equations derived from Eurocode 2004 and ACI 318 successfully and safely predict the physical yielding behavior of hybrid concrete elements based on their prescribed minimum reinforcement.

4.4.4 Evaluation of Experimental Ductility Against Non-Dimensional Parameter

This subsequent analytical phase evaluates the interaction between the physical yielding behavior of the hybrid elements and the non-dimensional parameter introduced by Fantilli. The vertical axis maps the actual experimental ductility observed during physical testing. The horizontal axis represents the theoretical non-dimensional parameter, calculated specifically using the minimum longitudinal steel area and the minimum fiber volume fraction mandated by each respective international design code.

By plotting the experimental ductility against this calculated non-dimensional parameter, the analysis tests the fundamental validity of the code provisions within the context of established hybrid concrete mechanics. According to the theoretical model, a stable and accurate regulatory framework should produce a clear, predictable relationship where the calculated non-dimensional parameter aligns with the physical transition from brittle fracture to ductile yielding. If a design code accurately captures the synergistic effect of macroscopic steel and microscopic fibers, its data cluster will follow a rational trajectory. Conversely, extreme scatter, inversions, or mathematically impossible values within this interaction domain will explicitly demonstrate that the code-prescribed reinforcement equations fail to represent the true structural mechanics of hybrid fiber-reinforced concrete.

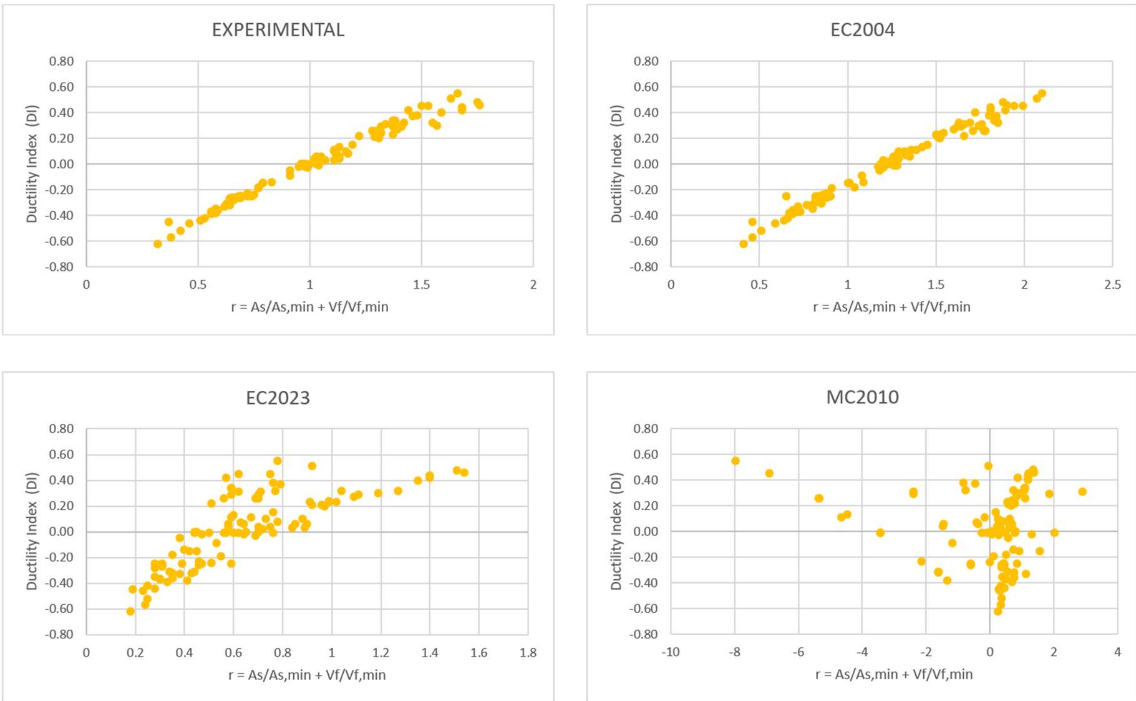

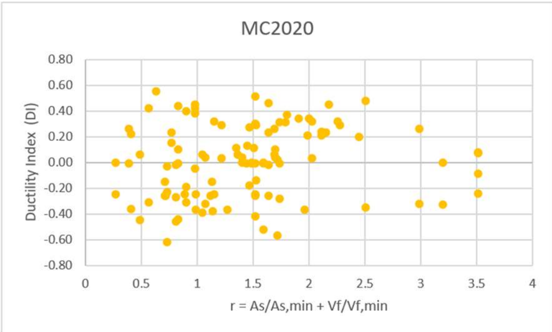

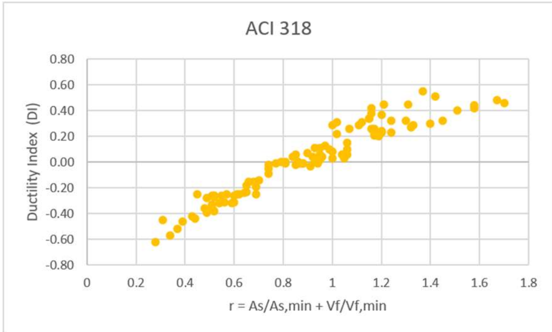

In the experimental baseline diagram, the data forms a highly distinct, tight linear progression that smoothly advances from the negative brittle zone into the positive ductile zone, establishing the true physical behavior of the hybrid elements.

When evaluating the international frameworks, Eurocode 2004 exhibits a shape that is remarkably close to the experimental baseline. The data points for Eurocode 2004 form an exceptionally tight, well-defined linear trajectory that perfectly mirrors the physical testing shape and safely tracks across the brittle-ductile transition zone. This proves that when utilizing the minimum reinforcement areas prescribed by Eurocode 2004, the non-dimensional parameter accurately and reliably represents the true structural mechanics of the hybrid elements.

The ACI 318 framework also demonstrates a highly stable and accurate interaction domain. Its distribution maintains a strong, continuous linear trend that very closely resembles the experimental shape, successfully capturing the synergistic effect of the macroscopic steel and microscopic fibers with only a minor degree of scatter at the uppermost limits.

Eurocode 2023 shows a generally correct upward trajectory but exhibits considerably more internal scatters and a visibly wider, more curved distribution than the experimental baseline. This lack of tightness indicates a noticeable loss of mathematical precision when its specific minimum reinforcement limits are applied to calculate the non-dimensional parameter.

The interaction domains for Model Code 2010 and Model Code 2020 reveal a complete mathematical breakdown. The data for both Model Codes scatters wildly and erratically without any discernible linear relationship. Notably, Model Code 2010 produces extreme negative values on the horizontal axis, plummeting down to negative 8.0 due to the negative minimum steel areas calculated by its formulas. This chaotic, formless scatter definitively proves that the highly unstable minimum reinforcement equations prescribed by the Model Codes cannot be realistically or reliably utilized to calculate the non-dimensional parameter for hybrid fiber-reinforced concrete.

5. Conclusions

This comprehensive analytical investigation evaluated the structural safety and predictive accuracy of five major international design frameworks, Eurocode 2004, Eurocode 2023, the fib Model Code 2010, the fib Model Code 2020, and ACI 318, in dictating the minimum reinforcement required to prevent brittle fracture. By systematically mapping the physical experimental ductility against the theoretical code-prescribed reinforcement limits for both conventional lightly reinforced concrete and hybrid fiber-reinforced concrete elements, critical disparities between mathematical models and physical realities were identified.

Regarding the macroscopic longitudinal steel provisions in conventional concrete elements, ACI 318 proved to be the most reliable and mathematically stable framework. It closely aligned with the experimental boundary between brittle fracture and ductile yielding, effectively minimizing the risk of unsafe structural classifications. Conversely, Eurocode 2004, Eurocode 2023, and the Model Codes demonstrated systemic calculation discrepancies, often underestimating the required minimum longitudinal reinforcement and exposing conventional structures to a high risk of false positives, while in other specific member geometries, they can mathematically overcompensate. This regulatory scatter is corroborated by the article "Minimum reinforcement revisited"[22], which confirms that current European code formulations do not always address practical cases accurately and suffer from calculation discrepancies that misestimate necessary reinforcement values.

The introduction of microscopic steel fibers to create hybrid matrices exposed severe mathematical instabilities within several of the international codes. When evaluating the code-prescribed minimum longitudinal steel area for hybrid elements, the Model Code 2010 and Model Code 2020 frequently calculated physically impossible negative reinforcement requirements. This anomaly occurs because their underlying theoretical formulas assume the tensile contribution of the fibers mathematically exceeds the cracking strength of the concrete matrix itself, also this mathematical breakdown is explicitly confirmed in the article "Investigation in the realm of fiber reinforced concrete[23]", which verifies that whenever the theoretical minimum reinforcement area calculates to a negative value, the minimal reinforcement requirement is being satisfied entirely by the fiber contribution, rendering the longitudinal steel equation unstable. As a result, the Model Codes produce extreme scatter and fail to provide a usable minimum longitudinal steel provision for highly efficient hybrid matrices. Eurocode 2023 avoided negative values but severely overcompensated by mandating excessively high minimum steel areas, thereby forcing unnecessary material congestion and failing to optimize the structural benefits of the fibers. ACI 318, however, maintained a stable and logical correlation for hybrid elements, avoiding both the extreme material over-prescription of Eurocode 2023 and the negative mathematical anomalies of the Model Codes.

A critical phase of this research involved calculating the theoretical ductility of the codes using the non-dimensional parameter published by Fantilli. By utilizing the relationship between this non-dimensional parameter and the code-prescribed minimum steel areas, the ultimate predictive capability of each framework was tested against the experimental ductility. Because the Model Code 2010 and Model Code 2020 generated negative minimum steel requirements, calculating Fantilli's parameter resulted in highly diverse, out-of-range values. This conclusively proves that the reinforcement equations in the Model Codes cannot be reliably used in conjunction with this theoretical ductility model. In stark contrast, Eurocode 2004 and ACI 318 demonstrated exceptional mathematical stability when applied to Fantilli's equations. The validity of utilizing this specific non-dimensional relationship is fully supported by the article "Scaled Approach to Designing the Minimum Hybrid Reinforcement of Concrete Beams[1]", which establishes that the minimum reinforcement corresponding to a zero-ductility state can be reliably designed by testing and expressed as a linear combination of the rebar area and the fiber volume fraction. The theoretical ductility derived for these two codes closely matched the real experimental ductility, correctly confining the predictive data to safe quadrants and validating their theoretical safety margins.

The experimental program also highlighted how specific geometrical and mechanical parameters profoundly affect the minimum reinforcement calculations demanded by the codes. Analyzing paired samples isolated the primary variables driving structural ductility. Comparing identical geometrical samples with varying longitudinal steel, such as S1-C30-A80-Φ4-1 and S1-C30-A80-Φ4-2, demonstrated that altering the provided reinforcement strictly impacts the yielding plateau, shifting the element across the brittle-ductile boundary.

The influence of the fiber aspect ratio proved to be highly significant. When comparing S2-C60-A80-Φ10-3 against S2-C60-A40-Φ10-3, as well as S1-C45-A80-Φ5-1 against S1-C45-A40-Φ5-1, it was evident that increasing the fiber dimension ratio significantly enhanced the post-cracking residual strength. This mechanical alteration changes the microscopic stress transfer mechanism, directly influencing the theoretical minimum reinforcement calculations required by the codes to maintain ductility. Variations in fiber volume and concrete compressive strength also triggered major shifts in code demands. Evaluating S1-C60-A40-Φ6-1 against S1-C60-A40-Φ6-3 revealed how different fiber volume fractions and aspect ratios interact to change the experimental ductility capacity. Furthermore, contrasting S2-C30-A80-Φ8-1 with S2-C30-A60-Φ8-1 demonstrated that increasing the concrete compressive strength alters the inherent brittleness of the matrix. These findings regarding parameter influence are directly supported by the article "Effects of Hooked-End Steel Fiber Geometry and Volume Fraction on the Flexural Behavior of Concrete Pedestrian Decks"[24], which validates that altering specific fiber geometries and volume fractions fundamentally dictates the flexural behavior and alters the minimum flexural reinforcement area required to prevent sudden failure.

Finally, the structural efficiency gained by transitioning from conventional concrete to hybrid fiber-reinforced concrete was explicitly proven by cross-referencing the two datasets. The conventional sample S1-C30-Φ4-1 and the hybrid sample S1-C30-A80-Φ4-1 shared identical dimensions and longitudinal steel areas, isolating the pure ductility enhancement provided exclusively by the inclusion of fibers. Most drastically, comparing the conventional sample S1-C60-Φ10-3, which required a massive longitudinal steel area to achieve safe yielding, with the hybrid sample S1-C60-A80-Φ10-3 showed that the introduction of fibers allowed for a severe reduction in macroscopic steel while fully maintaining structural integrity and ductile behavior, it is interesting to mention that also this principle of structural substitution is verified by the article "Effects of Hooked-End Steel Fiber Geometry and Volume Fraction on the Flexural Behavior of Concrete Pedestrian Decks"[24], which confirms that a precisely calibrated volume of steel fibers can safely replace minimum longitudinal steel rebars to guarantee a ductile flexural failure mode in accordance with frameworks like ACI 318 and Eurocode.

Furthermore, the direct visual correlation between the physical experimental ductility and the theoretical non-dimensional parameter, denoted as r, provided a definitive assessment of regulatory reliability regarding interaction domain trajectories. For conventional concrete elements lacking fibers, the ACI 318 framework produced a tightly clustered linear trajectory that accurately mirrored the physical baseline, whereas the European standards exhibited a pronounced rightward shift and increased scatter that compromised their predictive precision. When evaluating hybrid matrices, the trajectory distributions exposed even deeper structural misalignments. Eurocode 2004 and ACI 318 generated highly stable, linear interaction domains that seamlessly tracked the physical brittle-ductile transition, mimicking the exact shape of the experimental baseline. Conversely, Eurocode 2023 displayed significant internal scatter and a visible loss of mathematical tightness. Most critically, both Model Code 2010 and Model Code 2020 suffered a total mathematical collapse in this domain. The erratic, formless scatter and severe negative horizontal values generated by the Model Codes unequivocally confirm that their minimum reinforcement equations fail to capture the internal mechanics of hybrid fiber-reinforced concrete and cannot be utilized to model this non-dimensional structural parameter.

Ultimately, this investigation demonstrates that while ACI 318 and Eurocode 2004 provide relatively stable and accurate predictions for structural ductility using established mathematical models, current international frameworks, particularly the fib Model Codes, require significant recalibration. The theoretical equations governing minimum reinforcement must be updated to prevent the calculation of negative values, ensuring that modern engineering standards can safely and reliably optimize the use of hybrid fiber-reinforced concrete in structural applications.

Appendix A: Lightly Reinforced Concrete (LRC) Database and Calculations

Table 1 Geometric and Material Properties of Lightly Reinforced Concrete (LRC) Beams

Group	Beam	H (mm)	B (mm)	d (mm)	f_c (Mpa)	f_y (Mpa)	A_s (mm^2)	Ref.
L_1	S1_C30_ϕ4_1	200	100	160	30	450	25	
	S1_C30_ϕ4_2	200	100	160	30	450	38	
	S1_C30_ϕ4_3	200	100	160	30	450	50	
L_2	S1_C30_ϕ5_1	200	100	160	30	450	20	
	S1_C30_ϕ5_2	200	100	160	30	450	39	
	S1_C30_ϕ5_3	200	100	160	30	450	59	
L_3	S2_C30_ϕ8_1	400	200	320	30	450	101	
	S2_C30_ϕ8_2	400	200	320	30	450	151	
	S2_C30_ϕ8_3	400	200	320	30	450	201	
L_4	S2_C30_ϕ10_1	400	200	320	30	450	79	
	S2_C30_ϕ10_2	400	200	320	30	450	157	[6]
	S2_C30_ϕ10_3	400	200	320	30	450	236	
L_5	S1_C45_ϕ5_1	200	100	160	45	450	39	
	S1_C45_ϕ5_2	200	100	160	45	450	59	
	S1_C45_ϕ5_3	200	100	160	45	450	79	
L_6	S1_C45_ϕ6_1	200	100	160	45	450	28	
	S1_C45_ϕ6_2	200	100	160	45	450	57	
	S1_C45_ϕ6_3	200	100	160	45	450	85	
L_7	S2_C45_ϕ8_1	400	200	320	45	450	101	
	S2_C45_ϕ8_2	400	200	320	45	450	201	
	S2_C45_ϕ8_3	400	200	320	45	450	302	
L_8	S2_C45_ϕ10_1	400	200	320	45	450	157	
	S2_C45_ϕ10_2	400	200	320	45	450	236	

	S2_C45_ϕ10_3	400	200	320	45	450	314	
L_9	S1_C60_ϕ5_1	200	100	160	60	450	39	
	S1_C60_ϕ5_2	200	100	160	60	450	59	
	S1_C60_ϕ5_3	200	100	160	60	450	79	
L_10	S1_C60_ϕ6_1	200	100	160	60	450	28	
	S1_C60_ϕ6_2	200	100	160	60	450	57	
	S1_C60_ϕ6_3	200	100	160	60	450	85	
L_11	S2_C60_ϕ8_1	400	200	320	60	450	201	
	S2_C60_ϕ8_2	400	200	320	60	450	251	
	S2_C60_ϕ8_3	400	200	320	60	450	302	
L_12	S2_C60_ϕ10_1	400	200	320	60	450	157	
	S2_C60_ϕ10_2	400	200	320	60	450	236	
	S2_C60_ϕ10_3	400	200	320	60	450	314	
L_I	A_1	100	150	80	75.7	637	13	[6]
L_I	A_2	100	150	80	75.7	569	39	
L_II	B_1	200	150	160	75.7	569	20	
L_II	B_2	200	150	160	75.7	569	59	
L_III	C_1	400	150	320	75.7	637	25	
L_III	C_2	400	150	320	75.7	569	79	
L_III	C_3	400	150	320	75.7	441	201	
L_IV	NSC_0,14	100	100	80	64	740	13	
L_IV	NSC_0,25	100	100	80	64	740	25	
L_V	HSC_0,14	100	100	80	98.5	740	13	
L_V	HSC_0,25	100	100	80	98.5	740	25	
L_VI	A_1	100	150	80	24.4	633	20	
L_VI	A_2	100	150	80	24.4	633	39	

L_VII	B_1	200	150	160	24.4	489	28	
L_VII	B_2	200	150	160	24.4	489	57	
L_VII	B_3	200	150	160	24.4	489	85	
L_VIII	C_1	400	150	320	24.4	480	50	
L_VIII	C_2	400	150	320	24.4	480	101	
L_IX	D_1	800	200	640	24.4	456	79	
L_IX	D_2	800	200	640	24.4	456	157	
L_IX	D_3	800	200	640	24.4	456	236	
L_X	A012-06	100	100	80	40	604	20	
L_X	A025-06	100	100	80	40	604	39	
L_XI	A012-12	100	100	80	40	604	20	
L_XI	A025-12	100	100	80	40	604	39	
L_XII	1ϕ8-2	200	100	160	35.9	484	50	
L_XII	1ϕ8-3	200	100	160	35.9	484	50	[6]
L_XII	1ϕ8-4	200	100	160	35.9	484	50	
L_XII	2ϕ8-1	200	100	160	35.9	484	101	
L_XII	2ϕ8-2	200	100	160	35.9	484	101	
L_XII	2ϕ8-3	200	100	160	35.9	484	101	
L_XII	2ϕ8-4	200	100	160	35.9	484	101	
L_XIII	B501	400	250	320	43.2	480	157	
L_XIII	B502	400	250	320	43.2	515	226	
L_XIV	B751	400	250	320	60.6	495	192	
L_XIV	B752	400	250	320	60.6	501	270	
L_XV	B1001	400	250	320	80.1	480	236	
L_XV	B1002	400	250	320	80.1	480	314	
L_XVI	A-4-9.8	95	100	76	78.3	588	10	

L_XVI	A-4-17.1	95	100	76	78.3	588	17	
L_XVII	A_012_06#1	100	100	80	43	485	13	
L_XVII	A_012_06#3	100	100	80	43	485	13	
L_XVII	A_025_06#1	100	100	80	43	485	25	
L_XVII	A_025_06#3	100	100	80	43	485	25	[6]
L_XVIII	D1-R2X	75	50	60	39.5	538	5	
L_XVIII	D1-R3X	75	50	60	39.5	538	10	
L_XIX	D2-R1X	150	50	120	39.5	538	5	
L_XIX	D2-R2X	150	50	120	39.5	538	10	
L_XX	D3-R1X	300	50	240	39.5	538	10	
L_XX	D3-R2X	300	50	240	39.5	538	20	

Table 2 Experimental Results and Theoretical Parameters of Lightly Reinforced Concrete (LRC) Beams

Group	Beam	P^*_{cr} (Mpa)	M^*_{cr} (Mpa)	P_u (Mpa)	M_u (Mpa)	$A_{s,min}$ (mm^2)	DI	r	Ref.
L_1	S1_C30_ϕ4_1	-	2.88	-	2.15	36	-0.25	0.69	
	S1_C30_ϕ4_2	-	2.98	-	3.13	36	0.05	1.04	
	S1_C30_ϕ4_3	-	3.11	-	4.02	36	0.29	1.39	
L_2	S1_C30_ϕ5_1	-	2.80	-	1.68	37	-0.40	0.53	
	S1_C30_ϕ5_2	-	2.92	-	3.16	37	0.08	1.07	
	S1_C30_ϕ5_3	-	3.10	-	4.60	37	0.49	1.60	
L_3	S2_C30_ϕ8_1	-	21.54	-	16.56	138	-0.23	0.73	
	S2_C30_ϕ8_2	-	22.23	-	24.23	138	0.09	1.09	
	S2_C30_ϕ8_3	-	23.03	-	31.45	138	0.37	1.46	
L_4	S2_C30_ϕ10_1	-	20.98	-	12.97	137	-0.38	0.57	
	S2_C30_ϕ10_2	-	21.63	-	24.93	137	0.15	1.15	[6]
	S2_C30_ϕ10_3	-	22.71	-	36.77	137	0.62	1.72	
L_5	S1_C45_ϕ5_1	-	3.80	-	3.22	48	-0.15	0.81	
	S1_C45_ϕ5_2	-	3.98	-	4.69	48	0.18	1.22	
	S1_C45_ϕ5_3	-	4.13	-	6.19	48	0.50	1.63	
L_6	S1_C45_ϕ6_1	-	3.69	-	2.39	48	-0.35	0.58	
	S1_C45_ϕ6_2	-	3.87	-	4.49	48	0.16	1.17	
	S1_C45_ϕ6_3	-	4.07	-	6.55	48	0.61	1.75	
L_7	S2_C45_ϕ8_1	-	28.29	-	16.76	187	-0.41	0.54	
	S2_C45_ϕ8_2	-	29.58	-	31.92	187	0.08	1.07	
	S2_C45_ϕ8_3	-	31.07	-	47.14	187	0.52	1.61	

L_8	S2_C45_ϕ10_1	-	28.61	-	24.90	184	-0.13	0.84	
	S2_C45_ϕ10_2	-	29.56	-	37.09	184	0.25	1.26	
	S2_C45_ϕ10_3	-	30.25	-	48.71	184	0.61	1.68	
L_9	S1_C60_ϕ5_1	-	4.59	-	3.30	59	-0.28	0.66	
	S1_C60_ϕ5_2	-	4.75	-	4.78	59	0.01	0.99	
	S1_C60_ϕ5_3	-	4.91	-	6.19	59	0.26	1.33	
L_10	S1_C60_ϕ6_1	-	4.42	-	2.40	59	-0.46	0.48	
	S1_C60_ϕ6_2	-	4.62	-	4.53	59	-0.02	0.96	
	S1_C60_ϕ6_3	-	4.86	-	6.66	59	0.37	1.44	
L_11	S2_C60_ϕ8_1	-	35.37	-	32.15	224	-0.09	0.90	
	S2_C60_ϕ8_2	-	36.15	-	40.11	224	0.11	1.12	
	S2_C60_ϕ8_3	-	37.05	-	47.45	224	0.28	1.34	
L_12	S2_C60_ϕ10_1	-	34.36	-	25.52	221	-0.26	0.70	
	S2_C60_ϕ10_2	-	35.34	-	37.53	221	0.06	1.05	
	S2_C60_ϕ10_3	-	36.06	-	49.17	221	0.36	1.40	
L_I	A_1	11.80	-	7.00	-	30	-0.41	0.42	
L_I	A_2	12.50	-	15.20	-	30	0.22	1.31	
L_II	B_1	19.60	-	10.30	-	52	-0.47	0.38	
L_II	B_2	20.90	-	23.10	-	52	0.11	1.14	
L_III	C_1	36.70	-	15.70	-	138	-0.57	0.18	
L_III	C_2	38.80	-	32.40	-	138	-0.17	0.57	[6]
L_III	C_3	43.20	-	54.00	-	138	0.25	1.46	
L_IV	NSC_0,14	2.90	-	3.10	-	11	0.08	1.12	
L_IV	NSC_0,25	3.20	-	5.80	-	11	0.84	2.24	
L_V	HSC_0,14	3.50	-	3.20	-	14	-0.07	0.91	
L_V	HSC_0,25	3.60	-	5.90	-	14	0.63	1.81	
L_VI	A_1	11.30	-	11.50	-	19	0.02	1.02	
L_VI	A_2	11.10	-	19.80	-	19	0.78	2.05	
L_VII	B_1	11.30	-	10.10	-	37	-0.11	0.76	
L_VII	B_2	14.10	-	17.70	-	37	0.26	1.53	
L_VII	B_3	12.10	-	24.90	-	37	1.06	2.29	
L_VIII	C_1	19.90	-	20.10	-	49	0.01	1.02	
L_VIII	C_2	21.70	-	31.30	-	49	0.44	2.05	
L_IX	D_1	35.20	-	27.80	-	141	-0.21	0.56	
L_IX	D_2	43.40	-	45.30	-	141	0.04	1.11	
L_IX	D_3	45.60	-	60.60	-	141	0.33	1.67	
L_X	A012-06	7.10	-	6.30	-	22	-0.11	0.89	
L_X	A025-06	7.00	-	12.30	-	22	0.76	1.77	
L_XI	A012-12	3.20	-	3.10	-	20	-0.03	0.97	
L_XI	A025-12	3.10	-	5.70	-	20	0.84	1.93	
L_XII	1ϕ8-2	14.70	-	19.00	-	41	0.30	1.23	
L_XII	1ϕ8-3	17.80	-	19.40	-	41	0.09	1.23	
L_XII	1ϕ8-4	16.40	-	19.60	-	41	0.19	1.23	
L_XII	2ϕ8-1	17.20	-	37.10	-	41	1.16	2.47	
L_XII	2ϕ8-2	14.70	-	38.20	-	41	1.59	2.47	
L_XII	2ϕ8-3	18.50	-	39.00	-	41	1.10	2.47	

L_XII	2ϕ8-4	18.40	-	36.30	-	41	0.97	2.47	
L_XIII	B501	37.60	-	44.00	-	135	0.17	1.17	
L_XIII	B502	44.50	-	75.50	-	135	0.70	1.68	
L_XIV	B751	39.30	-	50.50	-	140	0.28	1.36	
L_XIV	B752	46.10	-	79.40	-	140	0.72	1.92	
L_XV	B1001	43.90	-	65.20	-	131	0.49	1.80	
L_XV	B1002	47.80	-	88.40	-	131	0.85	2.40	
L_XVI	A-4-9.8	6.80	-	2.92	-	29	-0.57	0.34	
L_XVI	A-4-17.1	6.80	-	4.42	-	29	-0.35	0.59	[6]
L_XVII	A_012_06#1	6.90	-	4.40	-	20	-0.36	0.64	
L_XVII	A_012_06#3	7.00	-	4.80	-	20	-0.31	0.64	
L_XVII	A_025_06#1	7.00	-	8.80	-	20	0.26	1.28	
L_XVII	A_025_06#3	7.30	-	9.20	-	20	0.26	1.28	
L_XVIII	D1-R2X	3.60	-	2.70	-	7	-0.25	0.72	
L_XVIII	D1-R3X	3.60	-	5.00	-	7	0.39	1.44	
L_XIX	D2-R1X	6.80	-	2.80	-	12	-0.59	0.41	
L_XIX	D2-R2X	6.50	-	5.30	-	12	-0.19	0.81	
L_XX	D3-R1X	11.30	-	5.90	-	28	-0.48	0.35	
L_XX	D3-R2X	11.30	-	8.90	-	28	-0.22	0.70	

Table 3 Minimum Reinforcement Area ($A_{s, min}$) Requirements Across International Codes for Evaluated LRC Elements

Group	Beam	EC2004 (mm^2)	$EC2023$ (mm^2)	$MC2010$ (mm^2)	$MC2020$ (mm^2)	$ACI318$ (mm^2)
L_1	S1_C30_ϕ4_1	26.78	26.78	26.78	27.94	49.03
	S1_C30_ϕ4_2	26.78	26.78	26.78	27.94	49.03
	S1_C30_ϕ4_3	26.78	26.78	26.78	27.94	49.03
L_2	S1_C30_ϕ5_1	26.78	26.78	26.78	27.94	49.03
	S1_C30_ϕ5_2	26.78	26.78	26.78	27.94	49.03
	S1_C30_ϕ5_3	26.78	26.78	26.78	27.94	49.03
L_3	S2_C30_ϕ8_1	107.10	107.10	107.10	111.75	196.12
	S2_C30_ϕ8_2	107.10	107.10	107.10	111.75	196.12
	S2_C30_ϕ8_3	107.10	107.10	107.10	111.75	196.12
L_4	S2_C30_ϕ10_1	107.10	107.10	107.10	111.75	196.12
	S2_C30_ϕ10_2	107.10	107.10	107.10	111.75	196.12

	S2_C30_ϕ10_3	107.10	107.10	107.10	111.75	196.12
L_5	S1_C45_ϕ5_1	35.09	35.09	35.09	34.69	59.41
	S1_C45_ϕ5_2	35.09	35.09	35.09	34.69	59.41
	S1_C45_ϕ5_3	35.09	35.09	35.09	34.69	59.41
L_6	S1_C45_ϕ6_1	35.09	35.09	35.09	34.69	59.41
	S1_C45_ϕ6_2	35.09	35.09	35.09	34.69	59.41
	S1_C45_ϕ6_3	35.09	35.09	35.09	34.69	59.41
L_7	S2_C45_ϕ8_1	140.35	140.35	140.35	138.74	237.66
	S2_C45_ϕ8_2	140.35	140.35	140.35	138.74	237.66
	S2_C45_ϕ8_3	140.35	140.35	140.35	138.74	237.66
L_8	S2_C45_ϕ10_1	140.35	140.35	140.35	138.74	237.66
	S2_C45_ϕ10_2	140.35	140.35	140.35	138.74	237.66
	S2_C45_ϕ10_3	140.35	140.35	140.35	138.74	237.66
L_9	S1_C60_ϕ5_1	40.26	39.81	40.26	39.47	68.61
	S1_C60_ϕ5_2	40.26	39.81	40.26	39.47	68.61
	S1_C60_ϕ5_3	40.26	39.81	40.26	39.47	68.61
L_10	S1_C60_ϕ6_1	40.26	39.81	40.26	39.47	68.61
	S1_C60_ϕ6_2	40.26	39.81	40.26	39.47	68.61
	S1_C60_ϕ6_3	40.26	39.81	40.26	39.47	68.61
L_11	S2_C60_ϕ8_1	161.03	159.24	161.03	157.89	274.42
	S2_C60_ϕ8_2	161.03	159.24	161.03	157.89	274.42
	S2_C60_ϕ8_3	161.03	159.24	161.03	157.89	274.42
L_12	S2_C60_ϕ10_1	161.03	159.24	161.03	157.89	274.42
	S2_C60_ϕ10_2	161.03	159.24	161.03	157.89	274.42
	S2_C60_ϕ10_3	161.03	159.24	161.03	157.89	274.42
L_I	A_1	23.23	22.79	23.23	22.96	40.83

L_I	A_2	26.01	25.52	26.01	25.71	45.71
L_II	B_1	52.02	51.03	52.02	51.41	91.42
L_II	B_2	52.02	51.03	52.02	51.41	91.42
L_III	C_1	92.93	91.17	92.93	91.85	163.32
L_III	C_2	104.04	102.06	104.04	102.83	182.83
L_III	C_3	134.24	131.68	134.24	132.67	235.90
L_IV	NSC_0,14	12.54	12.37	12.54	12.33	21.54
L_IV	NSC_0,25	12.54	12.37	12.54	12.33	21.54
L_V	HSC_0,14	14.63	14.28	14.63	14.51	26.73
L_V	HSC_0,25	14.63	14.28	14.63	14.51	26.73
L_VI	A_1	12.44	12.44	12.44	13.06	26.14
L_VI	A_2	12.44	12.44	12.44	13.06	26.14
L_VII	B_1	32.21	32.21	32.21	33.82	67.68
L_VII	B_2	32.21	32.21	32.21	33.82	67.68
L_VII	B_3	32.21	32.21	32.21	33.82	67.68
L_VIII	C_1	65.62	65.62	65.62	68.91	137.89
L_VIII	C_2	65.62	65.62	65.62	68.91	137.89
L_IX	D_1	184.19	184.19	184.19	193.42	387.07
L_IX	D_2	184.19	184.19	184.19	193.42	387.07
L_IX	D_3	184.19	184.19	184.19	193.42	387.07
L_X	A012-06	12.08	12.08	12.08	12.19	20.87
L_X	A025-06	12.08	12.08	12.08	12.19	20.87
L_XI	A012-12	12.08	12.08	12.08	12.19	20.87
L_XI	A025-12	12.08	12.08	12.08	12.19	20.87
L_XII	1ϕ8-2	28.06	28.06	28.06	28.75	49.34
L_XII	1ϕ8-3	28.06	28.06	28.06	28.75	49.34

L_XII	1ϕ8-4	28.06	28.06	28.06	28.75	49.34
L_XII	2ϕ8-1	28.06	28.06	28.06	28.75	49.34
L_XII	2ϕ8-2	28.06	28.06	28.06	28.75	49.34
L_XII	2ϕ8-3	28.06	28.06	28.06	28.75	49.34
L_XII	2ϕ8-4	28.06	28.06	28.06	28.75	49.34
L_XIII	B501	160.05	160.05	160.05	159.40	272.88
L_XIII	B502	149.18	149.18	149.18	148.57	254.33
L_XIV	B751	183.67	181.56	183.67	180.17	313.40
L_XIV	B752	181.47	179.38	181.47	178.01	309.65
L_XV	B1001	209.77	205.47	209.77	207.56	371.57
L_XV	B1002	209.77	205.47	209.77	207.56	371.57
L_XVI	A-4-9.8	16.14	15.81	16.14	15.96	28.49
L_XVI	A-4-17.1	16.14	15.81	16.14	15.96	28.49
L_XVII	A_012_06#1	15.79	15.79	15.79	15.74	26.94
L_XVII	A_012_06#3	15.79	15.79	15.79	15.74	26.94
L_XVII	A_025_06#1	15.79	15.79	15.79	15.74	26.94
L_XVII	A_025_06#3	15.79	15.79	15.79	15.74	26.94
L_XVIII	D1-R2X	5.04	5.04	5.04	5.10	8.73
L_XVIII	D1-R3X	5.04	5.04	5.04	5.10	8.73
L_XIX	D2-R1X	10.09	10.09	10.09	10.20	17.46
L_XIX	D2-R2X	10.09	10.09	10.09	10.20	17.46
L_XX	D3-R1X	20.18	20.18	20.18	20.40	34.92
L_XX	D3-R2X	20.18	20.18	20.18	20.40	34.92

Table 4 Non-Dimensional Reinforcement Ratio (r) Based on Building codes $A_{s,\,min}$ Provisions for LRC Elements

Group	Beam	EC2004	EC2023	MC2010	MC2020	ACI318
L_1	S1_C30_ϕ4_1	0.93	0.93	0.93	0.89	0.51
	S1_C30_ϕ4_2	1.42	1.42	1.42	1.36	0.78
	S1_C30_ϕ4_3	1.87	1.87	1.87	1.79	1.02
L_2	S1_C30_ϕ5_1	0.75	0.75	0.75	0.72	0.41
	S1_C30_ϕ5_2	1.46	1.46	1.46	1.40	0.80
	S1_C30_ϕ5_3	2.20	2.20	2.20	2.11	1.20
L_3	S2_C30_ϕ8_1	0.94	0.94	0.94	0.90	0.51
	S2_C30_ϕ8_2	1.41	1.41	1.41	1.35	0.77
	S2_C30_ϕ8_3	1.88	1.88	1.88	1.80	1.02
L_4	S2_C30_ϕ10_1	0.74	0.74	0.74	0.71	0.40
	S2_C30_ϕ10_2	1.47	1.47	1.47	1.40	0.80
	S2_C30_ϕ10_3	2.20	2.20	2.20	2.11	1.20
L_5	S1_C45_ϕ5_1	1.11	1.11	1.11	1.12	0.66
	S1_C45_ϕ5_2	1.68	1.68	1.68	1.70	0.99
	S1_C45_ϕ5_3	2.25	2.25	2.25	2.28	1.33
L_6	S1_C45_ϕ6_1	0.80	0.80	0.80	0.81	0.47
	S1_C45_ϕ6_2	1.62	1.62	1.62	1.64	0.96
	S1_C45_ϕ6_3	2.42	2.42	2.42	2.45	1.43
L_7	S2_C45_ϕ8_1	0.72	0.72	0.72	0.73	0.42
	S2_C45_ϕ8_2	1.43	1.43	1.43	1.45	0.85
	S2_C45_ϕ8_3	2.15	2.15	2.15	2.18	1.27
L_8	S2_C45_ϕ10_1	1.12	1.12	1.12	1.13	0.66
	S2_C45_ϕ10_2	1.68	1.68	1.68	1.70	0.99
	S2_C45_ϕ10_3	2.24	2.24	2.24	2.26	1.32
L_9	S1_C60_ϕ5_1	0.97	0.98	0.97	0.99	0.57
	S1_C60_ϕ5_2	1.47	1.48	1.47	1.49	0.86
	S1_C60_ϕ5_3	1.96	1.98	1.96	2.00	1.15

L_10	S1_C60_ϕ6_1	0.70	0.70	0.70	0.71	0.41
	S1_C60_ϕ6_2	1.42	1.43	1.42	1.44	0.83
	S1_C60_ϕ6_3	2.11	2.14	2.11	2.15	1.24
L_11	S2_C60_ϕ8_1	1.25	1.26	1.25	1.27	0.73
	S2_C60_ϕ8_2	1.56	1.58	1.56	1.59	0.91
	S2_C60_ϕ8_3	1.88	1.90	1.88	1.91	1.10
L_12	S2_C60_ϕ10_1	0.97	0.99	0.97	0.99	0.57
	S2_C60_ϕ10_2	1.47	1.48	1.47	1.49	0.86
	S2_C60_ϕ10_3	1.95	1.97	1.95	1.99	1.14
L_I	A_1	0.56	0.57	0.56	0.57	0.32
L_I	A_2	1.50	1.53	1.50	1.52	0.85
L_II	B_1	0.38	0.39	0.38	0.39	0.22
L_II	B_2	1.13	1.16	1.13	1.15	0.65
L_III	C_1	0.27	0.27	0.27	0.27	0.15
L_III	C_2	0.76	0.77	0.76	0.77	0.43
L_III	C_3	1.50	1.53	1.50	1.52	0.85
L_IV	NSC_0,14	1.04	1.05	1.04	1.05	0.60
L_IV	NSC_0,25	1.99	2.02	1.99	2.03	1.16
L_V	HSC_0,14	0.89	0.91	0.89	0.90	0.49
L_V	HSC_0,25	1.71	1.75	1.71	1.72	0.94
L_VI	A_1	1.61	1.61	1.61	1.53	0.77
L_VI	A_2	3.14	3.14	3.14	2.99	1.49
L_VII	B_1	0.87	0.87	0.87	0.83	0.41
L_VII	B_2	1.77	1.77	1.77	1.69	0.84
L_VII	B_3	2.64	2.64	2.64	2.51	1.26
L_VIII	C_1	0.76	0.76	0.76	0.73	0.36
L_VIII	C_2	1.54	1.54	1.54	1.47	0.73
L_IX	D_1	0.43	0.43	0.43	0.41	0.20
L_IX	D_2	0.85	0.85	0.85	0.81	0.41

L_IX	D_3	1.28	1.28	1.28	1.22	0.61
L_X	A012-06	1.66	1.66	1.66	1.64	0.96
L_X	A025-06	3.23	3.23	3.23	3.20	1.87
L_XI	A012-12	1.66	1.66	1.66	1.64	0.96
L_XI	A025-12	3.23	3.23	3.23	3.20	1.87
L_XII	1ϕ8-2	1.78	1.78	1.78	1.74	1.01
L_XII	1ϕ8-3	1.78	1.78	1.78	1.74	1.01
L_XII	1ϕ8-4	1.78	1.78	1.78	1.74	1.01
L_XII	2ϕ8-1	3.60	3.60	3.60	3.51	2.05
L_XII	2ϕ8-2	3.60	3.60	3.60	3.51	2.05
L_XII	2ϕ8-3	3.60	3.60	3.60	3.51	2.05
L_XII	2ϕ8-4	3.60	3.60	3.60	3.51	2.05
L_XIII	B501	0.98	0.98	0.98	0.98	0.58
L_XIII	B502	1.51	1.51	1.51	1.52	0.89
L_XIV	B751	1.05	1.06	1.05	1.07	0.61
L_XIV	B752	1.49	1.51	1.49	1.52	0.87
L_XV	B1001	1.13	1.15	1.13	1.14	0.64
L_XV	B1002	1.50	1.53	1.50	1.51	0.85
L_XVI	A-4-9.8	0.62	0.63	0.62	0.63	0.35
L_XVI	A-4-17.1	1.05	1.07	1.05	1.07	0.60
L_XVII	A_012_06#1	0.82	0.82	0.82	0.83	0.48
L_XVII	A_012_06#3	0.82	0.82	0.82	0.83	0.48
L_XVII	A_025_06#1	1.58	1.58	1.58	1.59	0.93
L_XVII	A_025_06#3	1.58	1.58	1.58	1.59	0.93
L_XVIII	D1-R2X	0.99	0.99	0.99	0.98	0.57
L_XVIII	D1-R3X	1.98	1.98	1.98	1.96	1.15
L_XIX	D2-R1X	0.50	0.50	0.50	0.49	0.29
L_XIX	D2-R2X	0.99	0.99	0.99	0.98	0.57
L_XX	D3-R1X	0.50	0.50	0.50	0.49	0.29

L_XX	D3-R2X	0.99	0.99	0.99	0.98	0.57

Table 5 Ductility Index (DI) for LRC Elements Across Evaluated Building Codes

Group	**Beam**	$EC2004$	$EC2023$	$MC2010$	$MC2020$	$ACI318$
L_1	S1_C30_ϕ4_1	-0.05	-0.05	-0.05	-0.08	-0.39
	S1_C30_ϕ4_2	0.34	0.34	0.34	0.29	-0.18
	S1_C30_ϕ4_3	0.69	0.69	0.69	0.63	0.02
L_2	S1_C30_ϕ5_1	-0.20	-0.20	-0.20	-0.23	-0.47
	S1_C30_ϕ5_2	0.37	0.37	0.37	0.32	-0.16
	S1_C30_ϕ5_3	0.96	0.96	0.96	0.89	0.16
L_3	S2_C30_ϕ8_1	-0.05	-0.05	-0.05	-0.08	-0.39
	S2_C30_ϕ8_2	0.33	0.33	0.33	0.28	-0.18
	S2_C30_ϕ8_3	0.70	0.70	0.70	0.64	0.02
L_4	S2_C30_ϕ10_1	-0.21	-0.21	-0.21	-0.23	-0.48
	S2_C30_ϕ10_2	0.37	0.37	0.37	0.32	-0.16
	S2_C30_ϕ10_3	0.96	0.96	0.96	0.89	0.16
L_5	S1_C45_ϕ5_1	0.09	0.09	0.09	0.10	-0.27
	S1_C45_ϕ5_2	0.55	0.55	0.55	0.56	-0.01
	S1_C45_ϕ5_3	1.00	1.00	1.00	1.02	0.26
L_6	S1_C45_ϕ6_1	-0.16	-0.16	-0.16	-0.15	-0.42
	S1_C45_ϕ6_2	0.50	0.50	0.50	0.51	-0.03
	S1_C45_ϕ6_3	1.14	1.14	1.14	1.16	0.34
L_7	S2_C45_ϕ8_1	-0.22	-0.22	-0.22	-0.22	-0.46
	S2_C45_ϕ8_2	0.35	0.35	0.35	0.36	-0.12

	S2_C45_ϕ8_3	0.92	0.92	0.92	0.94	0.22
L_8	S2_C45_ϕ10_1	0.09	0.09	0.09	0.11	-0.27
	S2_C45_ϕ10_2	0.55	0.55	0.55	0.56	-0.01
	S2_C45_ϕ10_3	0.99	0.99	0.99	1.01	0.26
L_9	S1_C60_ϕ5_1	-0.02	-0.02	-0.02	-0.01	-0.35
	S1_C60_ϕ5_2	0.37	0.39	0.37	0.40	-0.11
	S1_C60_ϕ5_3	0.77	0.79	0.77	0.80	0.12
L_10	S1_C60_ϕ6_1	-0.24	-0.24	-0.24	-0.23	-0.47
	S1_C60_ϕ6_2	0.33	0.35	0.33	0.36	-0.14
	S1_C60_ϕ6_3	0.89	0.91	0.89	0.92	0.19
L_11	S2_C60_ϕ8_1	0.20	0.21	0.20	0.22	-0.21
	S2_C60_ϕ8_2	0.45	0.46	0.45	0.47	-0.07
	S2_C60_ϕ8_3	0.70	0.72	0.70	0.73	0.08
L_12	S2_C60_ϕ10_1	-0.02	-0.01	-0.02	0.00	-0.34
	S2_C60_ϕ10_2	0.37	0.39	0.37	0.40	-0.11
	S2_C60_ϕ10_3	0.76	0.78	0.76	0.79	0.12
L_I	A_1	-0.35	-0.34	-0.35	-0.35	-0.55
L_I	A_2	0.40	0.42	0.40	0.41	-0.12
L_II	B_1	-0.49	-0.49	-0.49	-0.49	-0.62
L_II	B_2	0.11	0.12	0.11	0.12	-0.28
L_III	C_1	-0.58	-0.58	-0.58	-0.58	-0.68
L_III	C_2	-0.19	-0.18	-0.19	-0.19	-0.45
L_III	C_3	0.40	0.42	0.40	0.41	-0.12
L_IV	NSC_0,14	0.03	0.04	0.03	0.04	-0.32
L_IV	NSC_0,25	0.80	0.82	0.80	0.82	0.13
L_V	HSC_0,14	-0.09	-0.07	-0.09	-0.08	-0.41

L_V	HSC_0,25	0.57	0.60	0.57	0.58	-0.05
L_VI	A_1	0.49	0.49	0.49	0.42	-0.19
L_VI	A_2	1.71	1.71	1.71	1.59	0.39
L_VII	B_1	-0.10	-0.10	-0.10	-0.14	-0.47
L_VII	B_2	0.62	0.62	0.62	0.55	-0.13
L_VII	B_3	1.31	1.31	1.31	1.21	0.20
L_VIII	C_1	-0.19	-0.19	-0.19	-0.22	-0.51
L_VIII	C_2	0.43	0.43	0.43	0.37	-0.21
L_IX	D_1	-0.46	-0.46	-0.46	-0.47	-0.64
L_IX	D_2	-0.12	-0.12	-0.12	-0.15	-0.48
L_IX	D_3	0.23	0.23	0.23	0.18	-0.31
L_X	A012-06	0.52	0.52	0.52	0.51	-0.03
L_X	A025-06	1.78	1.78	1.78	1.76	0.70
L_XI	A012-12	0.52	0.52	0.52	0.51	-0.03
L_XI	A025-12	1.78	1.78	1.78	1.76	0.70
L_XII	1ϕ8-2	0.63	0.63	0.63	0.59	0.01
L_XII	1ϕ8-3	0.63	0.63	0.63	0.59	0.01
L_XII	1ϕ8-4	0.63	0.63	0.63	0.59	0.01
L_XII	2ϕ8-1	2.08	2.08	2.08	2.01	0.84
L_XII	2ϕ8-2	2.08	2.08	2.08	2.01	0.84
L_XII	2ϕ8-3	2.08	2.08	2.08	2.01	0.84
L_XII	2ϕ8-4	2.08	2.08	2.08	2.01	0.84
L_XIII	B501	-0.02	-0.02	-0.02	-0.01	-0.34
L_XIII	B502	0.41	0.41	0.41	0.42	-0.09
L_XIV	B751	0.04	0.05	0.04	0.05	-0.31
L_XIV	B752	0.39	0.40	0.39	0.41	-0.10

L_XV	B1001	0.10	0.12	0.10	0.11	-0.29
L_XV	B1002	0.40	0.42	0.40	0.41	-0.12
L_XVI	A-4-9.8	-0.30	-0.29	-0.30	-0.30	-0.52
L_XVI	A-4-17.1	0.04	0.06	0.04	0.05	-0.32
L_XVII	A_012_06#1	-0.14	-0.14	-0.14	-0.14	-0.41
L_XVII	A_012_06#3	-0.14	-0.14	-0.14	-0.14	-0.41
L_XVII	A_025_06#1	0.47	0.47	0.47	0.47	-0.06
L_XVII	A_025_06#3	0.47	0.47	0.47	0.47	-0.06
L_XVIII	D1-R2X	-0.01	-0.01	-0.01	-0.02	-0.34
L_XVIII	D1-R3X	0.79	0.79	0.79	0.77	0.12
L_XIX	D2-R1X	-0.40	-0.40	-0.40	-0.41	-0.57
L_XIX	D2-R2X	-0.01	-0.01	-0.01	-0.02	-0.34
L_XX	D3-R1X	-0.40	-0.40	-0.40	-0.41	-0.57
L_XX	D3-R2X	-0.01	-0.01	-0.01	-0.02	-0.34

Appendix B: Hybrid Fiber-Reinforced Concrete (HRC) Database and Calculations

Table 6 Geometric and Material Properties of Hybrid Reinforced Concrete (HRC) Beams

Group	pBeam	H (mm)	B (mm)	d (mm)	f_c (Mpa)	f_y (Mpa)	A_s (mm^2)	V_f (%)	Lf/Φf	Ref.
H_1	S1_C30_A80_φ4_1	200	100	160	30	450	13	0.15	80.00	
H_1	S1_C30_A80_φ4_2	200	100	160	30	450	25	0.15	80.00	
H_1	S1_C30_A80_φ4_3	200	100	160	30	450	38	0.15	80.00	
H_2	S1_C30_A80_φ5_1	200	100	160	30	450	20	0.05	80.00	
H_2	S1_C30_A80_φ5_2	200	100	160	30	450	20	0.20	80.00	
H_2	S1_C30_A80_φ5_3	200	100	160	30	450	20	0.35	60.00	
H_3	S1_C30_A60_φ4_1	200	100	160	30	450	13	0.25	60.00	
H_3	S1_C30_A60_φ4_2	200	100	160	30	450	25	0.25	60.00	
H_3	S1_C30_A60_φ4_3	200	100	160	30	450	38	0.25	60.00	
H_4	S1_C30_A60_φ5_1	200	100	160	30	450	20	0.15	60.00	
H_4	S1_C30_A60_φ5_2	200	100	160	30	450	20	0.30	60.00	[6]
H_4	S1_C30_A60_φ5_3	200	100	160	30	450	20	0.45	40.00	
H_5	S1_C30_A40_φ4_1	200	100	160	30	450	13	0.30	40.00	
H_5	S1_C30_A40_φ4_2	200	100	160	30	450	25	0.30	40.00	
H_5	S1_C30_A40_φ4_3	200	100	160	30	450	38	0.30	40.00	
H_6	S1_C30_A40_φ5_1	200	100	160	30	450	20	0.10	40.00	
H_6	S1_C30_A40_φ5_2	200	100	160	30	450	20	0.40	40.00	
H_6	S1_C30_A40_φ5_3	200	100	160	30	450	20	0.70	80.00	
H_7	S1_C45_A80_φ5_1	200	100	160	45	450	20	0.15	80.00	
H_7	S1_C45_A80_φ5_2	200	100	160	45	450	39	0.15	80.00	
H_7	S1_C45_A80_φ5_3	200	100	160	45	450	59	0.15	80.00	
H_8	S1_C45_A80_φ6_1	200	100	160	45	450	28	0.10	80.00	

H_8	S1_C45_A80_φ6_2	200	100	160	45	450	28	0.25	80.00	
H_8	S1_C45_A80_φ6_3	200	100	160	45	450	28	0.40	60.00	
H_9	S1_C45_A60_φ5_1	200	100	160	45	450	20	0.10	60.00	
H_9	S1_C45_A60_φ5_2	200	100	160	45	450	39	0.10	60.00	
H_9	S1_C45_A60_φ5_3	200	100	160	45	450	59	0.10	60.00	
H_10	S1_C45_A60_φ6_1	200	100	160	45	450	28	0.05	60.00	
H_10	S1_C45_A60_φ6_2	200	100	160	45	450	28	0.25	60.00	
H_10	S1_C45_A60_φ6_3	200	100	160	45	450	28	0.45	40.00	
H_11	S1_C45_A40_φ5_1	200	100	160	45	450	20	0.15	40.00	
H_11	S1_C45_A40_φ5_2	200	100	160	45	450	39	0.15	40.00	
H_11	S1_C45_A40_φ5_3	200	100	160	45	450	59	0.15	40.00	
H_12	S1_C45_A40_φ6_1	200	100	160	45	450	28	0.10	40.00	
H_12	S1_C45_A40_φ6_2	200	100	160	45	450	28	0.40	40.00	
H_12	S1_C45_A40_φ6_3	200	100	160	45	450	28	0.70	80.00	[6]
H_13	S1_C60_A80_φ5_1	200	100	160	60	450	20	0.15	80.00	
H_13	S1_C60_A80_φ5_2	200	100	160	60	450	39	0.15	80.00	
H_13	S1_C60_A80_φ5_3	200	100	160	60	450	59	0.15	80.00	
H_14	S1_C60_A80_φ6_1	200	100	160	60	450	28	0.10	80.00	
H_14	S1_C60_A80_φ6_2	200	100	160	60	450	28	0.25	80.00	
H_14	S1_C60_A80_φ6_3	200	100	160	60	450	28	0.40	60.00	
H_15	S1_C60_A60_φ5_1	200	100	160	60	450	20	0.10	60.00	
H_15	S1_C60_A60_φ5_2	200	100	160	60	450	39	0.25	60.00	
H_15	S1_C60_A60_φ5_3	200	100	160	60	450	59	0.25	60.00	
H_16	S1_C60_A60_φ6_1	200	100	160	60	450	28	0.10	60.00	
H_16	S1_C60_A60_φ6_2	200	100	160	60	450	28	0.35	60.00	
H_16	S1_C60_A60_φ6_3	200	100	160	60	450	28	0.60	40.00	

H_17	S1_C60_A40_φ5_1	200	100	160	60	450	20	0.30	40.00	
H_17	S1_C60_A40_φ5_2	200	100	160	60	450	39	0.30	40.00	
H_17	S1_C60_A40_φ5_3	200	100	160	60	450	59	0.30	40.00	
H_18	S1_C60_A40_φ6_1	200	100	160	60	450	28	0.10	40.00	
H_18	S1_C60_A40_φ6_2	200	100	160	60	450	28	0.50	40.00	
H_18	S1_C60_A40_φ6_3	200	100	160	60	450	28	0.90	80.00	
H_19	S2_C30_A80_φ8_1	400	200	320	30	450	50	0.10	80.00	
H_19	S2_C30_A80_φ8_2	400	200	320	30	450	101	0.10	80.00	
H_19	S2_C30_A80_φ8_3	400	200	320	30	450	151	0.10	80.00	
H_20	S2_C30_A80_φ10_1	400	200	320	30	450	79	0.05	80.00	
H_20	S2_C30_A80_φ10_2	400	200	320	30	450	79	0.20	80.00	
H_20	S2_C30_A80_φ10_3	400	200	320	30	450	79	0.35	60.00	
H_21	S2_C30_A60_φ8_1	400	200	320	30	450	50	0.15	60.00	
H_21	S2_C30_A60_φ8_2	400	200	320	30	450	101	0.15	60.00	[6]
H_21	S2_C30_A60_φ8_3	400	200	320	30	450	151	0.15	60.00	
H_22	S2_C30_A60_φ10_1	400	200	320	30	450	79	0.05	60.00	
H_22	S2_C30_A60_φ10_2	400	200	320	30	450	79	0.20	60.00	
H_22	S2_C30_A60_φ10_3	400	200	320	30	450	79	0.35	40.00	
H_23	S2_C30_A40_φ8_1	400	200	320	30	450	50	0.35	40.00	
H_23	S2_C30_A40_φ8_2	400	200	320	30	450	101	0.35	40.00	
H_23	S2_C30_A40_φ8_3	400	200	320	30	450	151	0.35	40.00	
H_24	S2_C30_A40_φ10_1	400	200	320	30	450	79	0.10	40.00	
H_24	S2_C30_A40_φ10_2	400	200	320	30	450	79	0.50	40.00	
H_24	S2_C30_A40_φ10_3	400	200	320	30	450	79	0.90	80.00	
H_25	S2_C45_A80_φ8_1	400	200	320	45	450	50	0.15	80.00	
H_25	S2_C45_A80_φ8_2	400	200	320	45	450	151	0.15	80.00	

H_25	S2_C45_A80_φ8_3	400	200	320	45	450	251	0.15	80.00	
H_26	S2_C45_A80_φ10_1	400	200	320	45	450	79	0.10	80.00	
H_26	S2_C45_A80_φ10_2	400	200	320	45	450	79	0.35	80.00	
H_26	S2_C45_A80_φ10_3	400	200	320	45	450	79	0.60	60.00	
H_27	S2_C45_A60_φ8_1	400	200	320	45	450	50	0.10	60.00	
H_27	S2_C45_A60_φ8_2	400	200	320	45	450	151	0.10	60.00	
H_27	S2_C45_A60_φ8_3	400	200	320	45	450	251	0.10	60.00	
H_28	S2_C45_A60_φ10_1	400	200	320	45	450	79	0.10	60.00	
H_28	S2_C45_A60_φ10_2	400	200	320	45	450	79	0.45	60.00	
H_28	S2_C45_A60_φ10_3	400	200	320	45	450	79	0.80	40.00	
H_29	S2_C45_A40_φ8_1	400	200	320	45	450	50	0.10	40.00	
H_29	S2_C45_A40_φ8_2	400	200	320	45	450	151	0.10	40.00	[6]
H_29	S2_C45_A40_φ8_3	400	200	320	45	450	251	0.10	40.00	
H_30	S2_C45_A40_φ10_1	400	200	320	45	450	79	0.10	40.00	
H_30	S2_C45_A40_φ10_2	400	200	320	45	450	79	0.60	40.00	
H_30	S2_C45_A40_φ10_3	400	200	320	45	450	79	1.10	80.00	
H_31	S2_C60_A80_φ8_1	400	200	320	60	450	50	0.25	80.00	
H_31	S2_C60_A80_φ8_2	400	200	320	60	450	151	0.25	80.00	
H_31	S2_C60_A80_φ8_3	400	200	320	60	450	251	0.25	80.00	
H_32	S2_C60_A80_φ10_1	400	200	320	60	450	79	0.10	80.00	
H_32	S2_C60_A80_φ10_2	400	200	320	60	450	79	0.35	80.00	
H_32	S2_C60_A80_φ10_3	400	200	320	60	450	79	0.60	60.00	
H_33	S2_C60_A60_φ8_1	400	200	320	60	450	50	0.10	60.00	
H_33	S2_C60_A60_φ8_2	400	200	320	60	450	151	0.10	60.00	
H_33	S2_C60_A60_φ8_3	400	200	320	60	450	251	0.10	60.00	
H_34	S2_C60_A60_φ10_1	400	200	320	60	450	79	0.10	60.00	

H_34	S2_C60_A60_φ10_2	400	200	320	60	450	79	0.50	60.00	
H_34	S2_C60_A60_φ10_3	400	200	320	60	450	79	0.90	40.00	
H_35	S2_C60_A40_φ8_1	400	200	320	60	450	50	0.10	40.00	
H_35	S2_C60_A40_φ8_2	400	200	320	60	450	151	0.10	40.00	[6]
H_35	S2_C60_A40_φ8_3	400	200	320	60	450	251	0.10	40.00	
H_36	S2_C60_A40_φ10_1	400	200	320	60	450	79	0.10	40.00	
H_36	S2_C60_A40_φ10_2	400	200	320	60	450	79	0.75	40.00	
H_36	S2_C60_A40_φ10_3	400	200	320	60	450	79	1.40	80.00	

Table 7 Experimental Results and Theoretical Parameters of Hybrid Reinforced Concrete (HRC) Beams

Group	Beam	M_{cr}^{*} (Mpa)	M_u (Mpa)	$A_{s,min}$ (mm^2)	$V_{f,min}$ (%)	DI	r	Ref.
H_1	S1_C30_A80_φ4_1	2.73	2.05	36	0.44	-0.25	0.68	
H_1	S1_C30_A80_φ4_2	2.83	2.99	36	0.44	0.06	1.03	
H_1	S1_C30_A80_φ4_3	2.95	3.87	36	0.44	0.31	1.38	
H_2	S1_C30_A80_φ5_1	2.66	1.96	37	0.44	-0.26	0.65	
H_2	S1_C30_A80_φ5_2	2.78	2.78	37	0.44	0.00	0.98	
H_2	S1_C30_A80_φ5_3	2.90	3.61	37	0.44	0.24	1.32	
H_3	S1_C30_A60_φ4_1	2.76	2.25	36	0.59	-0.19	0.77	
H_3	S1_C30_A60_φ4_2	2.89	3.19	36	0.59	0.11	1.11	
H_3	S1_C30_A60_φ4_3	3.00	4.12	36	0.59	0.37	1.46	
H_4	S1_C30_A60_φ5_1	2.71	2.30	37	0.59	-0.15	0.79	
H_4	S1_C30_A60_φ5_2	2.82	2.94	37	0.59	0.04	1.04	
H_4	S1_C30_A60_φ5_3	2.93	3.55	37	0.59	0.21	1.29	
H_5	S1_C30_A40_φ4_1	2.77	2.04	36	0.90	-0.26	0.68	[6]
H_5	S1_C30_A40_φ4_2	2.86	2.98	36	0.90	0.04	1.02	
H_5	S1_C30_A40_φ4_3	2.98	3.86	36	0.90	0.29	1.37	
H_6	S1_C30_A40_φ5_1	2.66	1.95	37	0.90	-0.27	0.64	
H_6	S1_C30_A40_φ5_2	2.81	2.77	37	0.90	-0.02	0.98	
H_6	S1_C30_A40_φ5_3	3.00	3.60	37	0.90	0.20	1.31	
H_7	S1_C45_A80_φ5_1	3.59	2.77	48	0.48	-0.23	0.72	
H_7	S1_C45_A80_φ5_2	3.71	4.19	48	0.48	0.13	1.13	
H_7	S1_C45_A80_φ5_3	3.89	5.63	48	0.48	0.45	1.53	
H_8	S1_C45_A80_φ6_1	3.56	3.03	48	0.48	-0.15	0.79	
H_8	S1_C45_A80_φ6_2	3.64	4.02	48	0.48	0.10	1.11	
H_8	S1_C45_A80_φ6_3	3.79	4.98	48	0.48	0.32	1.42	
H_9	S1_C45_A60_φ5_1	3.53	2.23	48	0.64	-0.37	0.56	

H_9	S1_C45_A60_φ5_2	3.70	3.68	48	0.64	0.00	0.97	
H_9	S1_C45_A60_φ5_3	3.83	5.12	48	0.64	0.34	1.38	
H_10	S1_C45_A60_φ6_1	3.50	2.59	48	0.64	-0.26	0.66	
H_10	S1_C45_A60_φ6_2	3.64	3.59	48	0.64	-0.01	0.98	
H_10	S1_C45_A60_φ6_3	3.76	4.60	48	0.64	0.23	1.29	
H_11	S1_C45_A40_φ5_1	3.53	2.23	48	0.98	-0.37	0.56	
H_11	S1_C45_A40_φ5_2	3.70	3.68	48	0.98	-0.01	0.97	
H_11	S1_C45_A40_φ5_3	3.82	5.12	48	0.98	0.34	1.37	
H_12	S1_C45_A40_φ6_1	3.56	2.66	48	0.98	-0.25	0.69	
H_12	S1_C45_A40_φ6_2	3.69	3.67	48	0.98	-0.01	0.99	
H_12	S1_C45_A40_φ6_3	3.87	4.67	48	0.98	0.21	1.30	
H_13	S1_C60_A80_φ5_1	4.30	2.95	59	0.48	-0.31	0.64	
H_13	S1_C60_A80_φ5_2	4.45	4.41	59	0.48	-0.01	0.97	
H_13	S1_C60_A80_φ5_3	4.60	5.82	59	0.48	0.26	1.31	
H_14	S1_C60_A80_φ6_1	4.24	3.17	59	0.48	-0.25	0.69	
H_14	S1_C60_A80_φ6_2	4.35	4.34	59	0.48	0.00	1.00	
H_14	S1_C60_A80_φ6_3	4.44	5.48	59	0.48	0.23	1.31	
H_15	S1_C60_A60_φ5_1	4.31	3.24	59	0.65	-0.25	0.72	
H_15	S1_C60_A60_φ5_2	4.46	4.71	59	0.65	0.06	1.05	
H_15	S1_C60_A60_φ5_3	4.60	6.10	59	0.65	0.32	1.38	
H_16	S1_C60_A60_φ6_1	4.24	2.94	59	0.65	-0.31	0.63	
H_16	S1_C60_A60_φ6_2	4.35	4.44	59	0.65	0.02	1.02	[6]
H_16	S1_C60_A60_φ6_3	4.52	5.83	59	0.65	0.29	1.41	
H_17	S1_C60_A40_φ5_1	4.32	2.96	59	0.99	-0.32	0.64	
H_17	S1_C60_A40_φ5_2	4.45	4.40	59	0.99	-0.01	0.97	
H_17	S1_C60_A40_φ5_3	4.60	5.80	59	0.99	0.26	1.30	
H_18	S1_C60_A40_φ6_1	4.20	2.74	59	0.99	-0.35	0.58	
H_18	S1_C60_A40_φ6_2	4.43	4.31	59	0.99	-0.03	0.99	
H_18	S1_C60_A40_φ6_3	4.64	5.88	59	0.99	0.27	1.39	
H_19	S2_C30_A80_φ8_1	20.21	12.94	138	0.44	-0.36	0.59	
H_19	S2_C30_A80_φ8_2	20.79	20.40	138	0.44	-0.02	0.95	
H_19	S2_C30_A80_φ8_3	21.53	27.81	138	0.44	0.29	1.32	
H_20	S2_C30_A80_φ10_1	20.01	14.81	137	0.44	-0.26	0.69	
H_20	S2_C30_A80_φ10_2	20.72	20.78	137	0.44	0.00	1.03	
H_20	S2_C30_A80_φ10_3	21.65	26.66	137	0.44	0.23	1.37	
H_21	S2_C30_A60_φ8_1	20.40	13.67	138	0.59	-0.33	0.62	
H_21	S2_C30_A60_φ8_2	21.11	20.98	138	0.59	-0.01	0.98	
H_21	S2_C30_A60_φ8_3	21.66	28.33	138	0.59	0.31	1.34	
H_22	S2_C30_A60_φ10_1	19.84	14.31	137	0.59	-0.28	0.66	
H_22	S2_C30_A60_φ10_2	20.67	18.73	137	0.59	-0.09	0.91	
H_22	S2_C30_A60_φ10_3	21.38	23.06	137	0.59	0.08	1.17	
H_23	S2_C30_A40_φ8_1	21.07	16.02	138	0.90	-0.24	0.75	
H_23	S2_C30_A40_φ8_2	21.76	23.37	138	0.90	0.07	1.12	
H_23	S2_C30_A40_φ8_3	22.25	30.66	138	0.90	0.38	1.48	
H_24	S2_C30_A40_φ10_1	19.98	14.77	137	0.90	-0.26	0.69	
H_24	S2_C30_A40_φ10_2	21.58	22.49	137	0.90	0.04	1.13	

H_24	S2_C30_A40_φ10_3	23.49	30.45	137	0.90	0.30	1.57	
H_25	S2_C45_A80_φ8_1	27.24	16.96	187	0.48	-0.38	0.58	
H_25	S2_C45_A80_φ8_2	28.48	31.61	187	0.48	0.11	1.12	
H_25	S2_C45_A80_φ8_3	29.79	46.32	187	0.48	0.55	1.66	
H_26	S2_C45_A80_φ10_1	26.62	18.23	184	0.48	-0.32	0.64	
H_26	S2_C45_A80_φ10_2	28.10	30.77	184	0.48	0.10	1.16	
H_26	S2_C45_A80_φ10_3	29.83	43.01	184	0.48	0.44	1.68	
H_27	S2_C45_A60_φ8_1	26.70	12.90	187	0.64	-0.52	0.42	
H_27	S2_C45_A60_φ8_2	27.95	27.95	187	0.64	0.00	0.96	
H_27	S2_C45_A60_φ8_3	29.46	42.65	187	0.64	0.45	1.50	
H_28	S2_C45_A60_φ10_1	26.57	16.87	184	0.64	-0.37	0.58	
H_28	S2_C45_A60_φ10_2	28.35	30.01	184	0.64	0.06	1.13	
H_28	S2_C45_A60_φ10_3	30.25	43.01	184	0.64	0.42	1.68	
H_29	S2_C45_A40_φ8_1	26.69	14.68	187	0.98	-0.45	0.37	
H_29	S2_C45_A40_φ8_2	27.93	26.47	187	0.98	-0.05	0.91	
H_29	S2_C45_A40_φ8_3	29.19	41.37	187	0.98	0.42	1.44	
H_30	S2_C45_A40_φ10_1	26.55	15.42	184	0.98	-0.42	0.53	
H_30	S2_C45_A40_φ10_2	28.51	28.10	184	0.98	-0.01	1.04	
H_30	S2_C45_A40_φ10_3	30.67	40.56	184	0.98	0.32	1.55	
H_31	S2_C60_A80_φ8_1	32.73	24.71	224	0.49	-0.25	0.74	[6]
H_31	S2_C60_A80_φ8_2	34.24	39.49	224	0.49	0.15	1.19	
H_31	S2_C60_A80_φ8_3	35.43	53.65	224	0.49	0.51	1.63	
H_32	S2_C60_A80_φ10_1	31.82	19.37	221	0.49	-0.39	0.56	
H_32	S2_C60_A80_φ10_2	33.28	34.15	221	0.49	0.03	1.07	
H_32	S2_C60_A80_φ10_3	34.87	48.78	221	0.49	0.40	1.59	
H_33	S2_C60_A60_φ8_1	32.02	13.77	224	0.65	-0.57	0.38	
H_33	S2_C60_A60_φ8_2	33.45	28.80	224	0.65	-0.14	0.83	
H_33	S2_C60_A60_φ8_3	34.57	43.44	224	0.65	0.26	1.28	
H_34	S2_C60_A60_φ10_1	31.80	17.68	221	0.65	-0.44	0.51	
H_34	S2_C60_A60_φ10_2	33.57	35.41	221	0.65	0.06	1.13	
H_34	S2_C60_A60_φ10_3	35.68	52.87	221	0.65	0.48	1.75	
H_35	S2_C60_A40_φ8_1	31.99	12.19	224	0.99	-0.62	0.32	
H_35	S2_C60_A40_φ8_2	33.43	27.28	224	0.99	-0.18	0.77	
H_35	S2_C60_A40_φ8_3	34.50	42.10	224	0.99	0.22	1.22	
H_36	S2_C60_A40_φ10_1	31.75	17.03	221	0.99	-0.46	0.46	
H_36	S2_C60_A40_φ10_2	34.11	35.23	221	0.99	0.03	1.11	
H_36	S2_C60_A40_φ10_3	37.14	54.34	221	0.99	0.46	1.76	

Table 8 Minimum Reinforcement Area ($As_{, min}$) Requirements Across International Codes for Evaluated HRC Elements

Group	Beam	$EC2004$ (mm^2)	$EC2023$ (mm^2)	$MC2010$ (mm^2)	$MC2020$ (mm^2)	$ACI318$ (mm^2)
H_1	S1_C30_A80_φ4_1	26.78	102.99	-13.86	-9.39	49.03
H_1	S1_C30_A80_φ4_2	26.78	102.99	-13.86	-9.39	49.03
H_1	S1_C30_A80_φ4_3	26.78	102.99	-13.86	-9.39	49.03
H_2	S1_C30_A80_φ5_1	26.78	102.99	64.04	68.51	49.03
H_2	S1_C30_A80_φ5_2	26.78	102.99	-52.81	-48.34	49.03
H_2	S1_C30_A80_φ5_3	26.78	102.99	-169.66	-165.19	49.03
H_3	S1_C30_A60_φ4_1	26.78	102.99	-43.07	-38.60	49.03
H_3	S1_C30_A60_φ4_2	26.78	102.99	-43.07	-38.60	49.03
H_3	S1_C30_A60_φ4_3	26.78	102.99	-43.07	-38.60	49.03
H_4	S1_C30_A60_φ5_1	26.78	102.99	15.35	19.82	49.03
H_4	S1_C30_A60_φ5_2	26.78	102.99	-72.29	-67.82	49.03
H_4	S1_C30_A60_φ5_3	26.78	102.99	-159.92	-155.45	49.03
H_5	S1_C30_A40_φ4_1	26.78	102.99	-13.86	-9.39	49.03
H_5	S1_C30_A40_φ4_2	26.78	102.99	-13.86	-9.39	49.03
H_5	S1_C30_A40_φ4_3	26.78	102.99	-13.86	-9.39	49.03
H_6	S1_C30_A40_φ5_1	26.78	102.99	64.04	68.51	49.03
H_6	S1_C30_A40_φ5_2	26.78	102.99	-52.81	-48.34	49.03
H_6	S1_C30_A40_φ5_3	26.78	102.99	-169.66	-165.19	49.03
H_7	S1_C45_A80_φ5_1	35.09	134.95	-8.16	-9.70	59.41
H_7	S1_C45_A80_φ5_2	35.09	134.95	-8.16	-9.70	59.41
H_7	S1_C45_A80_φ5_3	35.09	134.95	-8.16	-9.70	59.41
H_8	S1_C45_A80_φ6_1	35.09	134.95	39.54	38.00	59.41
H_8	S1_C45_A80_φ6_2	35.09	134.95	-103.56	-105.11	59.41

H_8	S1_C45_A80_φ6_3	35.09	134.95	-246.67	-248.22	59.41
H_9	S1_C45_A60_φ5_1	35.09	134.95	63.40	61.85	59.41
H_9	S1_C45_A60_φ5_2	35.09	134.95	63.40	61.85	59.41
H_9	S1_C45_A60_φ5_3	35.09	134.95	63.40	61.85	59.41
H_10	S1_C45_A60_φ6_1	35.09	134.95	99.17	97.63	59.41
H_10	S1_C45_A60_φ6_2	35.09	134.95	-43.94	-45.48	59.41
H_10	S1_C45_A60_φ6_3	35.09	134.95	-187.04	-188.59	59.41
H_11	S1_C45_A40_φ5_1	35.09	134.95	63.40	61.85	59.41
H_11	S1_C45_A40_φ5_2	35.09	134.95	63.40	61.85	59.41
H_11	S1_C45_A40_φ5_3	35.09	134.95	63.40	61.85	59.41
H_12	S1_C45_A40_φ6_1	35.09	134.95	87.25	85.70	59.41
H_12	S1_C45_A40_φ6_2	35.09	134.95	-55.86	-57.41	59.41
H_12	S1_C45_A40_φ6_3	35.09	134.95	-198.97	-200.52	59.41
H_13	S1_C60_A80_φ5_1	40.26	153.11	-10.41	-13.43	68.61
H_13	S1_C60_A80_φ5_2	40.26	153.11	-10.41	-13.43	68.61
H_13	S1_C60_A80_φ5_3	40.26	153.11	-10.41	-13.43	68.61
H_14	S1_C60_A80_φ6_1	40.26	153.11	44.67	41.65	68.61
H_14	S1_C60_A80_φ6_2	40.26	153.11	-120.58	-123.60	68.61
H_14	S1_C60_A80_φ6_3	40.26	153.11	-285.82	-288.84	68.61
H_15	S1_C60_A60_φ5_1	40.26	153.11	72.21	69.19	68.61
H_15	S1_C60_A60_φ5_2	40.26	153.11	-51.72	-54.74	68.61
H_15	S1_C60_A60_φ5_3	40.26	153.11	-51.72	-54.74	68.61
H_16	S1_C60_A60_φ6_1	40.26	153.11	72.21	69.19	68.61
H_16	S1_C60_A60_φ6_2	40.26	153.11	-134.35	-137.37	68.61
H_16	S1_C60_A60_φ6_3	40.26	153.11	-340.91	-343.93	68.61
H_17	S1_C60_A40_φ5_1	40.26	153.11	-10.41	-13.43	68.61

H_17	S1_C60_A40_φ5_2	40.26	153.11	-10.41	-13.43	68.61
H_17	S1_C60_A40_φ5_3	40.26	153.11	-10.41	-13.43	68.61
H_18	S1_C60_A40_φ6_1	40.26	153.11	99.75	96.73	68.61
H_18	S1_C60_A40_φ6_2	40.26	153.11	-120.58	-123.60	68.61
H_18	S1_C60_A40_φ6_3	40.26	153.11	-340.91	-343.93	68.61
H_19	S2_C30_A80_φ8_1	107.10	411.94	93.32	109.95	196.12
H_19	S2_C30_A80_φ8_2	107.10	411.94	93.32	109.95	196.12
H_19	S2_C30_A80_φ8_3	107.10	411.94	93.32	109.95	196.12
H_20	S2_C30_A80_φ10_1	107.10	411.94	238.22	254.84	196.12
H_20	S2_C30_A80_φ10_2	107.10	411.94	-196.46	-179.83	196.12
H_20	S2_C30_A80_φ10_3	107.10	411.94	-631.13	-614.51	196.12
H_21	S2_C30_A60_φ8_1	107.10	411.94	57.10	73.73	196.12
H_21	S2_C30_A60_φ8_2	107.10	411.94	57.10	73.73	196.12
H_21	S2_C30_A60_φ8_3	107.10	411.94	57.10	73.73	196.12
H_22	S2_C30_A60_φ10_1	107.10	411.94	274.44	291.06	196.12
H_22	S2_C30_A60_φ10_2	107.10	411.94	-51.57	-34.94	196.12
H_22	S2_C30_A60_φ10_3	107.10	411.94	-377.57	-360.95	196.12
H_23	S2_C30_A40_φ8_1	107.10	411.94	-124.01	-107.39	196.12
H_23	S2_C30_A40_φ8_2	107.10	411.94	-124.01	-107.39	196.12
H_23	S2_C30_A40_φ8_3	107.10	411.94	-124.01	-107.39	196.12
H_24	S2_C30_A40_φ10_1	107.10	411.94	238.22	254.84	196.12
H_24	S2_C30_A40_φ10_2	107.10	411.94	-341.35	-324.72	196.12
H_24	S2_C30_A40_φ10_3	107.10	411.94	-920.91	-904.29	196.12
H_25	S2_C45_A80_φ8_1	140.35	539.80	-30.35	-36.10	237.66
H_25	S2_C45_A80_φ8_2	140.35	539.80	-30.35	-36.10	237.66
H_25	S2_C45_A80_φ8_3	140.35	539.80	-30.35	-36.10	237.66

H_26	S2_C45_A80_φ10_1	140.35	539.80	147.10	141.35	237.66
H_26	S2_C45_A80_φ10_2	140.35	539.80	-740.17	-745.92	237.66
H_26	S2_C45_A80_φ10_3	140.35	539.80	-1627.44	-1633.19	237.66
H_27	S2_C45_A60_φ8_1	140.35	539.80	235.83	230.08	237.66
H_27	S2_C45_A60_φ8_2	140.35	539.80	235.83	230.08	237.66
H_27	S2_C45_A60_φ8_3	140.35	539.80	235.83	230.08	237.66
H_28	S2_C45_A60_φ10_1	140.35	539.80	235.83	230.08	237.66
H_28	S2_C45_A60_φ10_2	140.35	539.80	-695.81	-701.55	237.66
H_28	S2_C45_A60_φ10_3	140.35	539.80	-1627.44	-1633.19	237.66
H_29	S2_C45_A40_φ8_1	140.35	539.80	324.56	318.81	237.66
H_29	S2_C45_A40_φ8_2	140.35	539.80	324.56	318.81	237.66
H_29	S2_C45_A40_φ8_3	140.35	539.80	324.56	318.81	237.66
H_30	S2_C45_A40_φ10_1	140.35	539.80	324.56	318.81	237.66
H_30	S2_C45_A40_φ10_2	140.35	539.80	-562.72	-568.46	237.66
H_30	S2_C45_A40_φ10_3	140.35	539.80	-1449.99	-1455.73	237.66
H_31	S2_C60_A80_φ8_1	161.03	612.46	-448.55	-459.78	274.42
H_31	S2_C60_A80_φ8_2	161.03	612.46	-448.55	-459.78	274.42
H_31	S2_C60_A80_φ8_3	161.03	612.46	-448.55	-459.78	274.42
H_32	S2_C60_A80_φ10_1	161.03	612.46	166.17	154.94	274.42
H_32	S2_C60_A80_φ10_2	161.03	612.46	-858.36	-869.59	274.42
H_32	S2_C60_A80_φ10_3	161.03	612.46	-1882.89	-1894.12	274.42
H_33	S2_C60_A60_φ8_1	161.03	612.46	268.63	257.39	274.42
H_33	S2_C60_A60_φ8_2	161.03	612.46	268.63	257.39	274.42
H_33	S2_C60_A60_φ8_3	161.03	612.46	268.63	257.39	274.42
H_34	S2_C60_A60_φ10_1	161.03	612.46	268.63	257.39	274.42
H_34	S2_C60_A60_φ10_2	161.03	612.46	-960.81	-972.04	274.42

H_34	S2_C60_A60_φ10_3	161.03	612.46	-2190.25	-2201.48	274.42
H_35	S2_C60_A40_φ8_1	161.03	612.46	371.08	359.85	274.42
H_35	S2_C60_A40_φ8_2	161.03	612.46	371.08	359.85	274.42
H_35	S2_C60_A40_φ8_3	161.03	612.46	371.08	359.85	274.42
H_36	S2_C60_A40_φ10_1	161.03	612.46	371.08	359.85	274.42
H_36	S2_C60_A40_φ10_2	161.03	612.46	-960.81	-972.04	274.42
H_36	S2_C60_A40_φ10_3	161.03	612.46	-2292.71	-2303.94	274.42

Table 9 Non-Dimensional Reinforcement Ratio (r) Based on Building codes $A_{s,\,min}$ Provisions for HRC Elements

Group	Beam	$EC2004$	$EC2023$	$MC2010$	$MC2020$	$ACI318$
H_1	S1_C30_A80_φ4_1	0.83	0.47	-0.60	0.89	0.61
H_1	S1_C30_A80_φ4_2	1.27	0.58	-1.46	1.36	0.85
H_1	S1_C30_A80_φ4_3	1.76	0.71	-2.40	1.79	1.12
H_2	S1_C30_A80_φ5_1	0.86	0.31	0.43	0.72	0.52
H_2	S1_C30_A80_φ5_2	1.20	0.65	0.08	1.40	0.86
H_2	S1_C30_A80_φ5_3	1.54	0.99	0.68	2.11	1.20
H_3	S1_C30_A60_φ4_1	0.91	0.55	0.12	0.90	0.69
H_3	S1_C30_A60_φ4_2	1.36	0.67	-0.16	1.35	0.93
H_3	S1_C30_A60_φ4_3	1.84	0.79	-0.46	1.80	1.20
H_4	S1_C30_A60_φ5_1	1.00	0.45	1.56	0.71	0.66
H_4	S1_C30_A60_φ5_2	1.26	0.70	0.23	1.40	0.92
H_4	S1_C30_A60_φ5_3	1.51	0.96	0.64	2.11	1.17
H_5	S1_C30_A40_φ4_1	0.82	0.46	-0.60	1.12	0.60
H_5	S1_C30_A40_φ4_2	1.27	0.58	-1.47	1.70	0.84

H_5	S1_C30_A40_φ4_3	1.75	0.70	-2.41	2.28	1.11
H_6	S1_C30_A40_φ5_1	0.86	0.31	0.42	0.81	0.52
H_6	S1_C30_A40_φ5_2	1.19	0.64	0.07	1.64	0.85
H_6	S1_C30_A40_φ5_3	1.52	0.97	0.66	2.45	1.19
H_7	S1_C45_A80_φ5_1	0.88	0.46	-2.14	0.73	0.65
H_7	S1_C45_A80_φ5_2	1.42	0.60	-4.47	1.45	0.97
H_7	S1_C45_A80_φ5_3	1.99	0.75	-6.92	2.18	1.31
H_8	S1_C45_A80_φ6_1	1.01	0.42	0.92	1.13	0.68
H_8	S1_C45_A80_φ6_2	1.32	0.73	0.25	1.70	0.99
H_8	S1_C45_A80_φ6_3	1.63	1.04	0.72	2.26	1.30
H_9	S1_C45_A60_φ5_1	0.73	0.30	0.47	0.99	0.49
H_9	S1_C45_A60_φ5_2	1.27	0.45	0.77	1.49	0.81
H_9	S1_C45_A60_φ5_3	1.84	0.59	1.09	2.00	1.15
H_10	S1_C45_A60_φ6_1	0.88	0.29	0.36	0.71	0.55
H_10	S1_C45_A60_φ6_2	1.19	0.60	-0.25	1.44	0.86
H_10	S1_C45_A60_φ6_3	1.50	0.91	0.55	2.15	1.17
H_11	S1_C45_A40_φ5_1	0.72	0.30	0.47	1.27	0.49
H_11	S1_C45_A40_φ5_2	1.26	0.44	0.77	1.59	0.81
H_11	S1_C45_A40_φ5_3	1.83	0.59	1.08	1.91	1.15
H_12	S1_C45_A40_φ6_1	0.90	0.31	0.42	0.99	0.57
H_12	S1_C45_A40_φ6_2	1.21	0.62	-0.09	1.49	0.88
H_12	S1_C45_A40_φ6_3	1.51	0.92	0.57	1.99	1.19
H_13	S1_C60_A80_φ5_1	0.81	0.44	-1.61	0.57	0.60
H_13	S1_C60_A80_φ5_2	1.28	0.57	-3.43	1.52	0.88
H_13	S1_C60_A80_φ5_3	1.78	0.70	-5.35	0.39	1.17
H_14	S1_C60_A80_φ6_1	0.90	0.39	0.84	1.15	0.62

H_14	S1_C60_A80_φ6_2	1.22	0.70	0.29	0.27	0.93
H_14	S1_C60_A80_φ6_3	1.53	1.02	0.74	0.77	1.24
H_15	S1_C60_A60_φ5_1	0.65	0.28	0.43	1.52	0.45
H_15	S1_C60_A60_φ5_2	1.35	0.64	-0.37	1.05	0.95
H_15	S1_C60_A60_φ5_3	1.85	0.77	-0.76	2.03	1.24
H_16	S1_C60_A60_φ6_1	0.85	0.34	0.54	0.90	0.56
H_16	S1_C60_A60_φ6_2	1.23	0.72	0.33	1.72	0.95
H_16	S1_C60_A60_φ6_3	1.62	1.11	0.84	1.53	1.33
H_17	S1_C60_A40_φ5_1	0.80	0.43	-1.62	2.99	0.59
H_17	S1_C60_A40_φ5_2	1.27	0.56	-3.44	0.83	0.87
H_17	S1_C60_A40_φ5_3	1.77	0.69	-5.36	1.69	1.16
H_18	S1_C60_A40_φ6_1	0.80	0.28	0.38	2.51	0.51
H_18	S1_C60_A40_φ6_2	1.20	0.69	0.27	0.73	0.91
H_18	S1_C60_A40_φ6_3	1.60	1.09	0.83	1.47	1.32
H_19	S2_C30_A80_φ8_1	0.69	0.35	0.76	0.41	0.48
H_19	S2_C30_A80_φ8_2	1.17	0.47	1.31	0.81	0.74
H_19	S2_C30_A80_φ8_3	1.64	0.59	1.85	1.22	1.00
H_20	S2_C30_A80_φ10_1	0.85	0.31	0.45	1.64	0.52
H_20	S2_C30_A80_φ10_2	1.19	0.65	0.05	3.20	0.86
H_20	S2_C30_A80_φ10_3	1.53	0.99	0.67	1.64	1.20
H_21	S2_C30_A60_φ8_1	0.72	0.38	1.13	3.20	0.51
H_21	S2_C30_A60_φ8_2	1.20	0.50	2.02	1.74	0.77
H_21	S2_C30_A60_φ8_3	1.66	0.62	2.90	1.74	1.02
H_22	S2_C30_A60_φ10_1	0.82	0.28	0.37	1.74	0.49
H_22	S2_C30_A60_φ10_2	1.08	0.53	-1.19	3.51	0.74
H_22	S2_C30_A60_φ10_3	1.33	0.78	0.38	3.51	1.00

H_23	S2_C30_A40_φ8_1	0.86	0.51	-0.01	3.51	0.64
H_23	S2_C30_A40_φ8_2	1.33	0.63	-0.43	3.51	0.90
H_23	S2_C30_A40_φ8_3	1.80	0.76	-0.83	0.98	1.16
H_24	S2_C30_A40_φ10_1	0.85	0.30	0.44	1.52	0.51
H_24	S2_C30_A40_φ10_2	1.29	0.75	0.32	1.07	0.96
H_24	S2_C30_A40_φ10_3	1.74	1.19	0.91	1.52	1.40
H_25	S2_C45_A80_φ8_1	0.67	0.41	-1.33	1.14	0.52
H_25	S2_C45_A80_φ8_2	1.39	0.59	-4.66	1.51	0.95
H_25	S2_C45_A80_φ8_3	2.10	0.78	-7.96	0.63	1.37
H_26	S2_C45_A80_φ10_1	0.77	0.35	0.75	1.07	0.54
H_26	S2_C45_A80_φ10_2	1.29	0.88	0.62	0.83	1.06
H_26	S2_C45_A80_φ10_3	1.81	1.40	1.20	0.83	1.58
H_27	S2_C45_A60_φ8_1	0.51	0.25	0.37	1.59	0.37
H_27	S2_C45_A60_φ8_2	1.23	0.44	0.80	1.59	0.79
H_27	S2_C45_A60_φ8_3	1.94	0.62	1.22	0.98	1.21
H_28	S2_C45_A60_φ10_1	0.72	0.30	0.49	1.96	0.49
H_28	S2_C45_A60_φ10_2	1.27	0.85	0.59	0.49	1.04
H_28	S2_C45_A60_φ10_3	1.81	1.40	1.20	0.98	1.58
H_29	S2_C45_A40_φ8_1	0.46	0.19	0.26	0.49	0.31
H_29	S2_C45_A40_φ8_2	1.18	0.38	0.57	0.98	0.74
H_29	S2_C45_A40_φ8_3	1.89	0.57	0.88	0.57	1.16
H_30	S2_C45_A40_φ10_1	0.66	0.25	0.35	1.52	0.43
H_30	S2_C45_A40_φ10_2	1.18	0.76	0.47	0.39	0.94
H_30	S2_C45_A40_φ10_3	1.69	1.27	1.07	1.15	1.45
H_31	S2_C60_A80_φ8_1	0.82	0.59	0.40	0.27	0.69
H_31	S2_C60_A80_φ8_2	1.45	0.76	0.17	0.77	1.06

H_31	S2_C60_A80_φ8_3	2.07	0.92	-0.05	1.52	1.42
H_32	S2_C60_A80_φ10_1	0.69	0.33	0.68	1.05	0.49
H_32	S2_C60_A80_φ10_2	1.20	0.84	0.62	2.03	1.00
H_32	S2_C60_A80_φ10_3	1.72	1.35	1.18	0.90	1.51
H_33	S2_C60_A60_φ8_1	0.46	0.24	0.34	1.72	0.34
H_33	S2_C60_A60_φ8_2	1.09	0.40	0.72	1.53	0.70
H_33	S2_C60_A60_φ8_3	1.71	0.56	1.09	2.99	1.07
H_34	S2_C60_A60_φ10_1	0.64	0.28	0.45	0.83	0.44
H_34	S2_C60_A60_φ10_2	1.26	0.90	0.69	1.69	1.06
H_34	S2_C60_A60_φ10_3	1.88	1.51	1.35	2.51	1.67
H_35	S2_C60_A40_φ8_1	0.41	0.18	0.24	0.73	0.28
H_35	S2_C60_A40_φ8_2	1.04	0.35	0.51	1.47	0.65
H_35	S2_C60_A40_φ8_3	1.66	0.51	0.78	0.41	1.02
H_36	S2_C60_A40_φ10_1	0.59	0.23	0.31	0.81	0.39
H_36	S2_C60_A40_φ10_2	1.25	0.89	0.68	1.22	1.05
H_36	S2_C60_A40_φ10_3	1.90	1.54	1.38	1.64	1.70

Table 10 Ductility Index (DI) for HRC Elements Across Evaluated Building Codes

Group	Beam	$EC2004$	$EC2023$	$MC2010$	$MC2020$	$ACI318$
H_1	S1_C30_A80_φ4_1	-0.14	-0.43	-2.03	-2.74	-0.39
H_1	S1_C30_A80_φ4_2	0.22	-0.33	-3.41	-4.79	-0.15
H_1	S1_C30_A80_φ4_3	0.61	-0.23	-4.91	-7.00	0.12
H_2	S1_C30_A80_φ5_1	-0.11	-0.55	-0.21	-0.24	-0.48
H_2	S1_C30_A80_φ5_2	0.16	-0.28	-1.04	-1.10	-0.14
H_2	S1_C30_A80_φ5_3	0.43	-0.01	-0.35	-0.36	0.20

H_3	S1_C30_A60_φ4_1	-0.07	-0.36	-0.94	-1.00	-0.31
H_3	S1_C30_A60_φ4_2	0.29	-0.27	-1.39	-1.50	-0.07
H_3	S1_C30_A60_φ4_3	0.67	-0.17	-1.87	-2.04	0.20
H_4	S1_C30_A60_φ5_1	0.00	-0.44	1.49	1.02	-0.34
H_4	S1_C30_A60_φ5_2	0.20	-0.24	-0.84	-0.87	-0.08
H_4	S1_C30_A60_φ5_3	0.41	-0.03	-0.39	-0.40	0.17
H_5	S1_C30_A40_φ4_1	-0.14	-0.43	-2.03	-2.75	-0.40
H_5	S1_C30_A40_φ4_2	0.21	-0.34	-3.42	-4.79	-0.16
H_5	S1_C30_A40_φ4_3	0.60	-0.24	-4.92	-7.01	0.11
H_6	S1_C30_A40_φ5_1	-0.11	-0.56	-0.21	-0.24	-0.48
H_6	S1_C30_A40_φ5_2	0.15	-0.29	-1.05	-1.11	-0.15
H_6	S1_C30_A40_φ5_3	0.42	-0.02	-0.37	-0.37	0.19
H_7	S1_C45_A80_φ5_1	-0.09	-0.43	-4.47	-3.85	-0.35
H_7	S1_C45_A80_φ5_2	0.34	-0.32	-8.20	-6.98	-0.03
H_7	S1_C45_A80_φ5_3	0.80	-0.20	-12.12	-10.28	0.31
H_8	S1_C45_A80_φ6_1	0.01	-0.47	0.50	0.55	-0.32
H_8	S1_C45_A80_φ6_2	0.26	-0.22	-0.82	-0.81	-0.01
H_8	S1_C45_A80_φ6_3	0.51	0.03	-0.31	-0.31	0.30
H_9	S1_C45_A60_φ5_1	-0.22	-0.56	-0.17	-0.16	-0.51
H_9	S1_C45_A60_φ5_2	0.21	-0.44	0.31	0.33	-0.19
H_9	S1_C45_A60_φ5_3	0.67	-0.33	0.81	0.85	0.15
H_10	S1_C45_A60_φ6_1	-0.10	-0.57	-0.29	-0.28	-0.45
H_10	S1_C45_A60_φ6_2	0.15	-0.32	-1.51	-1.47	-0.14
H_10	S1_C45_A60_φ6_3	0.40	-0.07	-0.48	-0.48	0.17
H_11	S1_C45_A40_φ5_1	-0.22	-0.56	-0.17	-0.16	-0.51
H_11	S1_C45_A40_φ5_2	0.21	-0.45	0.31	0.33	-0.19

H_11	S1_C45_A40_φ5_3	0.67	-0.33	0.81	0.85	0.15
H_12	S1_C45_A40_φ6_1	-0.08	-0.55	-0.20	-0.20	-0.43
H_12	S1_C45_A40_φ6_2	0.16	-0.31	-1.28	-1.25	-0.12
H_12	S1_C45_A40_φ6_3	0.41	-0.06	-0.45	-0.45	0.19
H_13	S1_C60_A80_φ5_1	-0.15	-0.45	-3.62	-2.93	-0.40
H_13	S1_C60_A80_φ5_2	0.23	-0.35	-6.54	-5.20	-0.12
H_13	S1_C60_A80_φ5_3	0.62	-0.24	-9.62	-7.58	0.17
H_14	S1_C60_A80_φ6_1	-0.08	-0.49	0.37	0.44	-0.38
H_14	S1_C60_A80_φ6_2	0.17	-0.24	-0.75	-0.75	-0.07
H_14	S1_C60_A80_φ6_3	0.42	0.01	-0.29	-0.29	0.24
H_15	S1_C60_A60_φ5_1	-0.28	-0.57	-0.23	-0.21	-0.55
H_15	S1_C60_A60_φ5_2	0.28	-0.29	-1.70	-1.63	-0.05
H_15	S1_C60_A60_φ5_3	0.68	-0.18	-2.32	-2.22	0.24
H_16	S1_C60_A60_φ6_1	-0.12	-0.53	-0.06	-0.03	-0.44
H_16	S1_C60_A60_φ6_2	0.19	-0.22	-0.70	-0.70	-0.05
H_16	S1_C60_A60_φ6_3	0.49	0.08	-0.19	-0.19	0.33
H_17	S1_C60_A40_φ5_1	-0.16	-0.45	-3.63	-2.94	-0.41
H_17	S1_C60_A40_φ5_2	0.22	-0.35	-6.55	-5.20	-0.13
H_17	S1_C60_A40_φ5_3	0.61	-0.25	-9.62	-7.59	0.16
H_18	S1_C60_A40_φ6_1	-0.16	-0.57	-0.27	-0.26	-0.49
H_18	S1_C60_A40_φ6_2	0.16	-0.25	-0.77	-0.76	-0.09
H_18	S1_C60_A40_φ6_3	0.48	0.07	-0.20	-0.20	0.32
H_19	S2_C30_A80_φ8_1	-0.24	-0.52	0.24	0.11	-0.52
H_19	S2_C30_A80_φ8_2	0.14	-0.42	1.11	0.85	-0.26
H_19	S2_C30_A80_φ8_3	0.51	-0.32	1.97	1.58	0.00
H_20	S2_C30_A80_φ10_1	-0.12	-0.56	-0.18	-0.21	-0.48

H_20	S2_C30_A80_φ10_2	0.15	-0.28	-1.08	-1.14	-0.14
H_20	S2_C30_A80_φ10_3	0.43	-0.01	-0.36	-0.37	0.20
H_21	S2_C30_A60_φ8_1	-0.22	-0.50	0.80	0.49	-0.49
H_21	S2_C30_A60_φ8_2	0.16	-0.40	2.23	1.60	-0.23
H_21	S2_C30_A60_φ8_3	0.53	-0.30	3.63	2.68	0.02
H_22	S2_C30_A60_φ10_1	-0.14	-0.58	-0.27	-0.30	-0.51
H_22	S2_C30_A60_φ10_2	0.06	-0.38	-2.98	-4.15	-0.26
H_22	S2_C30_A60_φ10_3	0.26	-0.17	-0.66	-0.68	0.00
H_23	S2_C30_A40_φ8_1	-0.12	-0.39	-1.13	-1.23	-0.36
H_23	S2_C30_A40_φ8_2	0.27	-0.29	-1.79	-1.99	-0.10
H_23	S2_C30_A40_φ8_3	0.64	-0.20	-2.44	-2.74	0.16
H_24	S2_C30_A40_φ10_1	-0.12	-0.56	-0.18	-0.22	-0.49
H_24	S2_C30_A40_φ10_2	0.23	-0.20	-0.73	-0.74	-0.04
H_24	S2_C30_A40_φ10_3	0.59	0.15	-0.14	-0.14	0.40
H_25	S2_C45_A80_φ8_1	-0.26	-0.48	-3.19	-2.77	-0.48
H_25	S2_C45_A80_φ8_2	0.31	-0.33	-8.51	-7.24	-0.05
H_25	S2_C45_A80_φ8_3	0.88	-0.18	-13.78	-11.67	0.37
H_26	S2_C45_A80_φ10_1	-0.18	-0.52	0.23	0.26	-0.46
H_26	S2_C45_A80_φ10_2	0.23	-0.10	-0.39	-0.39	0.06
H_26	S2_C45_A80_φ10_3	0.65	0.32	0.12	0.12	0.58
H_27	S2_C45_A60_φ8_1	-0.39	-0.60	-0.34	-0.33	-0.63
H_27	S2_C45_A60_φ8_2	0.19	-0.45	0.35	0.38	-0.21
H_27	S2_C45_A60_φ8_3	0.76	-0.30	1.03	1.07	0.21
H_28	S2_C45_A60_φ10_1	-0.22	-0.56	-0.14	-0.13	-0.51
H_28	S2_C45_A60_φ10_2	0.21	-0.12	-0.42	-0.42	0.04
H_28	S2_C45_A60_φ10_3	0.65	0.32	0.12	0.12	0.58

H_29	S2_C45_A40_φ8_1	-0.43	-0.64	-0.47	-0.47	-0.69
H_29	S2_C45_A40_φ8_2	0.14	-0.49	0.03	0.04	-0.26
H_29	S2_C45_A40_φ8_3	0.71	-0.35	0.52	0.54	0.16
H_30	S2_C45_A40_φ10_1	-0.27	-0.60	-0.33	-0.32	-0.57
H_30	S2_C45_A40_φ10_2	0.14	-0.19	-0.53	-0.53	-0.06
H_30	S2_C45_A40_φ10_3	0.55	0.22	0.01	0.01	0.45
H_31	S2_C60_A80_φ8_1	-0.14	-0.33	-0.57	-0.57	-0.31
H_31	S2_C60_A80_φ8_2	0.36	-0.19	-0.93	-0.92	0.06
H_31	S2_C60_A80_φ8_3	0.86	-0.06	-1.29	-1.27	0.42
H_32	S2_C60_A80_φ10_1	-0.24	-0.53	0.12	0.18	-0.51
H_32	S2_C60_A80_φ10_2	0.16	-0.13	-0.38	-0.37	0.00
H_32	S2_C60_A80_φ10_3	0.57	0.28	0.11	0.11	0.51
H_33	S2_C60_A60_φ8_1	-0.43	-0.61	-0.38	-0.37	-0.66
H_33	S2_C60_A60_φ8_2	0.07	-0.48	0.22	0.26	-0.30
H_33	S2_C60_A60_φ8_3	0.57	-0.35	0.82	0.88	0.07
H_34	S2_C60_A60_φ10_1	-0.28	-0.57	-0.21	-0.19	-0.56
H_34	S2_C60_A60_φ10_2	0.21	-0.08	-0.32	-0.31	0.06
H_34	S2_C60_A60_φ10_3	0.70	0.41	0.25	0.25	0.67
H_35	S2_C60_A40_φ8_1	-0.47	-0.65	-0.50	-0.50	-0.72
H_35	S2_C60_A40_φ8_2	0.03	-0.52	-0.07	-0.05	-0.35
H_35	S2_C60_A40_φ8_3	0.53	-0.39	0.36	0.40	0.02
H_36	S2_C60_A40_φ10_1	-0.33	-0.62	-0.38	-0.37	-0.61
H_36	S2_C60_A40_φ10_2	0.20	-0.09	-0.33	-0.32	0.05
H_36	S2_C60_A40_φ10_3	0.72	0.43	0.28	0.28	0.70

Table 11 Minimum Fiber Volume ($V_{f,min}$) Based on Minimum Reinforcement Area Requirements Across International Codes

Group	Beam	$EC2004$ (%)	$EC2023$ (%)	$MC2010$ (%)	$MC2020$ (%)	$ACI318$ (%)
H_1	S1_C30_A80_φ4_1	0.77	0.26	0.07	0.05	0.36
H_1	S1_C30_A80_φ4_2	1.56	0.18	0.04	0.03	0.29
H_1	S1_C30_A80_φ4_3	-3.83	0.14	0.03	0.02	0.25
H_2	S1_C30_A80_φ5_1	-0.52	0.10	0.33	0.27	0.21
H_2	S1_C30_A80_φ5_2	0.86	0.24	0.13	0.12	0.35
H_2	S1_C30_A80_φ5_3	0.61	0.30	0.23	0.23	0.38
H_3	S1_C30_A60_φ4_1	0.88	0.37	0.20	0.19	0.50
H_3	S1_C30_A60_φ4_2	1.42	0.27	0.12	0.12	0.42
H_3	S1_C30_A60_φ4_3	6.12	0.21	0.09	0.08	0.36
H_4	S1_C30_A60_φ5_1	3.48	0.24	-0.12	-0.18	0.39
H_4	S1_C30_A60_φ5_2	1.02	0.34	0.20	0.20	0.47
H_4	S1_C30_A60_φ5_3	0.83	0.40	0.30	0.30	0.51
H_5	S1_C30_A40_φ4_1	1.54	0.52	0.14	0.10	0.72
H_5	S1_C30_A40_φ4_2	3.47	0.36	0.08	0.06	0.59
H_5	S1_C30_A40_φ4_3	-6.10	0.28	0.05	0.04	0.50
H_6	S1_C30_A40_φ5_1	-0.94	0.21	0.71	0.58	0.43
H_6	S1_C30_A40_φ5_2	1.72	0.49	0.25	0.24	0.70
H_6	S1_C30_A40_φ5_3	1.24	0.61	0.47	0.47	0.78
H_7	S1_C45_A80_φ5_1	1.00	0.25	0.03	0.04	0.39
H_7	S1_C45_A80_φ5_2	8.12	0.17	0.02	0.02	0.32
H_7	S1_C45_A80_φ5_3	-0.99	0.13	0.01	0.01	0.28
H_8	S1_C45_A80_φ6_1	-12.47	0.16	-0.29	-0.26	0.31
H_8	S1_C45_A80_φ6_2	0.80	0.26	0.16	0.16	0.39

H_8	S1_C45_A80_φ6_3	0.64	0.32	0.25	0.25	0.42
H_9	S1_C45_A60_φ5_1	-9.99	0.23	1.81	2.35	0.45
H_9	S1_C45_A60_φ5_2	-0.71	0.14	-6.99	-2.57	0.32
H_9	S1_C45_A60_φ5_3	-0.33	0.10	-0.92	-0.68	0.26
H_10	S1_C45_A60_φ6_1	-0.36	0.10	0.24	0.25	0.26
H_10	S1_C45_A60_φ6_2	1.37	0.31	0.13	0.13	0.49
H_10	S1_C45_A60_φ6_3	0.91	0.40	0.29	0.29	0.55
H_11	S1_C45_A40_φ5_1	-14.98	0.34	2.72	3.52	0.67
H_11	S1_C45_A40_φ5_2	-1.06	0.20	-10.49	-3.86	0.48
H_11	S1_C45_A40_φ5_3	-0.48	0.15	-1.26	-0.96	0.40
H_12	S1_C45_A40_φ6_1	-0.93	0.19	0.57	0.60	0.46
H_12	S1_C45_A40_φ6_2	2.08	0.49	0.22	0.23	0.77
H_12	S1_C45_A40_φ6_3	1.39	0.62	0.46	0.46	0.84
H_13	S1_C60_A80_φ5_1	1.05	0.28	0.04	0.05	0.43
H_13	S1_C60_A80_φ5_2	122.09	0.20	0.02	0.03	0.37
H_13	S1_C60_A80_φ5_3	-0.96	0.15	0.01	0.02	0.33
H_14	S1_C60_A80_φ6_1	-18.09	0.18	-0.32	-0.26	0.35
H_14	S1_C60_A80_φ6_2	0.82	0.29	0.18	0.18	0.42
H_14	S1_C60_A80_φ6_3	0.65	0.34	0.27	0.27	0.44
H_15	S1_C60_A60_φ5_1	0.45	0.16	0.36	0.39	0.23
H_15	S1_C60_A60_φ5_2	3.08	0.30	0.11	0.11	0.52
H_15	S1_C60_A60_φ5_3	-2.92	0.23	0.08	0.08	0.48
H_16	S1_C60_A60_φ6_1	-1.53	0.21	10.42	-5.72	0.45
H_16	S1_C60_A60_φ6_2	1.08	0.40	0.26	0.26	0.57
H_16	S1_C60_A60_φ6_3	0.84	0.47	0.39	0.39	0.60
H_17	S1_C60_A40_φ5_1	2.10	0.56	0.08	0.10	0.86

H_17	S1_C60_A40_φ5_2	244.19	0.39	0.04	0.05	0.75
H_17	S1_C60_A40_φ5_3	-1.81	0.30	0.03	0.04	0.68
H_18	S1_C60_A40_φ6_1	-0.87	0.23	0.76	0.86	0.58
H_18	S1_C60_A40_φ6_2	1.70	0.59	0.37	0.37	0.86
H_18	S1_C60_A40_φ6_3	1.30	0.72	0.59	0.59	0.92
H_19	S2_C30_A80_φ8_1	0.81	0.20	-0.37	-0.73	0.30
H_19	S2_C30_A80_φ8_2	14.29	0.13	-0.13	-0.19	0.23
H_19	S2_C30_A80_φ8_3	-1.11	0.10	-0.08	-0.11	0.18
H_20	S2_C30_A80_φ10_1	-1.05	0.09	0.31	0.26	0.17
H_20	S2_C30_A80_φ10_2	0.68	0.23	0.12	0.12	0.32
H_20	S2_C30_A80_φ10_3	0.55	0.29	0.22	0.22	0.36
H_21	S2_C30_A60_φ8_1	0.98	0.29	-0.19	-0.32	0.41
H_21	S2_C30_A60_φ8_2	4.05	0.19	-0.08	-0.12	0.32
H_21	S2_C30_A60_φ8_3	-2.15	0.14	-0.05	-0.08	0.26
H_22	S2_C30_A60_φ10_1	-0.64	0.10	0.25	0.22	0.19
H_22	S2_C30_A60_φ10_2	1.16	0.26	0.06	0.04	0.39
H_22	S2_C30_A60_φ10_3	0.81	0.34	0.23	0.23	0.46
H_23	S2_C30_A40_φ8_1	1.24	0.54	0.25	0.23	0.71
H_23	S2_C30_A40_φ8_2	1.98	0.38	0.14	0.13	0.58
H_23	S2_C30_A40_φ8_3	4.99	0.29	0.10	0.09	0.49
H_24	S2_C30_A40_φ10_1	-2.10	0.19	0.63	0.52	0.35
H_24	S2_C30_A40_φ10_2	1.27	0.51	0.33	0.33	0.69
H_24	S2_C30_A40_φ10_3	1.08	0.64	0.53	0.53	0.77
H_25	S2_C45_A80_φ8_1	0.67	0.30	0.05	0.05	0.41
H_25	S2_C45_A80_φ8_2	3.40	0.17	0.02	0.02	0.31
H_25	S2_C45_A80_φ8_3	-1.17	0.12	0.01	0.01	0.25

H_26	S2_C45_A80_φ10_1	1.30	0.19	-0.46	-0.39	0.33
H_26	S2_C45_A80_φ10_2	0.59	0.34	0.26	0.26	0.42
H_26	S2_C45_A80_φ10_3	0.54	0.38	0.34	0.34	0.45
H_27	S2_C45_A60_φ8_1	1.57	0.29	1.24	1.38	0.48
H_27	S2_C45_A60_φ8_2	-0.86	0.14	-1.55	-1.11	0.31
H_27	S2_C45_A60_φ8_3	-0.35	0.09	-0.49	-0.41	0.23
H_28	S2_C45_A60_φ10_1	5.84	0.22	2.27	3.26	0.40
H_28	S2_C45_A60_φ10_2	0.79	0.44	0.34	0.34	0.56
H_28	S2_C45_A60_φ10_3	0.72	0.51	0.46	0.46	0.59
H_29	S2_C45_A40_φ8_1	7.28	0.34	0.81	0.84	0.63
H_29	S2_C45_A40_φ8_2	-0.60	0.15	0.60	0.66	0.36
H_29	S2_C45_A40_φ8_3	-0.29	0.09	0.49	0.55	0.26
H_30	S2_C45_A40_φ10_1	-3.04	0.24	0.71	0.75	0.51
H_30	S2_C45_A40_φ10_2	1.26	0.65	0.47	0.48	0.85
H_30	S2_C45_A40_φ10_3	1.11	0.77	0.67	0.67	0.90
H_31	S2_C60_A80_φ8_1	0.58	0.37	0.27	0.27	0.45
H_31	S2_C60_A80_φ8_2	0.99	0.25	0.14	0.15	0.39
H_31	S2_C60_A80_φ8_3	3.51	0.19	0.10	0.10	0.35
H_32	S2_C60_A80_φ10_1	1.44	0.22	-0.50	-0.39	0.37
H_32	S2_C60_A80_φ10_2	0.60	0.36	0.29	0.29	0.45
H_32	S2_C60_A80_φ10_3	0.55	0.40	0.36	0.36	0.46
H_33	S2_C60_A60_φ8_1	1.44	0.32	1.22	1.45	0.51
H_33	S2_C60_A60_φ8_2	-0.93	0.16	-1.44	-0.92	0.36
H_33	S2_C60_A60_φ8_3	-0.36	0.11	-0.47	-0.36	0.27
H_34	S2_C60_A60_φ10_1	5.15	0.25	2.53	5.28	0.45
H_34	S2_C60_A60_φ10_2	0.78	0.49	0.40	0.40	0.59

H_34	S2_C60_A60_φ10_3	0.71	0.55	0.50	0.50	0.62
H_35	S2_C60_A40_φ8_1	10.53	0.39	0.96	1.02	0.73
H_35	S2_C60_A40_φ8_2	-0.60	0.17	0.84	1.01	0.46
H_35	S2_C60_A40_φ8_3	-0.30	0.11	0.73	0.96	0.33
H_36	S2_C60_A40_φ10_1	-3.27	0.28	0.84	0.92	0.58
H_36	S2_C60_A40_φ10_2	1.21	0.74	0.60	0.60	0.91
H_36	S2_C60_A40_φ10_3	1.10	0.84	0.77	0.77	0.95

Table 12 Minimum Fiber Volume ($V_{f,min}$) Based on Minimum Reinforcement Area Requirements Across International Codes When $r = 1$ $(DI = 0)$

Group	**Beam**	$EC2004$ (%)	$EC2023$ (%)	$MC2010$ (%)	$MC2020$ (%)	$ACI318$ (%)
H_1	S1_C30_A80_φ4_1	0.29	0.17	0.06	0.05	0.20
H_1	S1_C30_A80_φ4_2	2.26	0.19	0.04	0.03	0.31
H_1	S1_C30_A80_φ4_3	-0.36	0.21	0.03	0.02	0.67
H_2	S1_C30_A80_φ5_1	0.20	0.06	0.10	0.09	0.08
H_2	S1_C30_A80_φ5_2	0.79	0.24	0.12	0.12	0.34
H_2	S1_C30_A80_φ5_3	1.38	0.41	0.29	0.29	0.59
H_3	S1_C30_A60_φ4_1	0.49	0.28	0.17	0.16	0.34
H_3	S1_C30_A60_φ4_2	3.77	0.31	0.13	0.12	0.51
H_3	S1_C30_A60_φ4_3	-0.60	0.35	0.10	0.10	1.11
H_4	S1_C30_A60_φ5_1	0.59	0.18	-0.14	-0.24	0.25
H_4	S1_C30_A60_φ5_2	1.19	0.36	0.21	0.20	0.51
H_4	S1_C30_A60_φ5_3	1.78	0.53	0.37	0.37	0.76
H_5	S1_C30_A40_φ4_1	0.58	0.33	0.12	0.09	0.41
H_5	S1_C30_A40_φ4_2	4.52	0.37	0.08	0.06	0.61

H_5	S1_C30_A40_φ4_3	-0.72	0.43	0.06	0.04	1.33
H_6	S1_C30_A40_φ5_1	0.40	0.12	0.20	0.19	0.17
H_6	S1_C30_A40_φ5_2	1.58	0.47	0.25	0.24	0.68
H_6	S1_C30_A40_φ5_3	2.77	0.83	0.59	0.59	1.18
H_7	S1_C45_A80_φ5_1	0.35	0.17	0.03	0.03	0.23
H_7	S1_C45_A80_φ5_2	-1.34	0.20	0.02	0.02	0.44
H_7	S1_C45_A80_φ5_3	-0.22	0.23	0.01	0.01	21.49
H_8	S1_C45_A80_φ6_1	0.50	0.12	-0.75	-0.56	0.19
H_8	S1_C45_A80_φ6_2	1.24	0.30	0.17	0.18	0.47
H_8	S1_C45_A80_φ6_3	1.98	0.48	0.34	0.34	0.76
H_9	S1_C45_A60_φ5_1	0.23	0.11	0.20	0.21	0.15
H_9	S1_C45_A60_φ5_2	-0.90	0.13	6.37	-11.25	0.29
H_9	S1_C45_A60_φ5_3	-0.15	0.15	-0.20	-0.19	14.33
H_10	S1_C45_A60_φ6_1	0.25	0.06	0.09	0.09	0.09
H_10	S1_C45_A60_φ6_2	1.24	0.30	0.12	0.13	0.47
H_10	S1_C45_A60_φ6_3	2.23	0.54	0.36	0.36	0.85
H_11	S1_C45_A40_φ5_1	0.35	0.17	0.30	0.31	0.23
H_11	S1_C45_A40_φ5_2	-1.34	0.20	9.56	-16.87	0.44
H_11	S1_C45_A40_φ5_3	-0.22	0.23	-0.31	-0.29	21.49
H_12	S1_C45_A40_φ6_1	0.50	0.12	0.21	0.21	0.19
H_12	S1_C45_A40_φ6_2	1.98	0.48	0.22	0.22	0.76
H_12	S1_C45_A40_φ6_3	3.47	0.84	0.57	0.57	1.32
H_13	S1_C60_A80_φ5_1	0.30	0.17	0.04	0.04	0.21
H_13	S1_C60_A80_φ5_2	4.80	0.19	0.02	0.03	0.35
H_13	S1_C60_A80_φ5_3	-0.32	0.22	0.01	0.02	1.07
H_14	S1_C60_A80_φ6_1	0.33	0.12	-34.47	-1.32	0.17

H_14	S1_C60_A80_φ6_2	0.82	0.29	0.18	0.18	0.42
H_14	S1_C60_A80_φ6_3	1.31	0.47	0.35	0.35	0.68
H_15	S1_C60_A60_φ5_1	0.20	0.11	0.18	0.19	0.14
H_15	S1_C60_A60_φ5_2	8.01	0.31	0.11	0.12	0.58
H_15	S1_C60_A60_φ5_3	-0.54	0.36	0.09	0.09	1.79
H_16	S1_C60_A60_φ6_1	0.33	0.12	0.26	0.28	0.17
H_16	S1_C60_A60_φ6_2	1.15	0.41	0.26	0.26	0.59
H_16	S1_C60_A60_φ6_3	1.97	0.70	0.53	0.53	1.01
H_17	S1_C60_A40_φ5_1	0.60	0.34	0.07	0.09	0.42
H_17	S1_C60_A40_φ5_2	9.61	0.38	0.04	0.05	0.70
H_17	S1_C60_A40_φ5_3	-0.64	0.43	0.03	0.04	2.14
H_18	S1_C60_A40_φ6_1	0.33	0.12	0.18	0.19	0.17
H_18	S1_C60_A40_φ6_2	1.64	0.59	0.36	0.37	0.84
H_18	S1_C60_A40_φ6_3	2.96	1.05	0.80	0.80	1.52
H_19	S2_C30_A80_φ8_1	0.19	0.11	0.70	0.37	0.13
H_19	S2_C30_A80_φ8_2	1.75	0.12	-0.14	-0.21	0.21
H_19	S2_C30_A80_φ8_3	-0.24	0.14	-0.06	-0.08	0.43
H_20	S2_C30_A80_φ10_1	0.19	0.06	0.11	0.10	0.08
H_20	S2_C30_A80_φ10_2	0.76	0.24	0.12	0.12	0.33
H_20	S2_C30_A80_φ10_3	1.33	0.41	0.29	0.29	0.59
H_21	S2_C30_A60_φ8_1	0.28	0.17	-0.37	-1.76	0.20
H_21	S2_C30_A60_φ8_2	2.63	0.19	-0.08	-0.13	0.31
H_21	S2_C30_A60_φ8_3	-0.37	0.21	-0.05	-0.07	0.65
H_22	S2_C30_A60_φ10_1	0.19	0.06	0.09	0.09	0.08
H_22	S2_C30_A60_φ10_2	0.76	0.24	0.06	0.04	0.33
H_22	S2_C30_A60_φ10_3	1.33	0.41	0.26	0.26	0.59

H_23	S2_C30_A40_φ8_1	0.66	0.39	0.21	0.20	0.47
H_23	S2_C30_A40_φ8_2	6.14	0.44	0.15	0.14	0.72
H_23	S2_C30_A40_φ8_3	-0.85	0.50	0.12	0.11	1.52
H_24	S2_C30_A40_φ10_1	0.38	0.12	0.21	0.20	0.17
H_24	S2_C30_A40_φ10_2	1.91	0.59	0.36	0.36	0.84
H_24	S2_C30_A40_φ10_3	3.43	1.06	0.79	0.79	1.51
H_25	S2_C45_A80_φ8_1	0.23	0.16	0.04	0.05	0.19
H_25	S2_C45_A80_φ8_2	-1.98	0.19	0.02	0.02	0.41
H_25	S2_C45_A80_φ8_3	-0.19	0.24	0.01	0.01	-2.67
H_26	S2_C45_A80_φ10_1	0.23	0.11	0.71	0.95	0.15
H_26	S2_C45_A80_φ10_2	0.80	0.40	0.30	0.30	0.52
H_26	S2_C45_A80_φ10_3	1.37	0.68	0.56	0.56	0.90
H_27	S2_C45_A60_φ8_1	0.16	0.11	0.15	0.15	0.13
H_27	S2_C45_A60_φ8_2	-1.32	0.13	-4.09	-2.00	0.27
H_27	S2_C45_A60_φ8_3	-0.13	0.16	-0.14	-0.13	-1.78
H_28	S2_C45_A60_φ10_1	0.23	0.11	0.22	0.22	0.15
H_28	S2_C45_A60_φ10_2	1.03	0.51	0.38	0.38	0.67
H_28	S2_C45_A60_φ10_3	1.83	0.91	0.74	0.74	1.20
H_29	S2_C45_A40_φ8_1	0.16	0.11	0.13	0.13	0.13
H_29	S2_C45_A40_φ8_2	-1.32	0.13	0.39	0.41	0.27
H_29	S2_C45_A40_φ8_3	-0.13	0.16	-0.42	-0.39	-1.78
H_30	S2_C45_A40_φ10_1	0.23	0.11	0.16	0.17	0.15
H_30	S2_C45_A40_φ10_2	1.37	0.68	0.49	0.49	0.90
H_30	S2_C45_A40_φ10_3	2.52	1.25	1.01	1.01	1.65
H_31	S2_C60_A80_φ8_1	0.36	0.27	0.21	0.21	0.31
H_31	S2_C60_A80_φ8_2	4.01	0.31	0.16	0.16	0.56

H_31	S2_C60_A80_φ8_3	-0.45	0.37	0.13	0.13	2.93
H_32	S2_C60_A80_φ10_1	0.20	0.11	0.42	0.54	0.14
H_32	S2_C60_A80_φ10_2	0.69	0.39	0.31	0.31	0.49
H_32	S2_C60_A80_φ10_3	1.18	0.67	0.56	0.56	0.84
H_33	S2_C60_A60_φ8_1	0.15	0.11	0.14	0.15	0.12
H_33	S2_C60_A60_φ8_2	1.61	0.12	0.99	1.63	0.22
H_33	S2_C60_A60_φ8_3	-0.18	0.15	-0.20	-0.18	1.17
H_34	S2_C60_A60_φ10_1	0.20	0.11	0.19	0.20	0.14
H_34	S2_C60_A60_φ10_2	0.98	0.56	0.44	0.44	0.70
H_34	S2_C60_A60_φ10_3	1.77	1.00	0.85	0.85	1.26
H_35	S2_C60_A40_φ8_1	0.15	0.11	0.13	0.13	0.12
H_35	S2_C60_A40_φ8_2	1.61	0.12	0.29	0.30	0.22
H_35	S2_C60_A40_φ8_3	-0.18	0.15	-1.22	-0.86	1.17
H_36	S2_C60_A40_φ10_1	0.20	0.11	0.15	0.15	0.14
H_36	S2_C60_A40_φ10_2	1.47	0.84	0.66	0.66	1.05
H_36	S2_C60_A40_φ10_3	2.75	1.56	1.33	1.33	1.97

References

[1] A. Gorino and A. Fantilli, "Scaled Approach to Designing the Minimum Hybrid Reinforcement of Concrete Beams," *Materials*, vol. 13, no. 22, p. 5166, Nov. 2020, doi: 10.3390/ma13225166.

[2] A. Rubino, A. Carpinteri, and F. Accornero, "Flexural behavior and minimum reinforcement condition in hybrid-reinforced concrete beams," *Struct. Concr.*, vol. 24, no. 4, pp. 4767–4778, Aug. 2023, doi: 10.1002/suco.202200674.

[3] C. Pleesudjai *et al.*, "Efficiency of hybrid reinforced concrete beams with low reinforcement ratios," *Mater. Struct.*, vol. 58, no. 6, p. 218, Aug. 2025, doi: 10.1617/s11527-025-02736-4.

[4] H. Lu, Q. Chen, Z. Gu, X. Wen, Z. Huang, and T. Ding, "Experimental study on flexural behavior of hybrid fiber-reinforced concrete beams based on DIC technology," *Structures*, vol. 85, p. 111084, Mar. 2026, doi: 10.1016/j.istruc.2026.111084.

[5] G. B. Xu X, Li Z, Zhao H, and Zhang T, "Study on shear resistance calculation of steel fiber reinforced concrete beams.," *J Railw Sci Eng 201815082006–13*.

[6] A. Gorino, "Ductility of lightly reinforced and fiber-reinforced concrete elements: A unified approach".

[7] A. Fantilli, B. Chiaia, and A. Gorino, "Minimum reinforcement and ductility index of lightly reinforced concrete beams," *Comput. Concr.*, vol. 18, pp. 1175–1194, Dec. 2016, doi: 10.12989/cac.2016.18.6.1175.

[8] A. P. Fantilli, B. Chiaia, and A. Gorino, "Fiber volume fraction and ductility index of concrete beams," *Cem. Concr. Compos.*, vol. 65, pp. 139–149, Jan. 2016, doi: 10.1016/j.cemconcomp.2015.10.019.

[9] A. E. Naaman, "Engineered Steel Fibers with Optimal Properties for Reinforcement of Cement Composites," *J. Adv. Concr. Technol.*, vol. 1, no. 3, pp. 241–252, 2003, doi: 10.3151/jact.1.241.

[10] Yang X, Wu H, Liu Y., "Experimental study on cracking behavior of reinforced steel fiber concrete axial tensile members.," *Water Power 20194505113–7 Httpsdoi Org103969jissn0559-9342201905025*.

[11] Cui H, Wang W, Cui N, Yang X, He J, Zhang Z., "Experimental study on horizontal bearing characteristics of steel fiber reinforced concrete pile.," *J Beijing Jiaotong Univ 20194303130–6 Httpsdoiorg1011860iissn1673-029120180178*.

[12] Sakthipriya C., "Experimental investigation on hybrid fiber reinforced green cement concrete.," *Int J Res Appl Sci Eng Technol 20219238–40 Httpsdoiorg 1022214ijraset202133066*.

[13] Wang J, Li M, Chen J, Zhao Z, Zhao H, Zhang L, et al., "Investigation on shrinkage characteristics of polyester-fiber-reinforced cement-stabilized concrete considering fiber length and content.," *Build. 2023132075-53091027 Httpsdoiorg 103390buildings13041027*.

[14] Fu X., "Experimental study on durability of basalt-cellulose hybrid fibre concrete.," *PhD Thesis 2021 Liaoning Univ. Technol. Liaoning China Chin. Httpsdoiorg1027211dcnkigIngc2021000259*.

[15] Zhang Y., "Study on the impact of different fibers on the toughness performance of lightweight aggregate concrete.," *Concr. 20020530–2 Httpsdoiorg 103969jissn1002-3550200205010*.

[16] "Model Code 2020. 1."

[17] "Eurocode 2. Design of concrete structures. Part 1-1 General rules and rules for buildings, bridges and civil engineering structures: BS EN 1992-1-1:2004."

[18] British Standards Institution, Ed., *Eurocode 2. Design of concrete structures. Part 1-1 General rules and rules for buildings, bridges and civil engineering structures: BS EN 1992-1-1:2023*. in British Standard, no. BS EN 1992-1-1:2023. London: British Standards Institution, 2023.

[19] "Model Code 2010. 2," in Bulletin / Fédération Internationale du Béton, no. 56., Lausanne: International Federation for Structural Concrete (fib), 2010.

[20] *318-19 Building Code Requirements for Structural Concrete and Commentary*. American Concrete Institute, 2019. doi: 10.14359/51716937.

[21] S. M. F. Mahmood, T. Akter, S. J. Foster, and H. Valipour, "Minimum tensile reinforcement ratio for conventionally reinforced-SFRC beams and slabs," *Structures*, vol. 63, p. 106320, May 2024, doi: 10.1016/j.istruc.2024.106320.

[22] A. Pérez Caldentey, R. Garcia, and H. Corres Peiretti, "Minimum reinforcement revisited," *Struct. Concr.*, vol. 19, no. 5, pp. 1448–1459, Oct. 2018, doi: 10.1002/suco.201700271.

[23] P. A. Capsoni, "INVESTIGATION IN THE REALM OF FIBER REINFORCED CONCRETE".

[24] S.-J. Lee, D.-Y. Yoo, and D.-Y. Moon, "Effects of Hooked-End Steel Fiber Geometry and Volume Fraction on the Flexural Behavior of Concrete Pedestrian Decks," *Appl. Sci.*, vol. 9, no. 6, p. 1241, Mar. 2019, doi: 10.3390/app9061241.